# Dry Deep Soil Mixing Soil-Cement column panels as bottom struts for excavation support

Revising of design methodology in Scandinavia

Andres Alfonso Santos Barros

| | |
|---|---|
| Dr. Mandy Korff | TU Delft |
| Dr. Wout Broere | TU Delft |
| Dr. Robert Lanzafame | TU Delft |
| Ir. Robin Vervoorn | Civil7 |

*Master of Science Thesis*

*Geo-Engineering*

*Geoscience and Engineering*

*Civil Engineering and Geosciences*

*Delft, The Netherlands, 2019*

TU Delft

Civil 7

# Table of Contents

# List of figures

# List of tables

# Abstract

Deep Soil Mixing is an often-applied technique in the reinforcement of embankments, but little has been done to investigate and understand its behavior when used in excavation projects. The present research presents a database of the results of previous studies on the Deep Soil Mixing technique in Scandinavian soils. An expression that can estimate the improved soil strength when a specific binder content and binder ratio is mixed with the soil is proposed and its pertinence is tested with two full-scale tests. The proposed mathematical expression to predict the improved strength yields a good representation of the available data. The full-scale tests, in which a braced steel sheet pile wall interacts with panels of DSM overlapping columns are used for back-calculating the improved soil strength and stiffness properties. It is observed that the weighted average procedure for calculating properties should be used with care and that the loading conditions affect the strength and stiffness that the improved soil can develop. The drained analysis with a fixed friction angle and a cohesion intercept estimated from the undrained shear strength is the suggested design procedure to assess deep excavations involving improved materials.

# Preface

The present research is the result of a journey of almost nine months of personal and professional growth and, of course, hard work. This would not have been possible without all the help and advice of my thesis committee; you played an important role during the conception and improvement of the investigation. Mandy, Wout, Robert and Robin, I only have gratitude to you for all the time spent with me helping and critically assessing all the steps of my work. You always trusted me and my capabilities to improve the quality of my work, thank you for all the pushes and advice.

To all my friends back in Colombia and all the wonderful people I met here in The Netherlands, thanks for all the support when I needed to talk or when having a beer or coffee in the many breaks and gatherings in all this time. This day to day psychological support was one of the keys to keeping the mood up even in the most difficult moments.

To my lovely girlfriend Juliana, who was always there to support, advice and listen to all I had to say regarding this process. You made this a little easier for me and for that I am eternally grateful with you. I love you with my heart.

To all my family, especially my dad, Elverth; my mom, Martha and my little sister, Tata, for making this journey possible, for always believing in me and for being my strongest motivation. I love you with my soul and this if for you.

# *Prefacio*

*El presente trabajo es el resultado de un viaje de casi nueve meses de crecimiento personal y profesional y, por supuesto, arduo trabajo. Esto no podría haber sido posible sin toda la ayuda y el consejo de mi comité de tesis; ustedes han jugado un papel importante durante la concepción y el mejoramiento de la investigación. Mandy, Wout, Robert y Robin, solo tengo palabras de gratitud para ustedes por todo el tiempo empleado conmigo para ayudarme y al evaluar todos los avances de mi trabajo. Siempre confiaron en mí y en mis capacidades para mejorar la calidad de mi trabajo, gracias por toda la motivación y consejo.*

*A todos mis amigos en Colombia y todas las personas que conocí aquí en los Países Bajos, gracias por todo su apoyo cuando necesité hablar o al tomar una cerveza o un café en los numerosos breaks y reuniones durante este tiempo. Este apoyo psicológico diario fue una de las claves para mantenerme con ánimos incluso en los momentos más duros.*

*A mi hermosa novia Juliana, quien siempre estuvo y esta ahí para apoyarme, aconsejarme y escuchar todo lo que tuve que decir durante este proceso. Tu lograste hacer esto un poco más fácil para mí y por eso te estoy eternamente agradecido. Te amo con todo mi corazón.*

*A toda mi familia, especialmente a mi padre, Elverth; a mi madre, Martha, y a mi hermana menor, Tata, por hacer esto posible, por siempre creer en mí y por ser mi mas fuerte motivación. Los amo con mi alma y esto es por ustedes.*

# 1. INTRODUCTION

## 1.1. Background and motivation

Deep soil mixing techniques have been used since mid-1970s to successfully improve natural soil properties. In Europe, its application in construction projects began in Sweden where a mixture of dry cement and lime binder is introduced in the soil using different mixing tools and compressed air, this process is denominated Dry Deep Mixing. Almost simultaneously, the use of cement slurry as a binder to improve soil properties started in Japan and has thereafter been used in Europe; it is referred to as Wet Deep Mixing. The present research focuses only on the Dry Deep Mixing (DDM) method and its application in Scandinavian countries.

Since the introduction of the DDM, it has mainly been used to reduce the settlements and for stability improvement of road embankments built in locations were soil conditions are unfavorable, but its application is also possible in bridge abutments, quay walls, breakwaters and to improve the lateral resistance of pile foundations. Due to urban development, large construction projects are taking place in densely populated cities and the DDM application has extended to include stability of constructions near to cut slopes, liquefaction mitigation, support of braced excavations and several others.

The installation of column-type ground improvement on the passive side of an excavation is an application of the DDM method that has been studied in the recent years, but it is still not well understood. The use of this application has been documented for some field cases (Hanson, 2012; Ignat, 2018) and it shows the engineering and economic advantages of it. The proposed approach is to install columns between the retaining wall in a continuous panel configuration of at least two rows of overlapping columns. The field studies showed that by improving the soil in the passive zone of an excavation, the passive earth pressure that can be mobilized in the retaining structure is increased. Reduction of excavation induced settlements behind the retaining structure and reduction of structural forces is also documented, therefore increasing the factor of safety of the system.

The design methodology implemented in the Swedish design guidelines assumes that the improved soil behaves as a composite material alongside with the natural soil and the governing failure mode is a shear failure through both the stabilized and the natural soil (Trafikverket, 2011). Full interaction between the soil volumes is also assumed, therefore the material properties of the soil volume in the passive zone are calculated as a weighted average between the stabilized and the natural soil. The guideline states that when employing stabilized soil in the passive zone, the strength properties should be significantly reduced compared to the active or direct shear loading cases, meaning that the effect of ground improvement in passive zones will be considerably reduced.

It is of common interest to develop a reliable and practical design method to predict the strength properties of laterally loaded columns in the passive zone of an excavation in order to increase the likelihood applying the DDM in future construction projects where the columns are to be subjected to lateral loading conditions.

## 1.2. Research Objectives

The present research project is aiming to increase understanding and knowledge basis regarding the design methodology of DDM acting in the passive zone of an excavation. As a result, the following research questions were formulated:

- Can the shear strength improvement be estimated only based on natural soil properties and binder content?
- How do laboratory and field tests relate to determine DSM properties?
- What is the best approach to translate from laboratory or field obtained values to design strength and stiffness parameters?
- How should the column placement variability be accounted for in the design parameters?

# 2. DEEP SOIL MIXING

In the deep soil mixing method, soft soil is stabilized in situ with binder without compaction. Deep soil mixing is presently most common in regions with deep deposits of soft, compressible clays or loose sands with low strength. It is an in-situ ground modification technology by which a wet or dry binder is introduced into the ground and is blended with the soil by mechanical or rotary mixing tools and it is used for various purposes such as stability, settlement reduction, excavation support and seepage control (Kitazume & Terashi, 2013). The result of mixing is a hardened ground with improved engineering properties compared to the natural ground. Deep mixing can be classified regarding the method of mixing (mixing tool used) or the type of binder being used (dry or wet). The latter classification is of interest for the present research.

Deep soil mixing techniques had been used since mid-1970s to successfully improve natural soil properties. In Sweden, the research and testing using lime started in the 1960s and since 1975 lime-cement columns have been used for ground improvements in construction projects. The Swedish Dry Deep Mixing development used a dry mixture of cement and lime introduced into the soil by means of compressed air through different mixing tools. The Wet Deep Mixing, originated in Japan almost simultaneously, uses cement slurry as a binder and its use has also extended to Europe, where it was first implemented in Germany, France and Italy (Massarsch & Topolnicki, 2005).

## 2.1. Dry Deep Mixing Method

In dry mixing, the binder is a powder, normally a mixture of cement and dehydrated lime. However, the binder can also consist of a mixture of cement, lime, gypsum, and other substances in granular or powdered form which are incorporated into the soil using compressed air. This method had become the predominant ground improvement technique in the Scandinavian countries.

The amount of binder required to stabilize the soil can vary considerably, depending on the soil conditions and the project requirements. It ranges typically between 80 and 200 kg/m$^3$, units that must be read as weight of stabilizer added per initial in-situ volume of soil to be treated. Normally, a mixture of 50 % lime and 50 % cement is used, and the stabilization ratio (stabilized soil/unimproved soil) is generally 10 to 30 %, unless block improvement is applied. The design strength of the stabilized soil is typically limited 100 to 200 kPa for the Scandinavian case. Figure 1 shows a mixing tool of two blades used in Sweden.

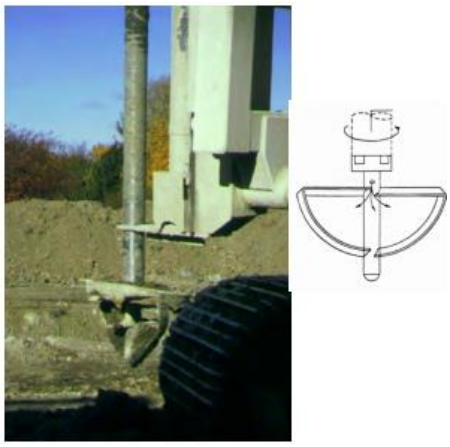

*Figure 1. Mixing tool of Swedish dry mixing method. Source:* (Massarsch & Topolnicki, 2005).

## 2.2. Wet Deep Mixing Method

Wet mixing can also use the same possible binders as the dry method, but they are fed in the form of a slurry, in some cases filler materials like sand are also added. The resulting columns behave similar to concrete piles and its installation is carried out using flight augers or by blades, depending on ground conditions. When necessary, reinforcement of the columns by means of beams or steel cages are also installed into the fresh mixed columns with the aid of a vibrator.

The development and initial trials of Bauer's Mixed-in-Place (MIP) system started in 1977 using the mixing tool shown in Figure 2. The original idea was to install vertical walls in the ground for soil nailing works in order to avoid shotcrete cover after excavation, but its application is also extended for settlement reduction under embankments and foundations. The walls are constructed using closely mounted augers arranged in a row.

*Figure 2. The first application of Mixed-in-place (MIP) piles. Source:* (Massarsch & Topolnicki, 2005).

## 2.3. Installation of soil cement columns

### 2.3.1. Installation procedure

Installation of soil cement columns is carried out by a mixing shaft which is lowered to the desired improvement depth, usually limited to 25 meters. Even though the binders could be added in either

lowering or withdrawing the mixing tool, it is a common practice to only introduce the binder into the soil when withdrawing the mixing tool. The rotational and withdrawal speed can be both adjusted depending on mixing requirements, the injecting pressure of the binder could also be modified depending on soil type, the use of too high pressure should be avoided as this may affect the soil pore pressure and therefore the stability of the surroundings (Andersson, 2010; Hanson, 2012).

Different column diameters are possible depending on the size of the mixing tool, typically ranging from 500 to 1000 mm. There are several types of mixing tools and its selection has been proven of importance for the stabilization result. For reasons of safety and environment, the binder injection is stopped when the mixing tool tip is about 1 meter below the ground surface. At installation of the piles, the material will present a reduction in strength for a certain period, as a result, the installing machinery will have a mobility restriction and installation should be carefully planned specially if cuts or slopes are to be stabilized. A general overview of the installation procedure is depicted in Figure 3.

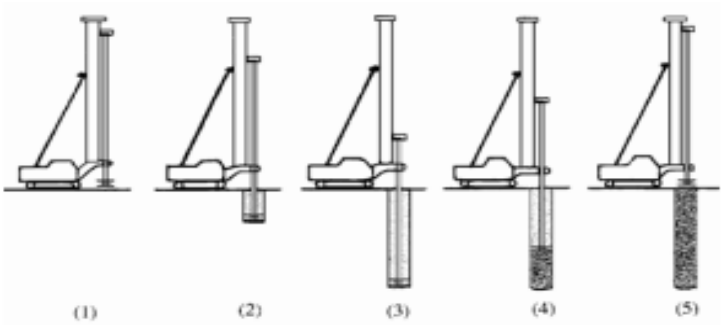


*Figure 3. Sequence of installation by Dry Deep Mixing: 1) the mixing tool is correctly positioned; 2) the mixing shaft penetrates to the desired depth of treatment with simultaneous disaggregation of the soil by the mixing tool; 3) after reaching the desired depth, the shaft is withdrawn and at the same time, the binder in granular or powder form is injected into the soil; 4) the mixing tool rotates in the horizontal plane and mixes the soil and the binder; 5) completion of the treated column. Source:* (Massarsch & Topolnicki, 2005).

### 2.3.2. Installation patterns

Depending on the intended purpose of the deep mixing, several different column installation patterns are used, from single columns to block improvement. Often the purpose of soil treatment is to stabilize slopes, embankments or trench walls. In these cases, the columns should be installed overlapped in several walls perpendicular to the slope, the embankment or the trench, see Figure 4 (1). Overlapping of columns has proven to be of importance when the columns are installed for stability or containment purposes (Ignat, Baker, Larsson, & Liedberg, 2015; Massarsch & Topolnicki, 2005). It is a common practice that the stability is analyzed based on the weighted mean strength properties of both the untreated and stabilized soil (Sukpunya & Jotisankasa, 2016). For settlement reduction purposes, the columns are placed in a triangular or quadrilateral pattern as shown in Figure 4 (2).

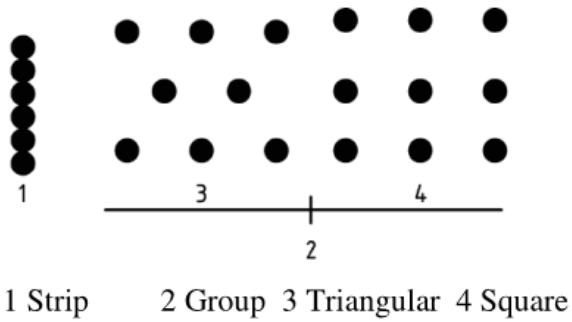


*Figure 4. Examples of installation patterns in the dry mixing method. Source:* (Massarsch & Topolnicki, 2005).

The columns will behave differently if situated in the active zone, in the pure shear zone, or in the passive zone of the potential failure surface. In the active zone, the axial load on the column contributes to increasing the shearing or bending resistance while in the passive zone the columns may even rupture in tension. Therefore, columns in the active zone benefit most to improving the stability condition. In the shear and passive zones columns arranged as buttress walls or as a block are more effective in preventing shear failure than single columns (Massarsch & Topolnicki, 2005).

In the case of improving future construction pits using braced excavations, the suggested approach is to use single or double ribs and block pattern inside the retaining walls, as the safety against bottom heave and improved strength and stiffness properties are obtained in the passive side of the excavation, resulting in reduced deformations and structural forces (Ignat, 2018). Also, extra piles are commonly set against the supporting wall to make the best contact possible, an example of this arrangement can be observed in Figure 5.

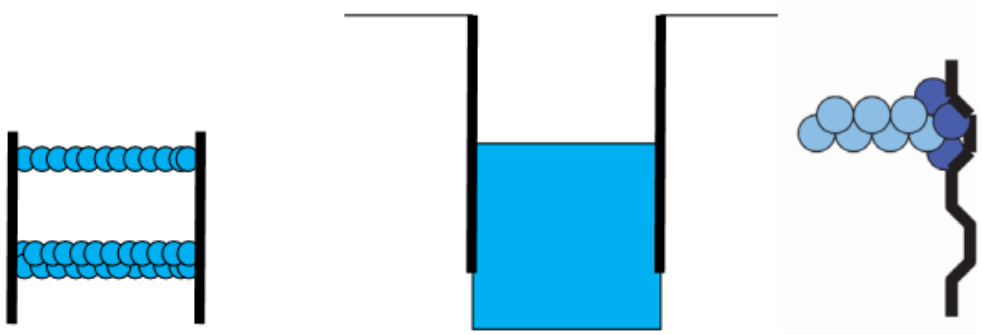

*Figure 5. Illustration of Dry DSM panel stabilization inside excavation. Source:* (Karlsrud, Eggen, Nerland, & Haugen, 2013).

It is important that the shear strength of the treated soil in the overlapping zone complies with design assumptions and that the overlap distance and strength of the columns is sufficient. It is also important that the verticality of overlapping columns is maintained over the whole length within stablished tolerances. The shear strength of the stabilized soil in the overlapping zone usually governs the lateral resistance of the columns (Massarsch & Topolnicki, 2005).

## 2.4. Design Methodology

### 2.4.1. Design guidelines

Different design methodologies agree that most of the strength and stiffness information about deep mixing method material should be obtained from unconfined compressive strength tests performed on laboratory mixed samples, wet grab samples taken during construction, and core samples obtained from deep mix elements constructed and cured in the field. Also, in-situ tests on field-cured materials are recommended as the laboratory curing conditions may differ from the ones on site.

The FHWA (Federal Highway Administration) Design Manual: *"Deep mixing for embankment and foundation support",* from the U.S. Department of Transportation, only considers the use of soil improvement method when supporting embankment constructions both using single columns and an arrangement that they call shear walls. The manual assesses two different internal stability modes of failure, a circular sliding surface, and vertical shearing of the shear walls, both can be observed in Figure 6. In the manual, no reference can be found about the implementation of DSM in the passive zone of an excavation. Therefore, the methodology there placed should be analyzed carefully when designing soil improvement subjected to other loading conditions.

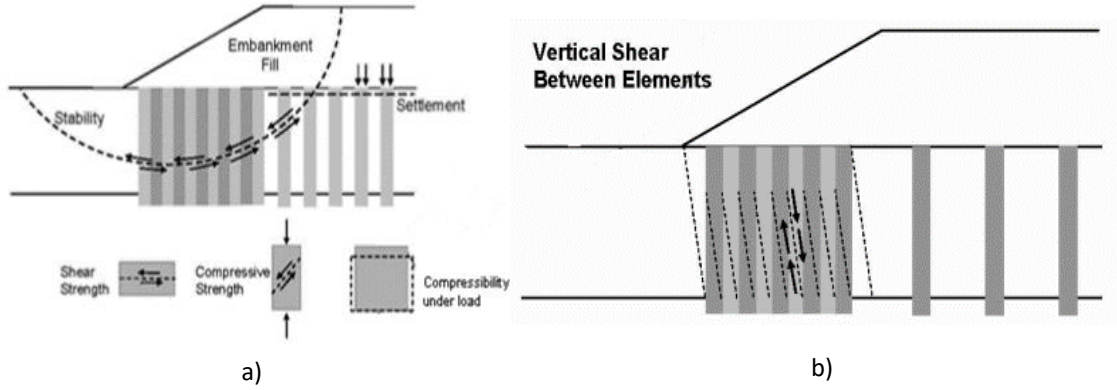


*Figure 6. Internal stability modes of failure: a) circular sliding surface; b) vertical shearing: Source:* (Bruce et al., 2013).

The current Swedish design guideline (TK Geo 13) establishes maximum strength properties for the improved soil depending on the loading condition. For undrained conditions, it sets a maximum undrained shear strength of 100 kPa using a factor of safety of 1.4, on the other hand, for drained conditions of improved material placed in the passive zone of an excavation the design code sets the drained cohesion at 0 kPa and a drained friction angle depending of the soil being mixed; 32° for clay and peat, 29° for gyttja, and 35° for silt (Trafikverket, 2011). Several studies suggest that these values could be increased, hence reducing construction costs while maintaining safety (Helen Åhnberg, 2007; Ignat, 2018).

The strength of deep mixed material is highly variable even at a single construction site, due to variability of the in-situ soil, of mixing effectiveness and many other possible factors. Given all the factors that affect the strength of treated soils, the Japanese Coastal Development Institute of Technology indicates that it is not possible to predict within a reasonable level of accuracy the strength that will result from adding a particular amount of binder to a given soil, based on the in-

situ characteristics of the soil (Kitazume & Terashi, 2013). Consequently, mix studies must be performed using soils obtained from a project site.

### 2.4.2. Design approach

In general, engineering property values for DSM materials can be obtained in the laboratory from unconfined compression tests, triaxial compression/extension tests, direct shear tests, oedometer tests, and hydraulic conductivity tests. Of the mentioned tests, the unconfined compression test is by far the most widely used. On the field, some of the used tests are the CPT, FKPS (reverse column test) and the MOPS (reverse column plate test). It has been proven that strength obtained from laboratory mixed and field mixed will differ because of different mixing and curing conditions. A scheme of the activities involved in DSM design is depicted in Figure 7.

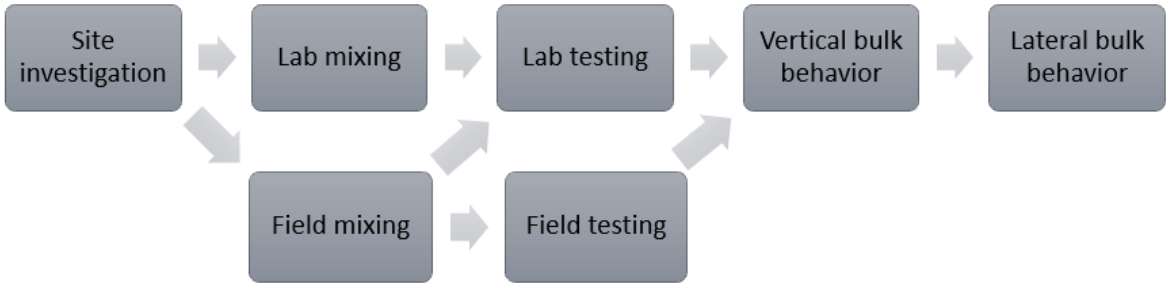


*Figure 7. Activities involved in DSM design. Source: own elaboration.*

Even though the scheme of the activities performed in the DSM design seems logical and ordered, it does not replicate the timeline of the design process. If a project has a potential to be designed using DSM, the site investigation will include more than the usual CPT profiles, it will include sample recovering and laboratory testing of the sampled soil, which would give the index properties of the natural soil. The site investigation is a crucial part of the geotechnical design because after analyzing all the results, the geotechnical designer will then decide which is the best approach to effectively fulfill the project requirements.

If the DSM is considered as the solution, then laboratory tests are arranged with different binder quantities and ratios mixed with soil samples coming from different boreholes and depths. Depending on the results obtained, field tests are then designed and performed, from which more laboratory and in-situ tests are made. After performing a statistical analysis, the characteristic values of the strength properties are then affected by a safety factor before being used for design. As the usual application of DSM is to support embankments, the safety factor suggested by the design codes should not be directly applied for lateral loading condition, therefore a new factor should be introduced. A scheme of the design timeline is depicted in Figure 8.


*Figure 8. Design timeline of a DSM project. Source: own elaboration*

From the design process timeline, it is clearly noted that even before performing laboratory mixing, the designer must be convinced that DSM is indeed the suitable solution of the faced problem. Therefore, it is an existing necessity that the designer could use the results from the site investigation to be able to predict the final lateral bulk behavior of an improved soil mass by means of correlations or a design chart. There has been a considerable amount of studies regarding the laboratory testing and results, as well as field testing and results; but it has not yet been presented a methodology that predicts the bulk behavior of an improved soil mass starting from only the index or the natural strength properties.

## 2.5. Factors Influencing Soil Strength Improvement

The magnitude of strength increase in stabilized soils by cement and other additives is influenced by the characteristics of the binder, natural soil conditions, mixing procedure and curing conditions (Kitazume & Terashi, 2013), for a more detailed list of influencing factors refer to Table 1. The characteristics of the binder will not be analyzed in the present research as for each of the analyzed projects, the binders were cement or a combination of lime and cement. The characteristics and conditions of soil are not easily modifiable and are unique for each project site, therefore these must be managed carefully in order to be able to compare results. The mixing conditions are not analyzed in the present research as contractors usually perform the installation of DSM using similar procedures. The curing conditions influence how the improved strength develops and it can be controlled easily in laboratory studies but cannot be influenced at project sites in most cases, this difference of strength development has to be carefully treated because difference in curing temperature highly influence how fast the chemical reactions take place between the soil and the binder.

*Table 1. Factors affecting strength increase of stabilized soil. Source:* (Kitazume & Terashi, 2013).

| | | |
|---|---|---|
| I. | Characteristics of binder | 1. Type of binder<br>2 . Quality<br>3. Mixing water and additives |
| II. | Characteristics and conditions of soil (especially important for clays) | 1. Physical, chemical and mineralogical properties of soil<br>2. Organic content<br>3. potential Hydrogen (*pH*) of pore water<br>4. Water content |
| III. | Mixing conditions | 1. Degree of mixing<br>2. Timing of mixing/re-mixing<br>3. Quantity of binder |
| IV. | Curing conditions | 1. Temperature<br>2. Curing period<br>3. Humidity<br>4. Wetting and drying/freezing and thawing, etc.<br>5. Overburden pressure |

### 2.5.1. Influence of water content

The influence of the natural water content of the soil on the unconfined compressive strength can be observed in Figure 9. To generate this graph, the same soil was prepared at different initial water contents and then stabilized using lime of two different binder factors and cured for three different time spans to also prove the strength development through time. In Figure 9, it can be observed that the maximum strength of the soil shifts to the dry side with increasing curing time. The strength

decreases considerably with increasing water content exceeding the liquid limit (Kitazume & Terashi, 2013).

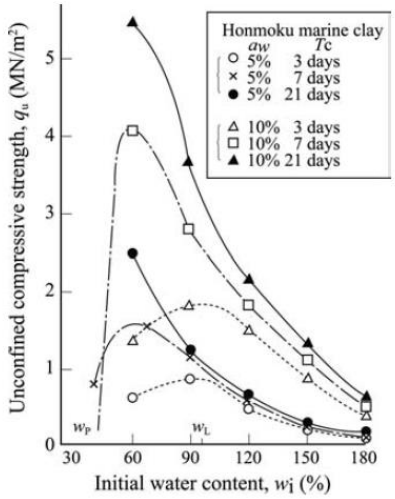


*Figure 9. Influence of initial water content on strength of quicklime stabilized soil. Source:* (Kitazume & Terashi, 2013).

Figure 10 shows the results of unconfined compression tests performed on two clays stabilized using cement. The unconfined compression strength decreases almost linearly with increasing initial water content regardless type of soil or cement.

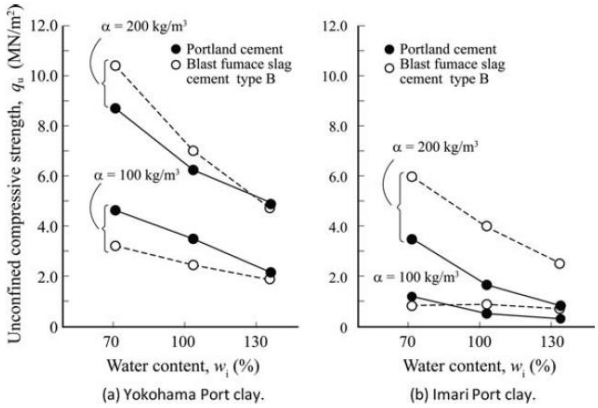


*Figure 10. Influence of initial water content on strength. Source:* (Kitazume & Terashi, 2013).

### 2.5.2. Influence of binder content

The improved shear strength is closely related to the amount of binder introduced into the soil regardless of the soil properties. In Figure 11 (left), the unconfined compressive strength increases almost linearly with the amount of quicklime used, irrespective of the curing period. However, Figure 11 (right) shows a clear peak strength at an optimal quicklime content, it can also be observed that the unconfined compressive strength becomes larger with longer curing period.

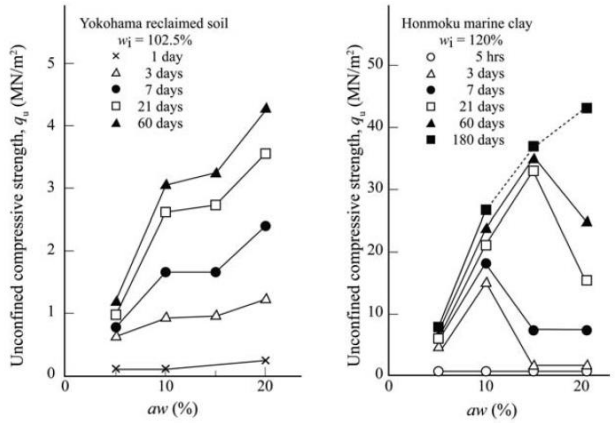


*Figure 2.10* Influence of amount of binder in quicklime stabilization (Terashi *et al.*, 1977).

*Figure 11. influence of amount of binder in quicklime stabilization. Source:* (Kitazume & Terashi, 2013).

A series of unconfined compression tests were reported in Skøyen, Oslo (Karlsrud et al., 2013) and the results are shown in Figure 12. The tests were referred to their 28-day strength to be able to compare the results properly. In general terms, a linear trend is observed with shear strength when the binder content is increased.

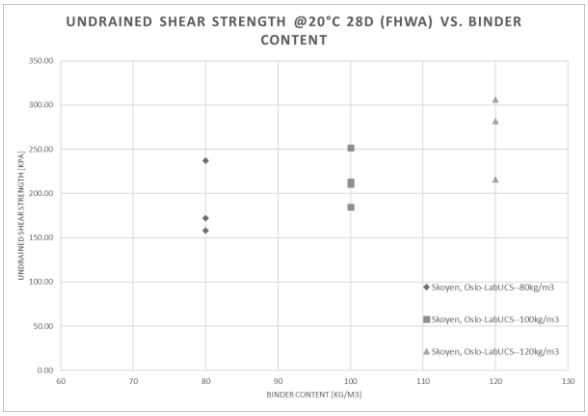


*Figure 12. Influence of binder content in cement stabilization. Source:* (Karlsrud et al., 2013).

According to the FHWA deep mixing manual, the binder content can be calculated and therefore specified by one of two methods (Bruce et al., 2013):

- Ratio of weight of dry binder to dry weight of soil to be treated, with units in %.
- Ratio of weight of dry binder to volume of soil to be treated, with units in kg/m$^3$.

The former is the one used in the present document and every binder content value should be interpreted in that way.

### 2.5.3. Influence of curing period

A series of unconfined compression tests were performed on cement stabilized soil, using 120 kg/m$^3$ of binder content (Ignat, 2018), the results of these tests are shown in Figure 13. In the figure, it is observed that the shear strength increases with the curing period. The FHWA deep mixing manual provides a relation that allows to predict the strength increase over time using a logarithmic trend.

It states, that based on the review of data by researchers, the following equation provides a conservative estimate of the strength increase with time for cement and cement-slag treatment, excluding highly organic soils (Bruce et al., 2013):

$$q_{u\_t}/q_{u\_28d} = 0.187\ln(t) + 0.375 \quad (1)$$

In a different publication, a relation to express the increase of strength in cement stabilized soils cured at 7 °C is presented (Helen Åhnberg, 2007):

$$q_{u\_t}/q_{u\_28d} = 0.3\ln(t) \quad (2)$$

For both equations the time, $t$, is given in days, and $q_{u\_t}$ and $q_{u\_28d}$ are the unconfined compressive strengths at $t$ days and at 28 days, respectively. Both relations are compared with the strength evolution observed in the gathered data to assess which equation better represents the general behavior of all the data points for the required purpose.

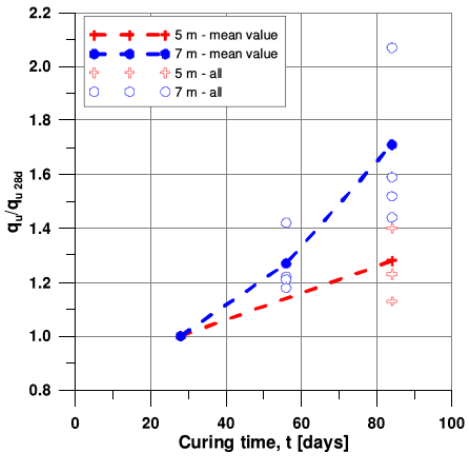


*Figure 13. Normalized unconfined compression strength versus curing time. Source:* (Ignat, 2018)

### 2.5.4. Influence of curing temperature

The influence of curing temperature is shown in Figure 14, in which two stabilized soils were cured at various temperatures up to 28 days. In the figure, the strength of stabilized soil cured at different temperatures is normalized by the strength of the stabilized soil cured at 20°C. The figure shows that the influence of curing temperature is more dominant on the short-term strength, but it becomes less dominant as the curing period increases, at the same time, it shows that larger strength can be achieved at a higher curing temperature for a given curing time.

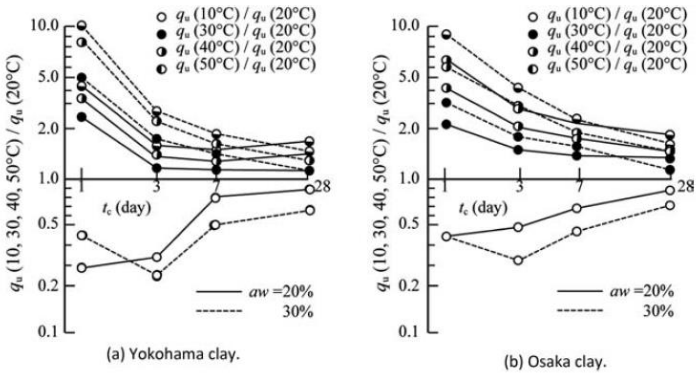


*Figure 2.37* Effects of curing temperature on strength of cement stabilized soils (Saitoh *et al.*, 1980).

*Figure 14. Effects of curing temperature in strength of cement stabilized soils. Source:* (Kitazume & Terashi, 2013).

### 2.5.5. Influence of Maturity

Maturity index is used in concrete engineering to relate the curing temperature and curing period to the strength development of samples; therefore, maturity is a concept that allows to combine the effects of time and temperature on strength gain. It has been proven that this concept is also applicable for stabilized soils, in literature, there are several equations defining the maturity index for stabilized soils, but as this research is focusing in Scandinavian soils, the equation proposed by Åhnberg and Holm in 1984 (Kitazume & Terashi, 2013) will be used and is expressed as follows:

$$M = \left(20 + 0.5 * (T_c - 20)\right)^2 * \sqrt{t_c} \qquad (3)$$

Where $M$ is the Maturity index; $T_c$ is the curing temperature [°C]; and $t_c$ is the curing period [day].

### 2.5.6. Influence of overburden pressure during curing

Soils mixed in situ are subjected to a curing overburden pressure due to the weight of the soil column during the curing period. Figure 15 shows the relationship between the unconfined compressive strength at 7 days curing with the curing overburden pressure. The figure suggests a linear relation between the two analyzed variables (Kitazume & Terashi, 2013).

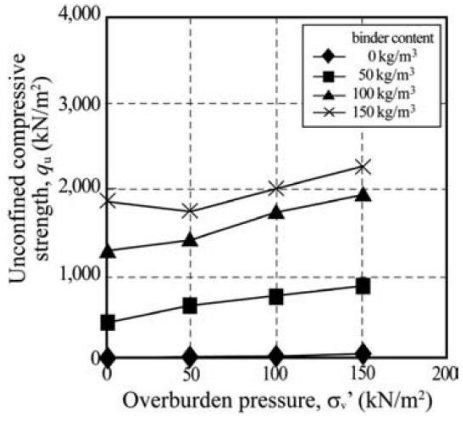


*Figure 15. Influence of overburden pressure during curing for a cement stabilized soil. Source:* (Kitazume & Terashi, 2013).

From laboratory studies, it is evident that subjecting stabilized samples to stresses during curing results in an increase in strength and an increase in quasi-preconsolidation pressure. As curing

stresses are applied, this causes compression of the samples hence allowing the cementation processes to take place with soil and binder grains arranged closer together. The increase of quasi-preconsolidation pressure has been reported to be of about 38% to 90% compared to samples cured with no external stress; the increase of the cohesion intercept, $c'$, was approximately proportional to the increase in $\sigma'_{qp}$ but the effective friction angle remained similar for samples cured with and without external stresses (Helen Åhnberg, 2007).

Increased stresses caused by load should preferably be applied in a way that produces certain compression of the material shortly after stabilization, if the load is applied with delay, the stabilized soil may have already partially hardened thus preventing significant compression and therefore inhibiting any further strength increase originated from this external pressure. When stabilizing soils under embankments, it is indeed a Swedish recommended practice to apply a load increment to the stabilized areas right after installation (Helen Åhnberg, 2007).

### 2.5.7. Differences between laboratory mixed and field mixed samples strength

It is well accepted that laboratory mixing is often more consistent than field mixing, as a result, it is expected that the strength of laboratory mixed samples is greater than the strength of field mixed materials at the same binder content. On the other hand, the effects of overburden pressure and higher curing temperature in the field tend to increase the strength of field mixed and cured materials compared to those in laboratory (Bruce et al., 2013).

According to the FHWA deep mixing manual , the strength of field mixed materials may be 20 to 100 percent of the strength of laboratory mixed samples (Bruce et al., 2013). The actual percentage depends on the quality of the mixing procedure and equipment on field and procedures used to prepare and cure laboratory specimens. It is proven that the strength of materials mixed and cured in situ can consistently achieve at least 50 percent of the strength of laboratory mixed samples.

## 2.6. Testing stabilized soil

In order to stablish the strength-strain properties of stabilized soil, tests can be performed both in field or in laboratory, with either laboratory mixed or in situ mixed specimens depending on the intended use of the soil stabilization or to industry standards. Due to the process of mixing and introducing a binder into the soil, the latter will have a different behavior than before stabilization, leading to a change in all its engineering properties. In most cases, the improvement of the undrained shear strength is the main purpose for soil stabilization, and it could be improved between 10 to 50 times its natural value (Hanson, 2012).

### 2.6.1. Laboratory testing

Laboratory tests can be performed on laboratory mixed samples, wet grab samples obtained from field or from cores of stabilized soil. It is important to understand the difference in mixing and curing conditions between the different specimens in order to compare test results in a consistent way.

#### *2.6.1.1. Unconfined compression test*

The unconfined compression test can be considered as a special case of a triaxial compression test in which no confining pressure is applied. These tests are only performed on samples which can stand without any lateral support, which is the case for stabilized soils. The test is an undrained test and is one of the simplest and quickest tests to determine the undrained shear strength.

Unconfined compression tests results are comparable to those of undrained triaxial tests at low confining pressures up to a shear strength of approximately 300 kPa (Helen Åhnberg, 2006). On the other hand, at higher strength levels, the unconfined tests yield higher strength values than the triaxial tests, therefore, it is considered that the results of unconfined compression tests for high strength may yield misleadingly high results and should be treated with caution (Helen Åhnberg, 2006), this effect is shown in Figure 16.

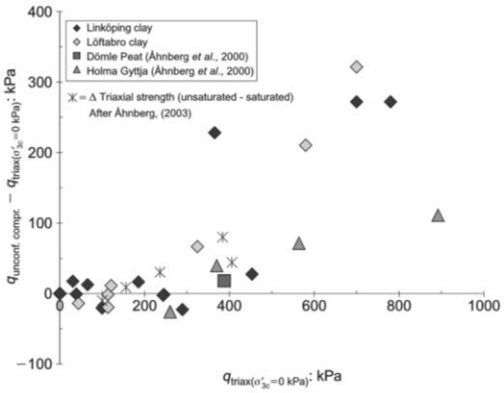


*Figure 16. Difference between compressive strength evaluated from unconfined compression tests and undrained triaxial tests. Source:* (Helen Åhnberg, 2006).

### *2.6.1.2. Triaxial test*

Triaxial test is not a common test to perform on stabilized samples in practice because it is time consuming and costly. Since this method applies a confining stress, it is expected that it offers a more accurate result of the stabilized material shear strength than the unconfined compression test. Both drained and undrained tests were performed on stabilized soils to investigate the effects of drainage and stress conditions, these tests showed that the drained and undrained strengths of stabilized materials are stress dependent, hence evidencing a behavior similar to natural clays (Helen Åhnberg, 2006). In drained tests, the strain at failure increased with the cell pressure and a peak strength suppression is evident, in the same way as in overconsolidated clays. Undrained tests showed a brittle behavior at low cell pressures with significant strength reduction after failure.

The existence of a quasi-preconsolidation pressure where yield occurs is evident in these tests, below which the stabilized soils behaved in an overconsolidated manner even though they had not been subjected to these stresses before. The stabilized soils behaves similar to overconsolidated soils when the consolidation pressure in the triaxial tests was lower than the quasi-preconsolidation pressure and in a normally consolidated manner when the opposite (Helen Åhnberg, 2007). This quasi-preconsolidation pressure or yield stress is governed by the cementation effects originated in the soil-binder reaction and is closely related to the strength of the stabilized soil. In order to determine these quasi-preconsolidation pressures or yield stresses, it is necessary to perform a series of oedometer tests on the same types of materials as those used in the triaxial tests (Helen Åhnberg, 2006, 2007).

### *2.6.1.3. Oedometer*

Oedometer tests can be performed in stabilized soils using the same procedures as for natural materials. In order to correctly perform an oedometer tests on a stabilized material, it is necessary to cure the mixture in the oedometer ring in order to allow full contact between the sample and the

ring (Hanson, 2012). Both CRS (constant rate of strain) or IL (incrementally loaded) oedometer tests can be performed on the stabilized samples to determine the quasi-preconsolidation pressure (Helen Åhnberg, 2006).

### 2.6.2. In situ testing

In early design stages, the strength of the stabilized material is tested in the laboratory using different types of binder and binder contents. The FHWA deep mixing manual strongly suggests to also perform full scale tests to assess the behavior of the stabilized soil in the field curing conditions, quality of mixing and field stress state of the material (Bruce et al., 2013). To measure the strength of the stabilized material there are different in situ tests that could be performed depending on availability and cost, the ones considered the most important are listed and explained below.

#### *2.6.2.1. KPS (push-in resistance test)*

One of the most commonly used methods to assess in-situ DSM column strength is the push-in resistance test (PIRT) or, in Swedish, Kalk-Pelar-Sondering (KPS). It is an in-situ test in which a winged penetrometer is advanced into the stabilized soil at a constant rate and the force-depth profile recorded, the Swedish Transport Administration (Trafikverket) offers suggested dimensions for the KPS probe (Trafikverket, 2011), a scheme and a picture of the probe can be observed in Figure 17.

The KPS offers some advantages over the most widely used CPT. While the CPT only probes a point location that will most likely follow the weak path of the stabilized soil, in the case of the KPS, a chord of the columns is tested, allowing to investigate more material at a time, feature that is of great importance due to the high variability of the stabilized soil (Timoney & McCabe, 2017).

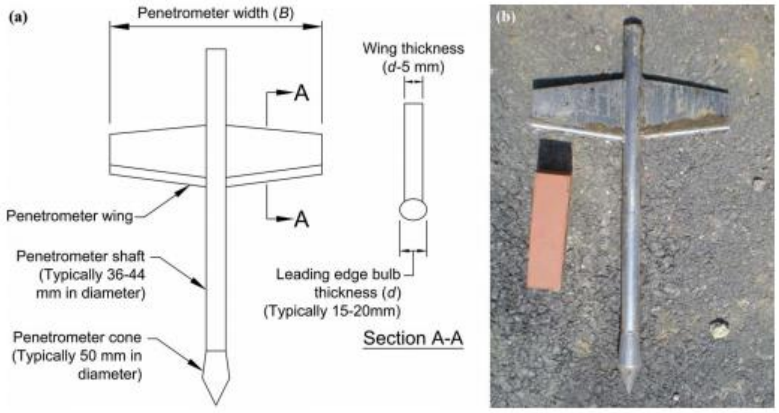


*Figure 17. Typical PIRT (KPS) penetrometer: (a) guideline dimensions (modified from* (Trafikverket, 2011)*) and (b) 400 mm PIRT penetrometer. Source:* (Timoney & McCabe, 2017)*.*

#### *2.6.2.2. FOPS (pull-out resistance test)*

Similar to the KPS, the Pull-Out Resistance Test (PORT) or, in Swedish, Förinstallerad Omvänd Pelar Sondering (FOPS), a winged probe is used to directly measure the resistance of the stabilized soil. In this case the blade is installed at the bottom of the improved soil column at the beginning of the mixing process and is pulled using a steel cable (Liyapathirana & Kelly, 2010). The probe has, in essence, the same shape as the one used in the KPS, but with the round edge of the wing placed in the top end, a scheme of the FOPS probe can be observed in Figure 18.

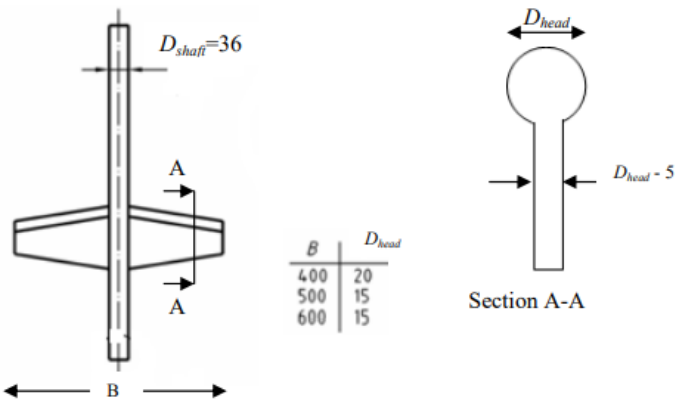


*Figure 18. Lime column probe used for PORT (FOPS) and cross section of the blade, dimensions in mm. Source:* (Liyapathirana & Kelly, 2010).

#### *2.6.2.3. CPT (cone penetration test)*

The Cone Penetration Test (CPT) is originally a method used to determine the soil properties and its stratigraphy. It is also used in quality control tests on stabilized soils and its results are comparable to those of KPS or FOPS (Hanson, 2012), allowing to measure the column shear strength and its homogeneity. Due to the high strength of the stabilized material, the CPT probe could be dragged out of the DSM column into the softer natural soil, a behavior also observed in the KPS and FOPS probes.

#### *2.6.2.4. Core sampling*

Core sampling could be used in nearly any situation to extract specimens from stabilized soil. Unlike the penetration methods, the coring bit allows the test verticality to be maintained despite the column strength and provides cylindrical specimens for unconfined compression tests or triaxial tests.

#### *2.6.2.5. PMT (pressuremeter Ménard test)*

The Pressuremeter Ménard Test (PMT) was introduced by Ménard in 1955 and it is a device that is placed in a borehole with a dilatable probe that is inflated and allows to relate the pressure applied for its expansion to a measure of soil deformation (Monnet, 2015). The test can determine the soil shear deformation modulus ($E_M$) and the limit pressure, which can be linked to soil shear resistance.

#### *2.6.2.6. Full column test*

Tests on whole single columns could be performed by installing a wire with a plate at the bottom of the column and applying a tension or by applying pressure on the top of the column similar to a plate load test, it has been proven that between both implementation there is no significant difference in the results (S Baker, Sällfors, & Alén, 2005).

## 2.7. Dimensioning

### 2.7.1. Undrained shear strength of stabilized soil

#### *2.7.1.1. Comparison between Triaxial and Unconfined Compression tests*

Results from unconfined compression tests show similar results to those of triaxial tests performed at low confining stresses, or when extrapolating results to a zero-confining stress. From section 2.6.1.1, however, it is observed that as the strength of the materials increase, the strength values

determined by means of unconfined compression tests became higher than those determined from triaxial tests, results remained consisted up to about 300 kPa, but when this value is surpassed, the consistency of the results disappeared (Helen Åhnberg, 2006).

#### *2.7.1.2. Stress dependence of the undrained strength*

In general, results from different undrained triaxial tests evidence a consolidation stress dependence. Nevertheless, scatter in some of the individual series of results make the evaluation of the magnitude of the stress dependence somewhat uncertain. The increase of strength seems to vary with the investigated stress interval and with the presence of organic matter in the soil (Helen Åhnberg, 2006).

As stated in section 2.6.1.2, to describe the stress dependence of stabilized material, an approach similar to the one used with natural clays is implemented. The stabilized soils behave similarly to overconsolidated soils and the existence of a quasi-preconsolidation pressure where yielding occurred is evident, pressure below which the improved soil behave in an overconsolidated manner even though it has not ever been subjected to these pressures earlier.

The influence of the stress level on the undrained strength was investigated by normalizing the latter to the vertical stress after consolidation, $q_u/\sigma'_{1c}$, and comparing with the ratio $\sigma'_{qp}/\sigma'_{1c}$; the results of this comparison can be observed in Figure 19. Samples consolidated at stresses higher than the quasi-preconsolidation pressure in the triaxial cell, are regarded as normally consolidated and are of low strength mainly because of a short curing time or for being stabilized with ineffective binders. According to the data presented in Figure 19, the unconfined compressive strength of the overconsolidated samples can be expressed as:

$$q_u = a \cdot \sigma'_{1c} \cdot \left(\sigma'_{qp}/\sigma'_{1c}\right)^b \qquad (4)$$

Where $a$ and $b$ are constants with values of 1.02 and 0.88 respectively. It is also observed that for the normally consolidated samples, the normalized strength ratio, $q_u/\sigma'_{1c}$, remained fairly constant at a value of 0.98.

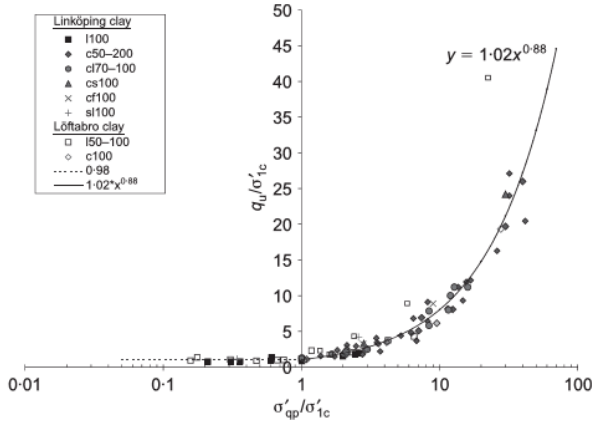


*Figure 19. Normalized undrained compressive strength at different overconsolidation ratio. Abbreviations represent binder type: c, cement; l, lime; f, fly ash; s, slag; quantity kg/m³. Source:* (Helen Åhnberg, 2006).

Figure 20 shows measured undrained strengths together with calculated strengths at different quasi-preconsolidation pressures for $a = 1.02$ and $b = 0.88$. As expected with stabilized soils, a

large scatter is encountered in the measured results, but the general trend of the calculated strength-stress curves if followed by the measured data. However, the stress dependence at low confining stresses is still not well understood. For low consolidation stresses, some of the test series show significantly low strength, whereas others indicate constant or even increased strength at these low stresses, as mentioned in section 2.6.1.1.

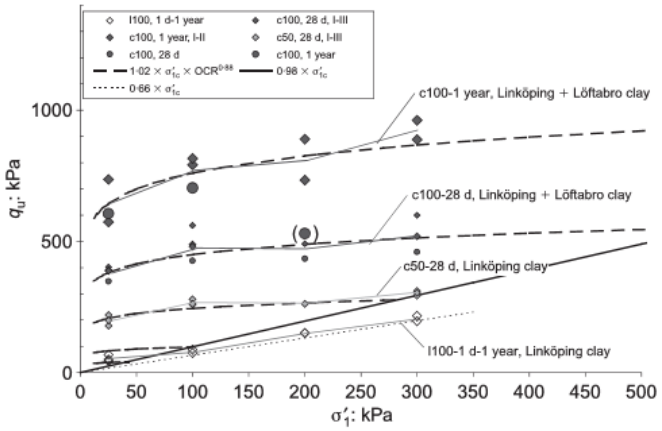


*Figure 20. Estimated undrained compressive strength at different strength levels together with examples of measured strength. Abbreviations represent binder type: c, cement; l, lime; f, fly ash; s, slag; quantity kg/m³. Source:* (Helen Åhnberg, 2006).

The vertical yield stresses or quasi-preconsolidation pressure have a great influence on the strength behavior of stabilized soils and can be evaluated from oedometer tests, as stated in section 2.6.1.3. The undrained strength can be considered dependent on the quasi-preconsolidation pressure and the overconsolidation ratio of the stabilized soils, in other terms, the location of the yield locus and its distance from the stresses before the start of undrained shearing. The unconfined compression strength is found to increase with the quasi-preconsolidation pressure with the approximate relation being (Helen Åhnberg, 2006):

$$\sigma'_{qp} = 1.34 q_u \qquad (5)$$

### 2.7.2. Drained strength of stabilized material

Drained triaxial test results also show stress dependence regardless of soil type or added binder and this dependence remained fairly the same for the investigated stress levels. This fairly similar stress dependence can be observed when comparing the obtained effective friction angles ($\phi'$) from the drained tests, these results can be observed in Figure 21. Moreover, no significant change in the effective friction angle was observed regardless the cohesion intercept ($c'$) value (Helen Åhnberg, 2006).

The mean magnitude of the measured effective friction angle is 33°, and even though the values varied from 26° to 38°, which is a relatively wide range, most of the test were performed as single tests and the expected scatter in the results may affect the effective friction angle determination (Helen Åhnberg, 2007). It is also relevant to mention that there is a tendency for a curvature in the strength envelopes, similar to what is observed in the undrained case in section 2.7.1.2, thus indicating a decrease in friction angle and an increase in cohesion intercept with increasing stress

level, depicted in Figure 22. This shows a decreasing dilatancy effect with increasing stress level that affects the friction angle, similar to natural soils.

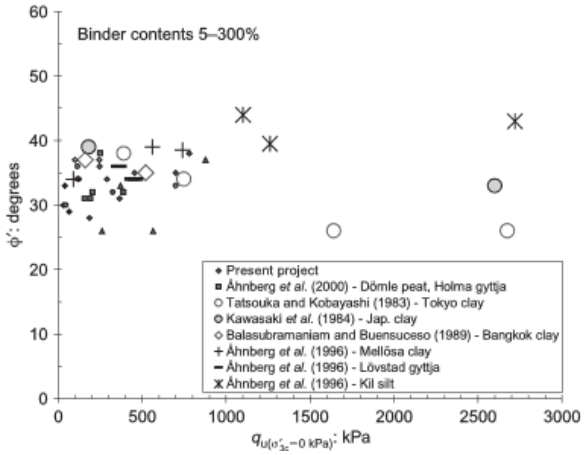


*Figure 21. Evaluated friction angle against undrained compressive strength level for different locations. Source:* (Helen Åhnberg, 2006).

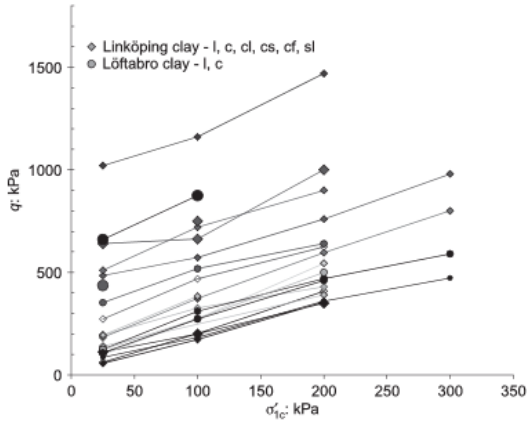


*Figure 22. Measured drained strength at failure against consolidation pressure. Abbreviations represent binder type: c, cement; l, lime; f, fly ash; s, slag. Source:* (Helen Åhnberg, 2006).

In contrast to the behavior observed in the variation of the effective friction angle, the evaluated cohesion intercept had a much considerable variation with curing time and type of binder. It increased with time following a similar trend to that of the undrained strength; the mean value of the cohesion intercept was approximately 0.23 of the unconfined compressive strength at zero effective cell pressure, estimated from extrapolation of results from triaxial tests ($q_{u(\sigma'_{3c=0})}$), while the individual relation varied between 0.12 and 0.33 (Helen Åhnberg, 2006, 2007).

Due to the individual variation of the effective friction angle, it is necessary to compare the evolution of the cohesion intercept and $q_{u(\sigma'_{3c=0})}$, this relation can be observed in Figure 23; it can also be observed that the strength ratio $c'/q_{u(\sigma'_{3c=0})}$ levels off towards a value in the order of 0.15 to 0.20 for the high strength samples. At lower confining stresses, where the overconsolidation ratio is high, the drained strength should be considered for design (Helen Åhnberg, 2006).

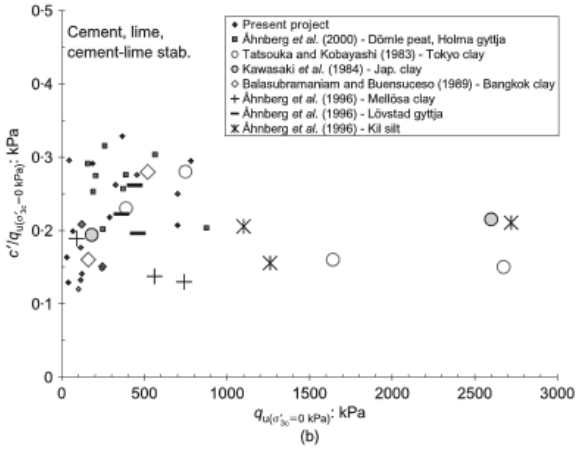


*Figure 23. Effective strength ratio against undrained strength evaluated in the present project and from data reported in earlier investigations. Source:* (Helen Åhnberg, 2006).

### 2.7.3. Measured effective stress paths in the various types of stabilized soils

Results of triaxial testing showed that the stabilized soils behave, in general, in an overconsolidated and a normally consolidated manner when the consolidation stress used in the triaxial tests was lower or higher than the quasi-preconsolidation pressure, respectively; as stated in section 2.6.1.2. The yielding model proposed by Larsson in 1977 for natural clays was found to be applicable to the stabilized soils (Helen Åhnberg, 2007). In this model, the limit state curves are schematically given as four segments, two of which correspond to the failure strength envelopes in compression and extension, and two of which correspond to $\sigma'_v = \sigma'_{vc}$ and $\sigma'_h = K_{0NC} \cdot \sigma'_{vc}$ (Larsson, 1977). Where $\sigma'_v$ is the vertical effective stress; $\sigma'_{vc}$ is the vertical effective consolidation stress; $\sigma'_h$ is the horizontal effective stress; and $K_{0NC}$ is the coefficient of earth pressure for normally consolidated soil.

The use of the former model to analyze results of stabilized soils is demonstrated in Figure 24 with the dashed lines, where results from active and passive tests performed on Linköping clay stabilized with lime-cement at a quantity of 70 kg/m$^3$ are shown. The evaluated effective stress parameters in the passive tests are of the same order as the values found for active tests (Helen Åhnberg, 2007). For the samples shown in Figure 24, an approximately isotropic yield surface could be adopted, meaning that the $K_{0NC}$ value is close to one.

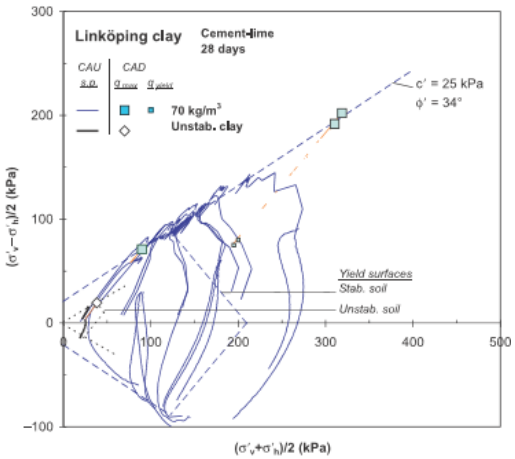


*Figure 24. Measured stress paths in the s'-t stress plane in active and passive triaxial tests on stabilized and unstabilized Linköping clay. Source:* (Helen Åhnberg, 2007).

From the results, it is evident that the quasi-preconsolidation pressure affects the stress paths to a high degree and is closely associated with the undrained strength of the stabilized soils. The stress paths can be normalized to the quasi-preconsolidation pressure in order to further investigate its influence, this can be observed in Figure 25; it is seen that the different soil samples all follow a common pattern, with a cohesion intercept of approximately 0.12 to 0.24 the quasi-preconsolidation pressure and an effective friction angle between 33° and 34°. If Equation (5), from section 2.7.1.2, which relates the peak strength from the triaxial tests, $q_u$, and the quasi-preconsolidation pressure, $\sigma'_{qp}$, , is combined with the relation between the cohesion intercept and the quasi-preconsolidation pressure, a direct relation between the peak strength and the cohesion intercept can be made:

$$c' = (0.10\ to\ 0.24) \cdot 1.34 \cdot q_u = (0.13\ to\ 0.33) \cdot q_u \qquad (6)$$

Equation (6) shows a good agreement with earlier studies conducted also on stabilized materials (Helen Åhnberg, 2006; Ignat, 2015) which presented values between 0.18 and 0.25. The compressive strength varies from approximately $0.6\sigma'_{qp}$ for highly overconsolidated samples to $1.0\sigma'_{qp}$ for normally consolidated samples (Helen Åhnberg, 2007). In the case where the consolidation stresses applied in the triaxial test where higher than the quasi-preconsolidation pressure, the specimens are considered to be normally consolidated and are expressed as dashed lines in Figure 25.

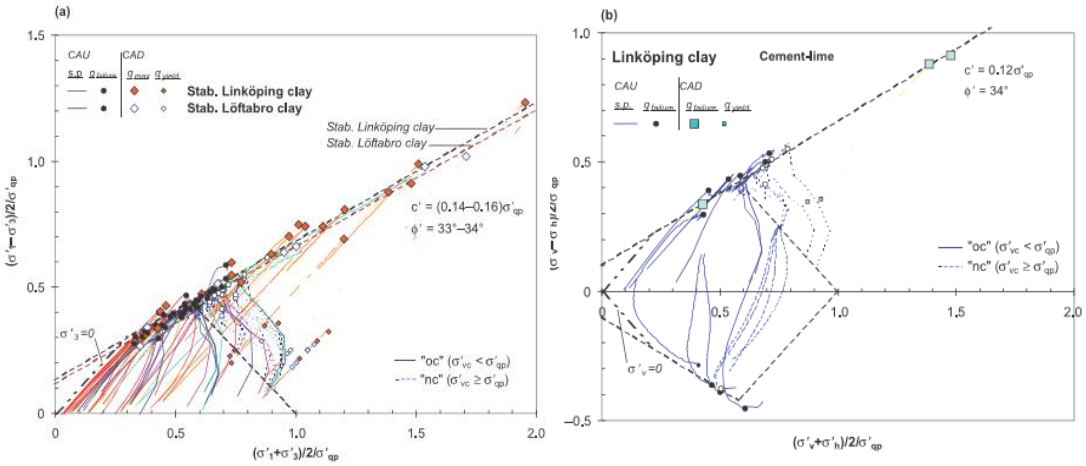


*Figure 25. Measured stress paths normalized to the quasi-preconsolidation pressures in the s'-t stress plane in (a) triaxial compression tests on stabilized Linköping and Löftabro clay, and (b) triaxial compression and extension tests on cement-lime stabilized Linköping clay. Source:* (Helen Åhnberg, 2007).

The stabilized material is considered to be of an isotropic nature, meaning that its natural $K_{0NC}$ would tend to the unity and both active and passive tests should have similar behavior. Nevertheless, as observed in Figure 25, when consolidated to a $K_{0NC}$ of around 0.5, this condition affects the outcome, but the effect of cementation has a greater impact on the results, therefore constraining the reduction of the apparent $K_{0NC}$ to approximately 0.85. As expressed in section 2.5.6, the shear strength of the stabilized material can be increased by applying an overburden pressure shortly after mixing, but it has also been found that the $K_{0NC}$ is also affected to some extend (Helen Åhnberg, 2007).

Results for triaxial tests on samples cured with and without stresses are shown in Figure 26 It is important to note that as the curing stresses were below the yield locus of the samples cured with no stresses and that a $K_0$ of 0.5 was used during this process, the expected results would be a corresponding ratio for vertical and horizontal yield stresses, but this was not the case (Helen Åhnberg, 2007). Even though a 0.5 relation was not obtained for the yield stresses, the used $K_0$ value for curing had an influence in the general behavior of the stabilized specimens. It is observed in Figure 26 that as the curing stress is increased, the ratio between the horizontal and vertical yield stress reduces.

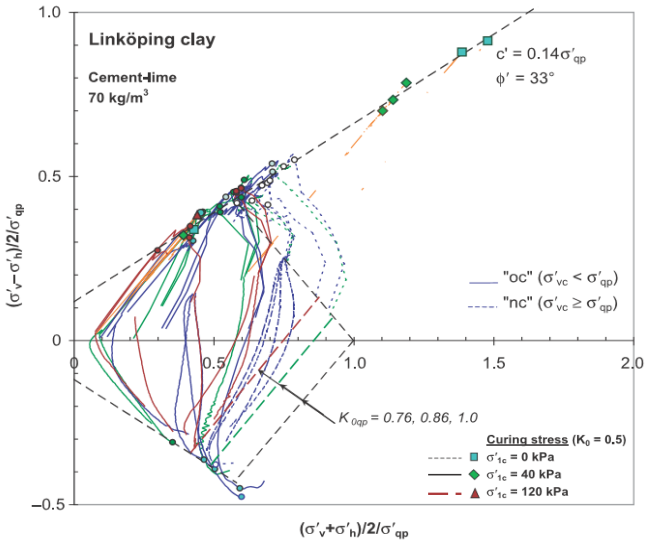


*Figure 26. Normalized measured stress paths to the quasi-preconsolidation pressure in the s'-t stress plane for cement-lime stabilized Linköping clay subjected to different curing stresses after mixing. Source:* (Helen Åhnberg, 2007)

### 2.7.4. Stiffness of stabilized soil

The secant modulus of elasticity, $E_{50}$, is defined as the slope of the line extending from the origin of the stress-strain plot to the point corresponding to half the maximum measured stress. The value of $E_{50}$ is frequently used as the Young's modulus of the stabilized material (Navin & Filz, 2005) and earlier studies have proposed values based on laboratory results (Helen Åhnberg et al., 1995; Sadek Baker, 2000; Ignat, 2015; Löfroth, 2005; Navin & Filz, 2005; Terashi, 2005; Trafikverket, 2011), which are presented in Table 2.

*Table 2. Proposed values for the Young's modulus over peak strength ratio. Source: own elaboration.*

| $E_{50}/q_u$ | Test | Source |
|---|---|---|
| **200** | Unconfined compression | (Terashi, 2005) |
| **190 to 200** | Triaxial | (Löfroth, 2005) |
| **250 to 300** | Unconfined compression | (Navin & Filz, 2005) |
| **44 to 92** | Unconfined compression | (Ignat, 2015) |
| **56 to 185** | Triaxial | (Ignat, 2015) |
| **50 to 200** | Triaxial | (Sadek Baker, 2000) |
| **50 to 200** | Triaxial | (Helen Åhnberg et al., 1995) |
| **250** | - | (Trafikverket, 2011) |

### 2.7.5. Horizontal strength and stiffness of stabilized soil

A laboratory study in which cores of stabilized material were extracted from block samples in both vertical and horizontal directions was performed (Hanson, 2012). The measured strength and stiffness properties are presented in Figure 27. From the measured values of strength and stiffness, it is possible to draw four conclusions:

- Vertical and horizontal strength of cored samples is virtually the same (Hanson, 2012).
- It does not appear that there is any difference in measured shear stress in drained and undrained condition for the same confining pressure (Hanson, 2012).

- The horizontal Young's modulus is slightly higher than the vertical.
- It appears that there is a limit in strength increase with increasing confining pressure.

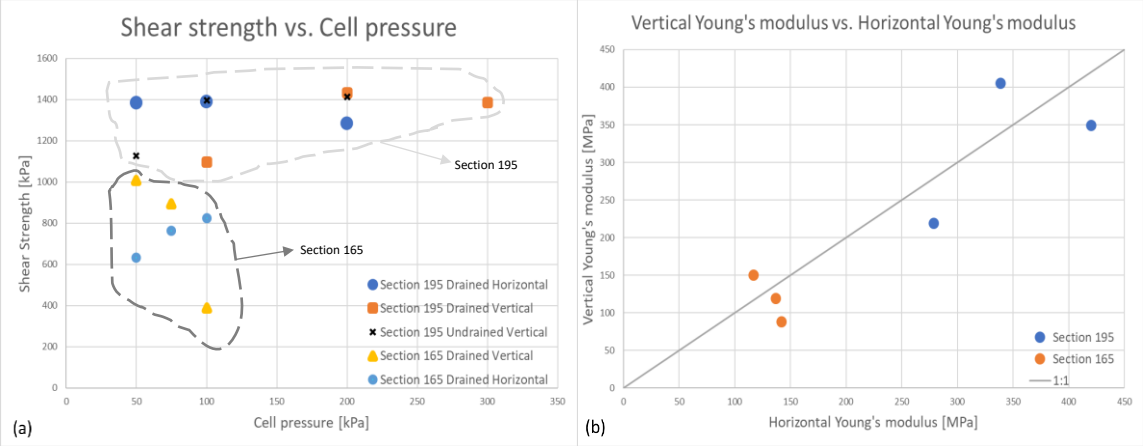


*Figure 27. (a) Shear strength vs. Cell pressure; and (b) vertical vs. horizontal Young's modulus of sections which had both vertical and horizontal core samples. Source: own elaboration from* (Hanson, 2012).

### 2.7.6. Design strength

The Swedish design guideline proposes a deterministic approach for calculating the design values and restricts the strength property values that can be used in design for the specific case of stabilized soils depending on the loading condition, as stated in section 2.4.1. For the case in which the stabilized soil is placed in the passive zone of an excavation, which is of most interest for the present research, it establishes differences and upper limit values for both the drained and undrained parameters that could be used for design (Trafikverket, 2011), namely:

- Drained loading condition:

$$Cohesion\ intercept\colon\ c' = 0\ kPa$$

$$Effective\ friction\ angle\colon\ \phi = 32\ ^\circ\ (for\ stabilized\ clays)$$

- Undrained loading condition:

$$Maximum\ undrained\ shear\ strength\colon\ s_u = 100\ kPa$$

$$Calculated\ as\colon\ s_u = s_{u,failure}/1.4$$

The Dutch design methodology proposes a reliability-based approach for calculating the design values for both ULS (Ultimate Limit State) and SLS (Serviceability Limit State) depending on the property statistics. A characteristic or representative value is defined, which is the value that offers a 95 % reliability in the lower limit for strength properties (CUR, 2008):

$$X_{gem;rep} = X_{gem} \cdot (1 - 1.65 \cdot V) \tag{7}$$

Where $X_{gem;rep}$ is the characteristic or representative value of the property $X$; $X_{gem}$ is the mean value of the property $X$; and $V$ is the coefficient of variation of the property $X$.

The design recommendation proposes an alternative way of calculating the representative value which is influenced by the number of tests performed to determine parameter $X$ and by using the Student-t distribution and usually yields higher values:

$$X_{gem;rep} = X_{gem} \cdot (1 - t_{0.05} \cdot V \cdot \sqrt{1/n}) \quad (8)$$

Where $t_{0.05}$ is the factor that according to the Student-t distribution gives a 5 % chance of occurring as a function of the number of observations; and $n$ is the number of observations.

The design value of a property $X$ can be calculated both from the $X_{gem}$ or the $X_{gem;rep}$, being the determination from the latter the most common:

$$X_d = X_{gem} \cdot (1 - \alpha\beta V) \quad (9)$$

$$X_d = X_{gem;rep}/\gamma_m \quad (10)$$

Where $X_d$ is the design value; $\alpha$ is the influence coefficient of property $X$; $\beta$ is the reliability index; and $\gamma_m$ is the partial material safety factor for parameter $X$. It has to be noted that both $\beta$ and $\gamma_m$ can be obtained from design tables depending on the building conditions in order to calculate the required design strength. From Equation (7), Equation (9) and Equation (10) $\gamma_m$ can be computed as the ratio of the representative over the design strength:

$$\gamma_m = \frac{X_{gem;rep}}{X_d} = \frac{(1 - 1.65 \cdot V)}{(1 - \alpha\beta V)} \quad (11)$$

### 2.7.7. Composite material approach

The current Swedish dimensioning method considers the columns of stabilized soil and the natural soil surrounding them as a composite material (Trafikverket, 2011). It is assumed that the peak shear strength of the columns is mobilized at the same time as the peak shear strength of the natural soil between the columns, meaning that there is a complete interaction between improved and natural soil (Charbit, 2009). A weighted average approach of the undrained shear strength is then applied to obtain the composite value of this parameter:

$$s_{u,comp} = s_{u,col} \cdot a + s_{u,soil} \cdot (1 - a) \quad (12)$$

Where $s_{u,comp}$, $s_{u,col}$ and $s_{u,soil}$ are the composite, stabilized and natural soil undrained shear strength; and $a$ is the area replacement ratio, which is the ratio of the improved area over the total area in the assessment.

Kitasume and Terashi (2013) proposed a modification of this weighted average approach presented in Equation (12) to include the cases in which the axial strain at failure of the stabilized soil is smaller than that of the natural soil, behavior that can be observed in Figure 28. In this specific case, the shear strength of the original soil is considered not fully mobilized at failure, behavior that could be incorporated in the equation by introducing a mobilization factor $k$, which is the ratio of the

undrained shear strength of soft soil mobilized at the peak shear strength of stabilized soil and the undrained shear strength of the soil.

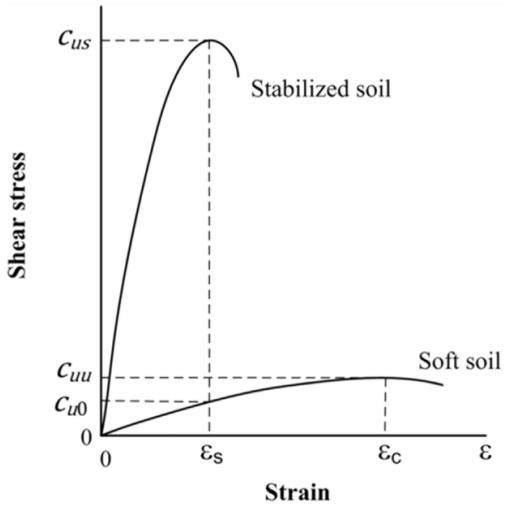


*Figure 28. Typical stress-strain curves for stabilized soil and natural soft soil. Source:* (Kitazume & Terashi, 2013).

After testing cement stabilized soil columns installed in different patterns in a large simple shear apparatus, the $k$ factor was found to remain in values between 0.90 to 0.97, thus a new correction factor, $f$, is proposed and included in Equation (12) to apply a reduction in the stabilized soil shear strength depending on the installation pattern (Sukpunya & Jotisankasa, 2016). The equation to calculate the composite shear strength, including both correction factors, can be written as:

$$s_{u,comp} = f \cdot s_{u,col} \cdot a + s_{u,soil} \cdot (1 - a) \cdot k \quad (13)$$

The present project focuses on improved soil columns installed in the passive zone of an excavation, therefore, the definition of the $f$ factor should be selected to match this installation pattern, which is similar to the mentioned longitudinal tangent wall pattern in the laboratory study (Sukpunya & Jotisankasa, 2016):

$$f = 0.0661 \cdot s_{u,soil} - 0.0695 \quad (14)$$

The determination of the mobilization factor seems to be a simple task, fulfilled by just comparing the stress-strain results of both the stabilized and the natural soil. Nevertheless, results from full-scale tests in which cement stabilized soil column walls, also called ribs, where installed as bottom struts in a shallow excavation, showed that the interaction between improved and natural soil depends on the rib-to-rib distance (Ignat, Baker, Liedberg, & Larsson, 2016). Therefore, more careful analysis of the $k$ factor should be made.

In the present research, the same set of weighted average equations will be used to calculate the composite stiffness properties as well as drained properties such as cohesion intercept and the internal friction angle of the composite material on account of the fact that on an earlier study this method was used (Andromalos, Hegazy, & Jasperse, 2001), the validity for this application will be contrasted with the limits set by the Swedish design guidelines and results of a full-scale test performed in an earlier study (Ignat et al., 2016).

# 3. DATA GATHERING AND CLASSIFICATION

## 3.1. Methodology

The currently available literature on deep soil mixing is abundant with research made all over the world with a special focus in regions such as North America, Scandinavian countries and Japan. However, the present study will focus on Scandinavian soils, mainly because of the information available. A literature study was performed to collect information from scientific publications including natural soil index and strength properties as well as strength and stiffness properties of stabilized soil. Besides the scientific information available, data from two locations of the West Link project in Gothenburg were provided in order to analyze it and compare with earlier studies. A total of 288 data points were collected from 9 different sites, the sites names and information precedence can be found in Table 3.

*Table 3. Sites and sources of the available information. Source: own elaboration.*

| Site | Source |
|---|---|
| **Enköping, Sweden** | (Ignat, 2015, 2018; Ignat et al., 2016) |
| **Gothenburg, Sweden** | West Link Project |
| **Linköping, Sweden** | (H. Åhnberg & Johansson, 2005; Helen Åhnberg, 2006, 2007) |
| **Löftabro, Sweden** | (H. Åhnberg & Johansson, 2005; Helen Åhnberg, 2006, 2007) |
| **Møllenberg, Trondheim, Norway** | (Hanson, 2012; Karlsrud et al., 2013) |
| **Schweigaardsgate, Oslo, Norway** | (Karlsrud et al., 2013) |
| **Trafikverket study** | (Trafikverket, 2011) |
| **Skøyen, Oslo, Norway** | (Karlsrud et al., 2013) |
| **Gothenburg, Sweden** | (Jonsson, 2017) |

Regarding the stabilized soil properties, the measured parameter of most importance for the present study is the shear strength since it is the most widely studied and can be also used to estimate stiffness properties. Two obstacles had to be overcome before being able to properly compare measured properties; first, the different curing temperature conditions that the stabilized specimens had; and second, the different curing times at which the samples were tested. To solve these issues, the concept of Maturity and Equation (1) from section 2.5.3 are used; the process is explained in section 3.1.1.

This step is of great importance because it will allow to better understand the influence of different natural soil properties in the final behavior of the improved material, besides, it will show the importance of the different soil conditions of every site when predicting the expected strength gain of the improved soil. Collected data includes information from both laboratory and field mixed samples with a variety of curing conditions and tested using most of the tests described in sections 2.6.1 and 2.6.2, therefore, a conclusion can be drawn regarding the influence of mixing and testing conditions. Also, at the site of Enköping, Sweden, a full-scale test was performed alongside with the laboratory study, therefore a more thorough analysis of the system response can be obtained, this is addressed in section 4.

From the available data, it is aimed to produce a mathematical expression that could allow estimating the undrained shear strength obtained from unconfined compression tests of improved soil using as input parameters the introduced binder content and the most relevant soil properties. The selection of the most relevant soil properties as well of the most suitable mathematical expression that could represent the available data and the expected behavior is presented in section 3.1.2 and 3.2.2.

### 3.1.1. Strength equivalence using the concept of Maturity

In order to compare results from different authors research, it was necessary to find a consistent way to evaluate the strength measurements in a common scale, for this purpose, the maturity index is used. The maturity index is a concept that allows creating an equivalency between curing temperature and curing time; Equation (3) introduced in section 2.5.5, is used to find the time equivalency between 7 °C and 20 °C, which are the common temperatures in which stabilized soil is cured in laboratory conditions. Figure 29 shows the plot of Equation (3) for 7°C and 20°C for varying curing ages, the Maturity concept allows to establish an equivalency of maturity or strength gain when the Maturity index values are the same for two given curing times, this equivalency is expressed with the horizontal line in the graph and it can be done for any desired value of curing time. To simplify the process, several equivalent times are presented in Table 4.

*Table 4. Curing days equivalence using the Maturity Index between 7 °C and 20 °C. Source: own elaboration.*

| Age 7 °C [days] | Age 20 °C [days] |
|---:|---:|
| 14 | 3 |
| 21 | 5 |
| 28 | 7 |
| 67 | 14 |
| 140 | 28 |
| 270 | 56 |
| 400 | 84 |
| 500 | 100 |

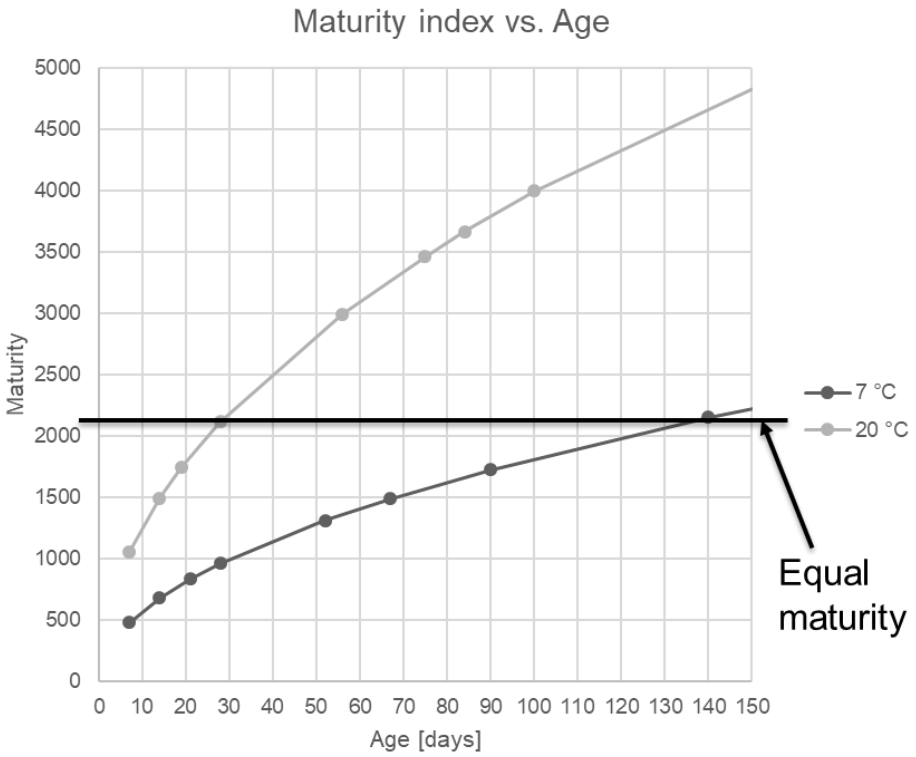


*Figure 29. Maturity index vs. Age for 7 °C and 20 °C. Source: own elaboration.*

Even though a time equivalency exists when curing temperatures are different, there is still the inconvenience that most of the data is not referred to a measured strength at a given curing period; in the present research, the measured 28-day strength with curing temperature of 20 °C is selected for comparison. It is then of importance finding a method to refer measurements at any given day to the selected criteria. To overcome this issue, a relation between measured shear strength at a given time with the 28-day shear strength has to be used; indeed, section 2.5.3 introduces Equation (1) and Equation (2) allowing to perform such estimations, but it is not well known whether any of those two relations would fit the behavior of the gathered data.

To assess the validity of Equation (1) and Equation (2), all the data is plotted alongside both equations. It is important to note that for each data series, their own equation of strength improvement was obtained by means of a logarithmic trendline using MS Excel, due to the fact that both Equation (1) and Equation (2) define the fraction between a strength at a given day over the 28-day strength. For all the samples that were cured at 7 °C, their measured value was associated now with an equivalent time at 20 °C by using the Maturity concept and an extended version of Table 4.

Figure 30 shows the result of the abovementioned process. Figure 30 shows a great scatter in the data, nonetheless, what is of great interest for the investigation is the general trend followed by the values, in order to use either equation for data interpretation. It is considered that Equation (1) better reflects the general trend presented in the plot and also has the added value that for strength estimation for curing periods of more than 28 days, offers a lower value than Equation (2). Figure 31 shows in a scatter plot, the average for each measured strength at a given curing time alongside a plot of Equation (1) with the corresponding error bars.

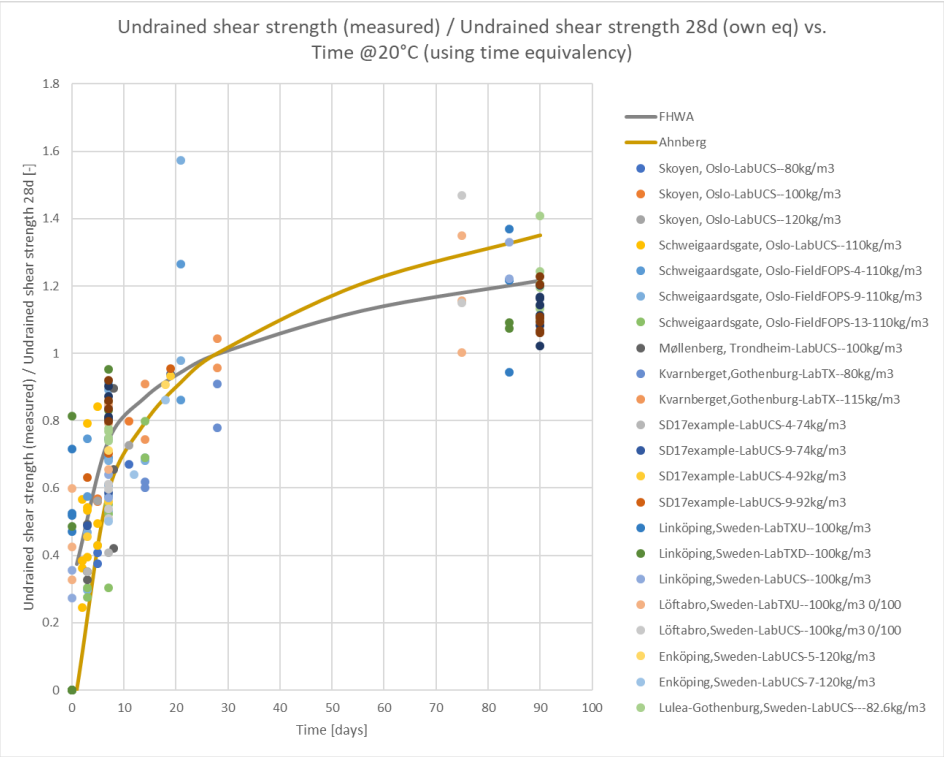


*Figure 30. Ratio of measured undrained strength of the stabilized soil over the 28-day strength calculated with their own strength development equation vs. curing time referred to 20 °C. Source: own elaboration.*

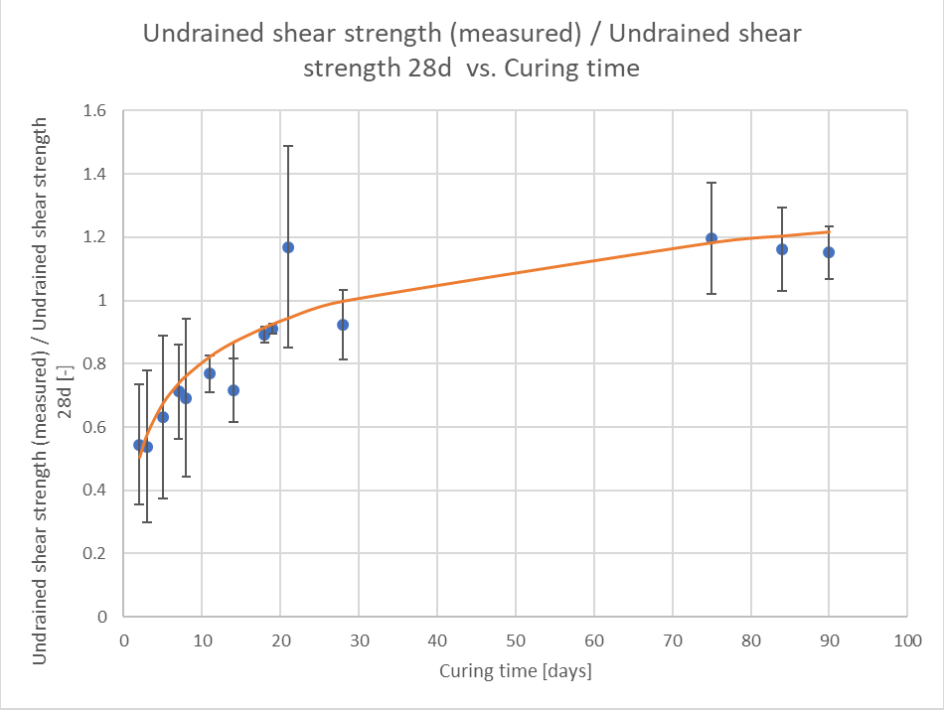


*Figure 31. Average, for each curing day period, of the undrained strength (scatter plot); FHWA equation with corresponding error bars. Source: own elaboration.*

The process of reaching a shear strength equivalence using the concept of maturity and Equation (1) is depicted in Figure 32 and is based on the time equivalence at 28 days of a sample cured at 20 °C, which in 7 °C curing temperature would mean a curing time of 140 days. Table 4 was built by setting the temperature as a fixed value while varying the curing time and then comparing the Maturity Index values. The curing time in which the Maturity Index values are the same at the two given temperatures, the equivalence is confirmed.

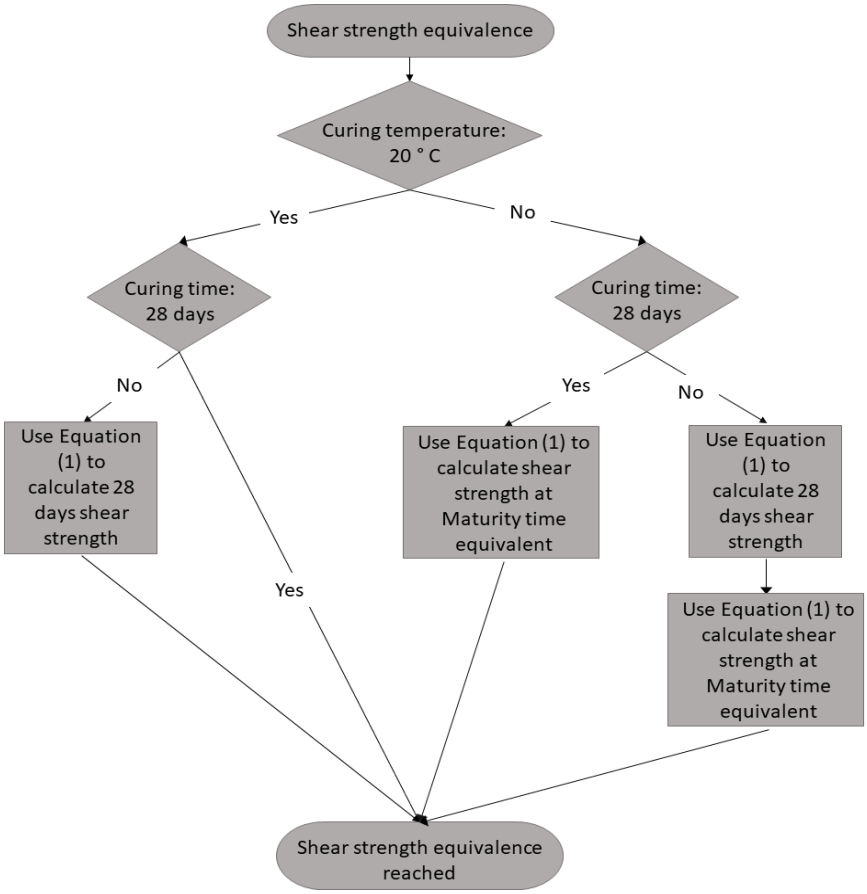


*Figure 32. Flowchart of the process to determine the shear strength equivalence using the Maturity Index. Source: own elaboration.*

### 3.1.2. Estimation of the improved undrained shear strength

In section 1.2 it was stated as one of the research questions if it was possible to estimate in any degree the expected undrained shear strength of the investigated soils by only using the natural soil properties and the introduced binder content. In order to answer the proposed research question, all the available data was condensed and compared using different graphs, firstly per site and secondly among sites in order to investigate if any common trend could be observed. In this step, the natural soil properties that were not considered to have an influence were not used for the expression that estimates the improved undrained shear strength.

The goal is to generate an expression that could estimate or predict the undrained shear strength of any soil for the Scandinavian countries and that would properly adjust to the data available. One

of the aspects to take into account is that not only data from different sites is available, but also among sites, different binder ratios were used for the samples, therefore it was decided to analyze separately the data from each binder ratio available because the magnitude of the improved undrained shear strength depends highly on the binder content and the binder ratio used.

## 3.2. Results

In the present section, all the gathered data will be analyzed site by site and considering the information from both natural and improved soil properties to obtain trends and compare between sites and testing methods. For each subsection, the reported natural soil properties are presented first and then the improved soil properties. It is important to note that in some cases, not all the index properties of the soils were available, a fact that is not well understood because when investigating soil, the index properties are of great importance, this presented a difficulty to compare the sites. It has to be pointed out the high variability present in the measured improved shear strength per site and for a given binder content, this fact has been analyzed previously with reported coefficient of variation typically ranging from 0.30 to 0.60 but values as low as 0.15 and as high as 1.35 have also been found (Navin & Filz, 2005).

### 3.2.1. Gathered data per site

#### *3.2.1.1. Enköping, Sweden*

The natural soil properties for Enköping are presented in Table 5. The reported improved soil data is from unconfined compression tests from laboratory mixed and tested samples. Figure 33 shows the improved shear strength of the laboratory mixed samples from the Enköping site. It appears to be a relation between the natural soil depth; hence the natural shear strength and the strength increase when a binder is introduced to the soil. Besides, it appears to be no difference between compression and extension triaxial tests results.

*Table 5. Soil properties of Enköping Sweden. Source:* (Ignat et al., 2016).

| **Depth [m]** | **Unit weight [kN/m3]** | **Water content, w [%]** | **Liquid limit, LL [%]** | **Sensitivity, $S_t$** | **Undrained shear strength [kPa]** | **$\sigma'_{pv}$ [kPa] pre-consolidation pressure** | **OCR** |
|---|---|---|---|---|---|---|---|
| **2** | 15 | 70 | 70 | 20 | 12.5 | - | - |
| **5** | 15 | 85 | 55 | 30 | 18.1 | 60 | 1.5 |
| **7** | 17.5 | 55 | 40 | 50 | 20.5 | 65 | 1.3 |

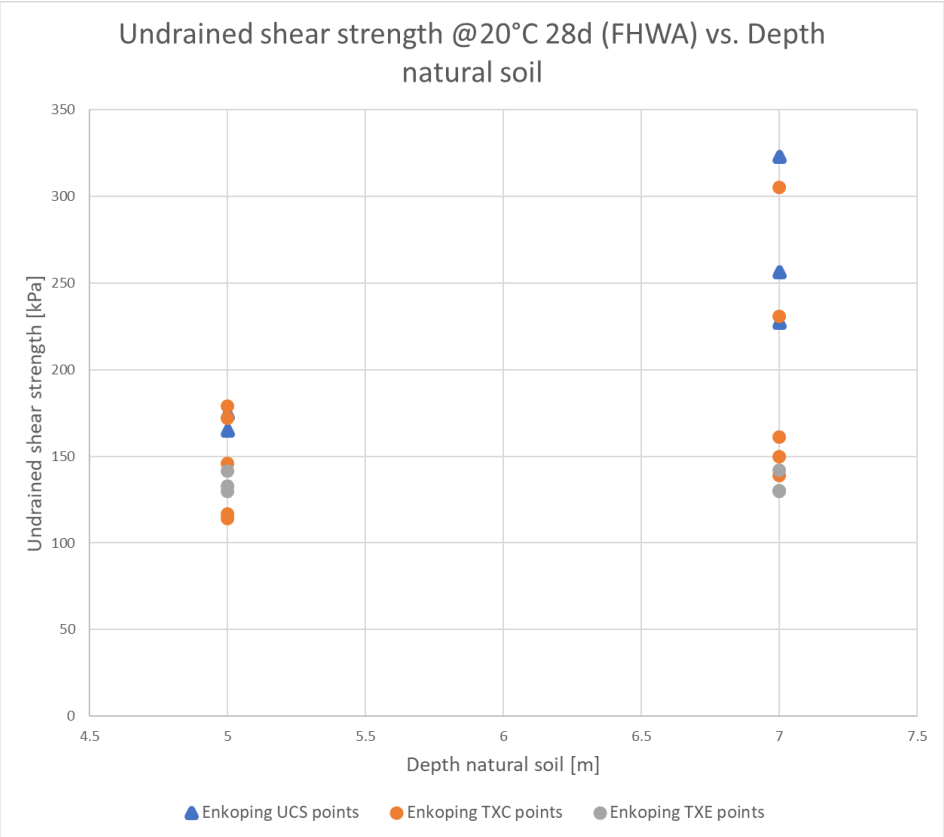


*Figure 33. Improved undrained shear strength for the Enköping soil compared to the natural sample depth. Source: own elaboration from* (Ignat et al., 2016).

### *3.2.1.2. Gothenburg, Sweden (West Link)*

Soil properties for different depths are presented in Table 6 for the present project site. For the present site, the improved soil data comes from laboratory mixed and tested data. Figure 34 shows the results of the unconfined compression tests over samples with different total binder contents and different binder ratios. The results show an increase in strength with increasing binder content, but also more spread in the results. As expected, the samples with more cement showed a higher strength for 28-day curing. Figure 35 shows both the results of unconfined compression and triaxial tests for different total binder contents, as expected, the samples subjected to confinement pressures resulted in higher shear strength (Helen Åhnberg, 2007).

*Table 6. Soil properties in Gothenburg, Sweden. Source: West Link project information.*

| Depth [m] | Level [m] | Density [t/m3] | Liquid Limit LL [%] | Water Content, w [%] | Sensitivity, $S_t$ | Undrained shear strength [kPa] | Soil type |
|---|---|---|---|---|---|---|---|
| **10** | -10 | 1.57 | 77 | 80 | 19 | 23 | Clay |
| **12** | -12 | 1.59 | 78 | 75 | 16 | 32 | Clay |
| **15** | -15 | 1.6 | 75 | 74 | 21 | 34 | Clay |
| **18** | -18 | 1.64 | 73 | 69 | 15 | 40 | Clay |
| **20** | -20 | 1.65 | 77 | 67 | 16 | 48 | Clay |

| | | | | | | | |
|---|---|---|---|---|---|---|---|
| **22** | -22 | 1.66 | 71 | 64 | 15 | 48 | Clay |
| **25** | -25 | 1.69 | 61 | 60 | 15 | 49 | Clay |
| **28** | -28 | 1.74 | 57 | 52 | 12 | 46 | Clay |

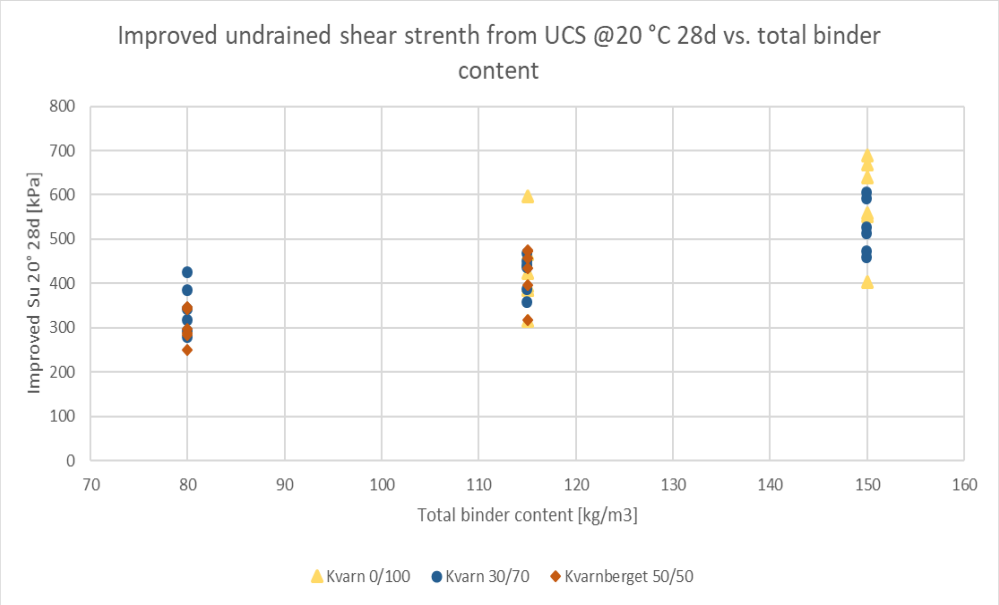


*Figure 34. Improved undrained shear strength from UCS tests compared to the total binder content at different binder ratios for the Gothenburg clay. Source: own elaboration from West Link project information.*

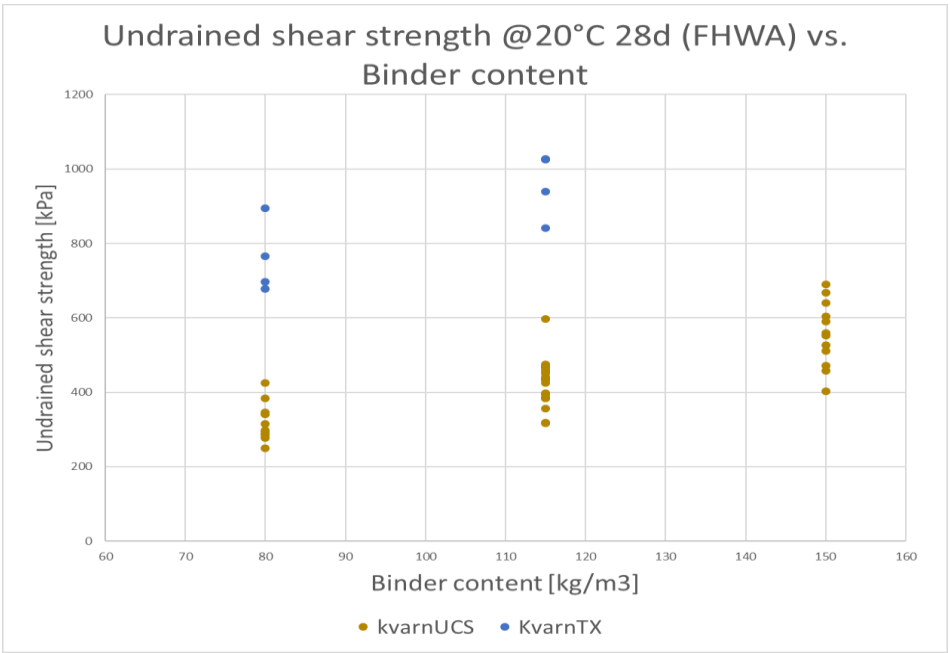


*Figure 35. Improved undrained shear strength vs. total binder content for both unconfined compression and triaxial tests: Source: own elaboration from West Link project information.*

Figure 36 and Figure 37 show the results of undrained triaxial tests over laboratory mixed samples, the stress paths in the s'-t plane is reported in them. Even though the test is undrained, the samples do not generate pore pressures during shearing, meaning that for the present case, the improved material is completely impermeable or non-porous, contrary to the behavior found in previous studies in which the samples generated pore pressures while shearing (Helen Åhnberg, 2006). Table 7 shows the ratio between the Young's modulus and the deviator stress in order to compare the present data with the recommended values exposed in Table 2; it can be observed that the values obtained in the present study are in the same order of magnitude than in previous research.

Table 8 shows the result of the undrained triaxial tests and allows to compare with the relations presented in 2.7.2 for the determination of the cohesion intercept; it also shows that the results of the unconfined compression tests can be a good estimation of the cohesion intercept for the investigated strength level but with slight tendency to the overestimation, therefore its use should be analyzed with care. Figure 38 shows the relation between the Young's modulus and the shear strength for different binder contents and sample origin from a different location of the West Link project, it is reported a ratio $E_{50}/s_u$ of 250, which is consistent with the data presented in Table 2 and Table 7. Figure 39 shows the comparison of the vertical and horizontal shear strength and Young's modulus, it is observed that there is no difference between the vertical and the horizontal shear strength; in contrast, there is a difference between the vertical and the horizontal Young's modulus being higher the latter, result which is consistent with previous studies (Hanson, 2012).

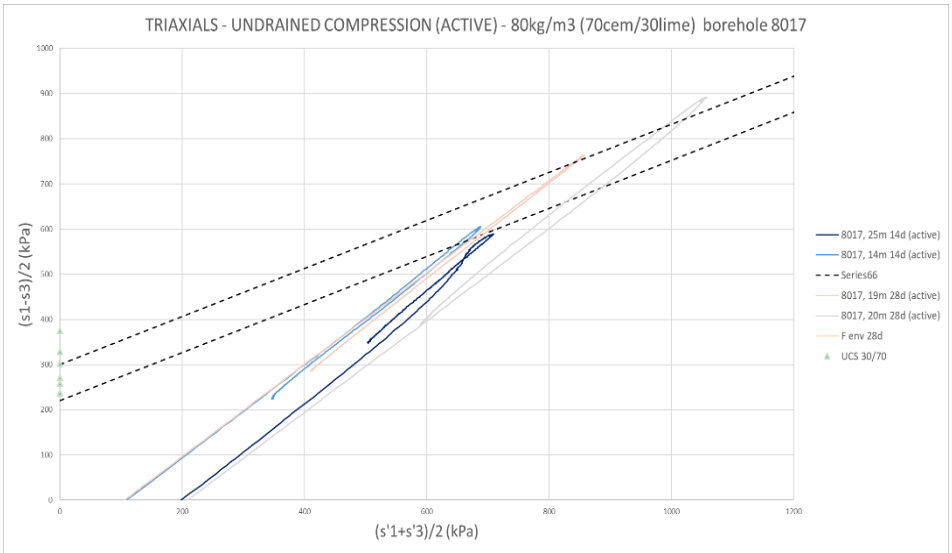


*Figure 36. Undrained triaxial compression test result in the s'-t plane over a sample with 80 kg/m3 total binder content with a 70 % cement content and 30 % lime content for 14- and 28-days curing time. Source: West Link project information.*

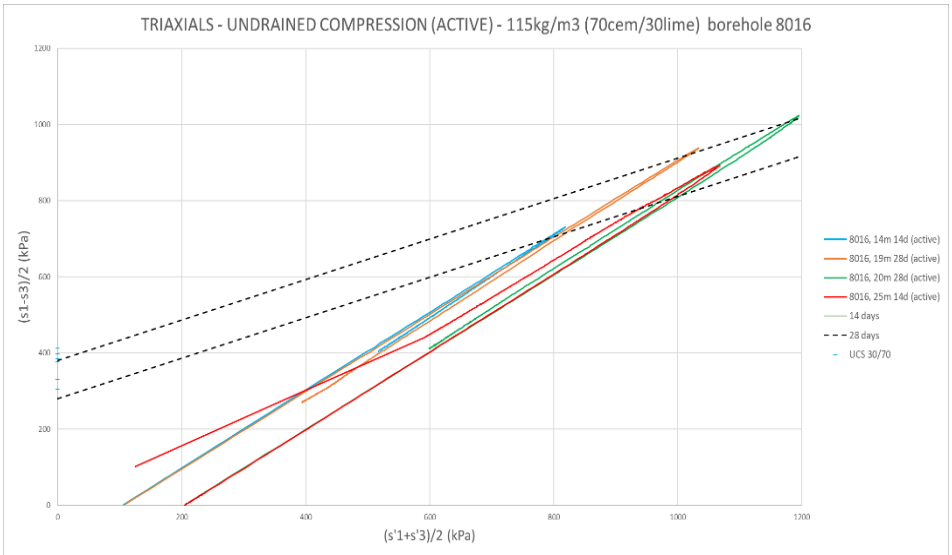


*Figure 37. Undrained triaxial compression test result in the s'-t plane over a sample with 115 kg/m3 total binder content with a 70 % cement content and 30 % lime content for 14 and 28 curing time. Source: West Link project information.*

*Table 7. Calculated $E_{50}/q_u$ from triaxial tests. Source: West Link project information.*

| Test | Binder content [kg/m³] | Depth [m] | $E_{50}/q_u$ @ 28 days |
|---|---|---|---|
| **Triaxial** | 80 | 19 | 100 |
| **Triaxial** | 80 | 20 | 79 |
| **Triaxial** | 115 | 19 | 98 |
| **Triaxial** | 115 | 20 | 77 |

*Table 8. Peak strength and cohesion intercept obtained from triaxial tests. Source: West Link project information.*

| Binder content | Depth [m] | Curing time [days] | c' calc. from triaxial [kPa] | Effective friction angle [°] | $q_u$ [kPa] | $c'/q_u$ | Avg UCS 30/70 |
|---|---|---|---|---|---|---|---|
| **80** | 14 | 14 | 259.76 | 32.12 | 1200 | 0.2164 | 294.88 |
| **80** | 25 | 14 | | | 1160 | 0.2239 | |
| **80** | 19 | 28 | 354.22 | 32.12 | 1540 | 0.2300 | 360.98 |
| **80** | 20 | 28 | | | 1800 | 0.196 | |
| **115** | 14 | 14 | 330.60 | 32.12 | 1500 | 0.2204 | 366.91 |
| **115** | 25 | 14 | | | 1740 | 0.1900 | |
| **115** | 19 | 28 | 448.68 | 32.12 | 1900 | 0.2361 | 456.41 |
| **115** | 20 | 28 | | | 2040 | 0.2199 | |

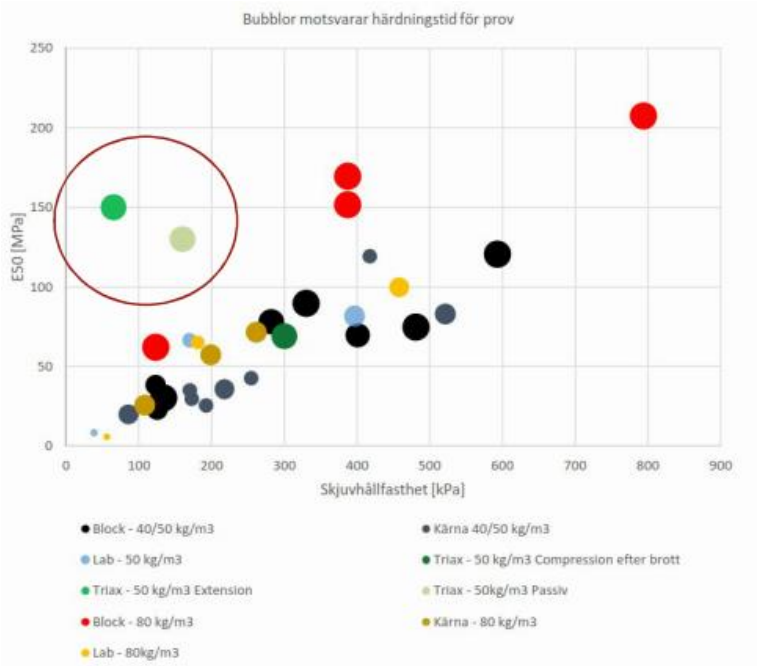


*Figure 38. Young's modulus vs. shear strength for different binder content and sample preparation. Source: West Link project information.*

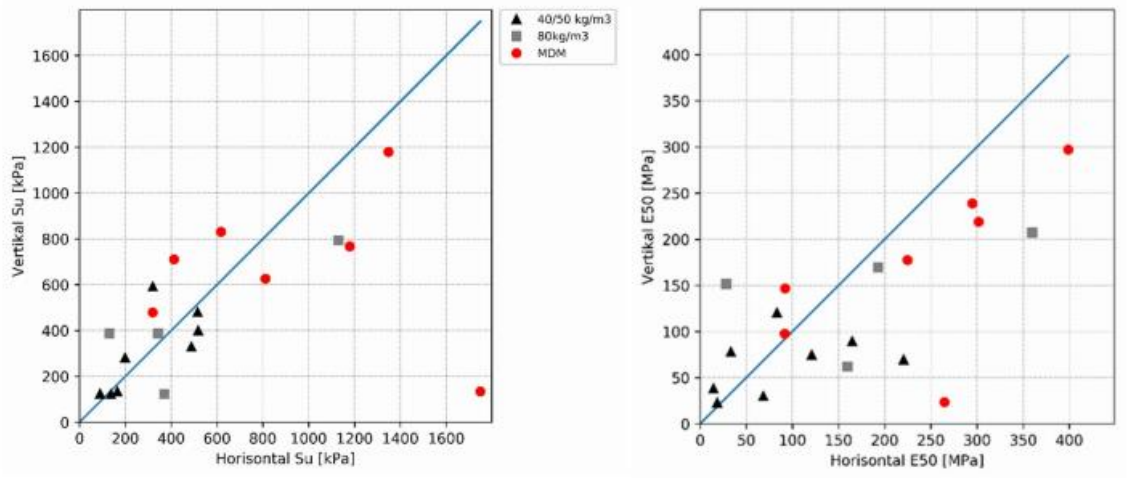


*Figure 3-9. Investigation of hållfasthetsanisotropi for uniaxial laboratory experiments on samples from the block. Horizontal and vertical Su plotted for all the blocks in order to give an indication of how the sample orientation affects the resistance.*

*Figure 39. Comparison between the vertical and the horizontal shear strength and Young's modulus. Source: West Link project information.*

### *3.2.1.3. Linköping, Sweden*

Natural soil properties of the present site are presented in Table 9. From the results of laboratory mixed and tested data, Figure 40 is reported showing the influence of the total binder content in the unconfined compression tests results, a clear direct relation is observed. Figure 41 shows the influence of the total binder content in the results of both drained and undrained compression triaxial tests, a direct relationship is evident and it can also be noted that, for the case of this soil, the drained and undrained triaxial evidence no difference at lower binder content, but a difference starts to appear with higher binder contents, yielding the drained test a higher strength.

*Table 9. Soil properties in Linköping, Sweden. Source:* (Helen Åhnberg, 2006, 2007).

| Depth [m] | Density [t/m3] | Plastic limit, PL [%] | Liquid Limit, LL [%] | Water content, w [%] | Undrained shear strength [kPa] | Sensitivity, $S_t$ |
|---|---|---|---|---|---|---|
| **3** | 1.55 | 24 | 70 | 78 | 15 | 20 |
| **4** | 1.55 | 24 | 70 | 78 | 15 | 20 |
| **5** | 1.55 | 24 | 70 | 78 | 15 | 20 |
| **6** | 1.55 | 24 | 70 | 78 | 15 | 20 |

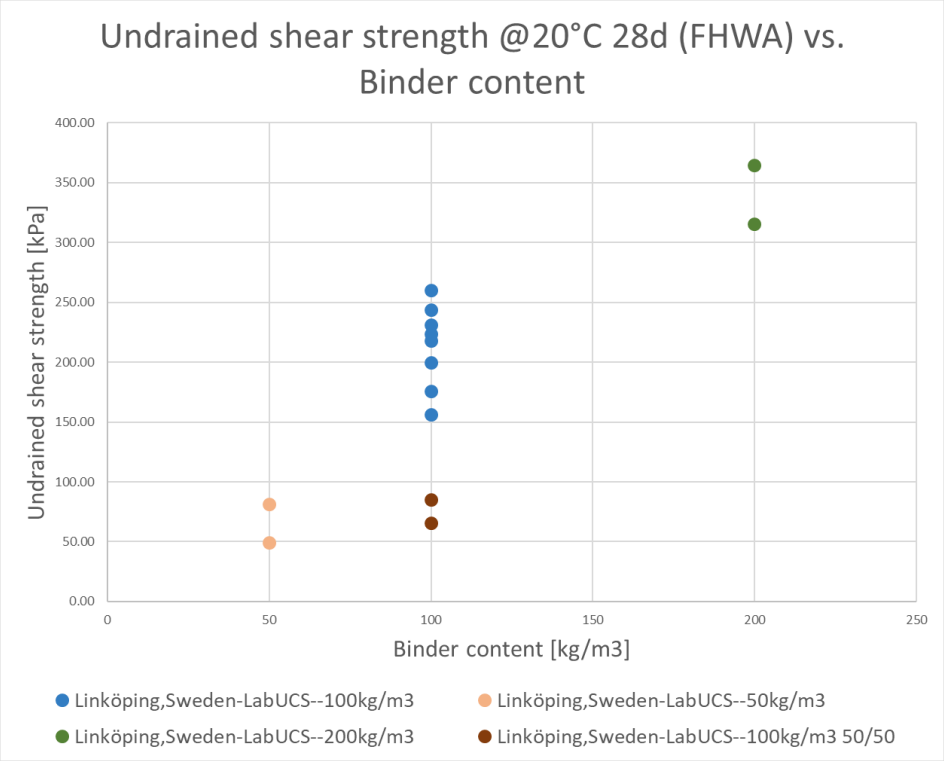


*Figure 40. Improved undrained shear strength from UCS with different binder contents. Source: own elaboration from* (Helen Åhnberg, 2006, 2007).

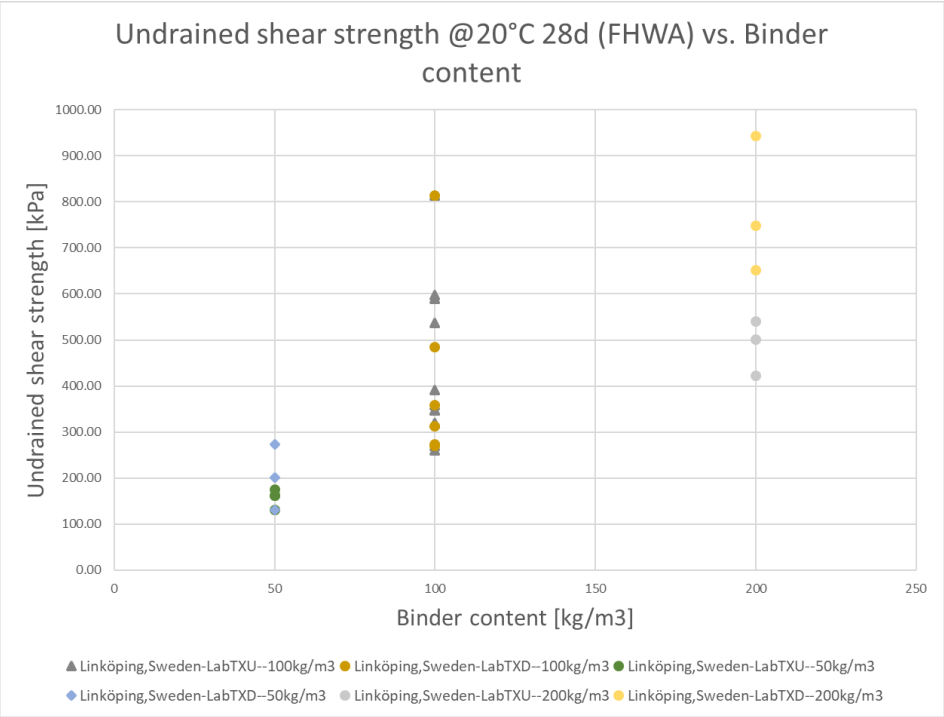


*Figure 41. Improved undrained shear strength from drained and undrained triaxial test with different binder contents. Source: own elaboration from* (Helen Åhnberg, 2006, 2007).

#### *3.2.1.4. Löftabro, Sweden*

Natural soil properties for the present site are presented in Table 10, it is observed that for every depth, the reported properties are the same, fact that could lead to inaccuracies in the predictions, because inherently, soil natural properties vary with the positioning and even between testing the same material. For the present site, the improved soil data is obtained from laboratory mixed and tested specimens. Figure 42 shows the undrained shear strength at different confining stress and for the present case it is not possible to stablish any trend due to the fact that the spread in the data is high and the data is limited.

*Table 10. Soil properties in Löftabro, Sweden. Source:* (Helen Åhnberg, 2006, 2007).

| Depth [m] | Density [t/m3] | Plastic limit, PL [%] | Liquid Limit, LL [%] | Water content, w [%] | Undrained shear strength [kPa] | Sensitivity, $S_t$ |
|---|---|---|---|---|---|---|
| **2** | 1.52 | 23 | 66 | 89 | 8 | 25 |
| **3** | 1.52 | 23 | 66 | 89 | 8 | 25 |
| **4** | 1.52 | 23 | 66 | 89 | 8 | 25 |
| **5** | 1.52 | 23 | 66 | 89 | 8 | 25 |

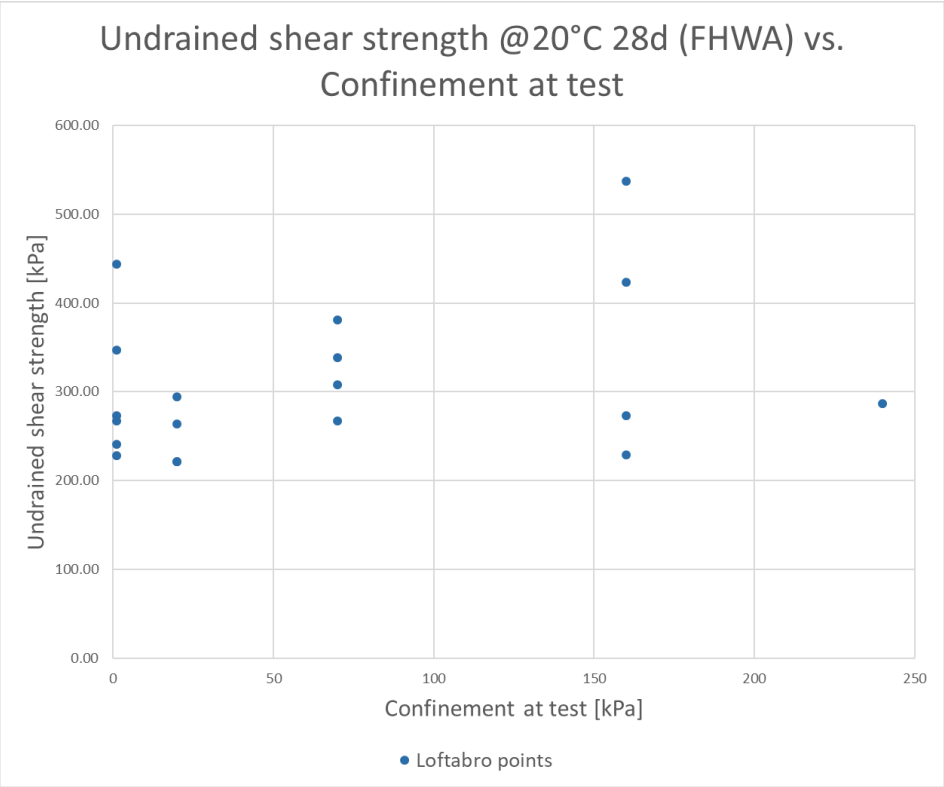


*Figure 42. Undrained shear strength at different confining stress. Source: own elaboration from* (Helen Åhnberg, 2006, 2007).

### *3.2.1.5. Møllenberg, Trondheim, Norway*

For the present site, the unconfined compression tests were performed on laboratory mixed samples, whereas the drained triaxial tests were performed on vertical and horizontal cores extracted from field mixed material, only little information could be found about the original soil properties, which is shown in Table 11. Figure 43 shows the undrained shear strength at different binder contents for unconfined compression and drained triaxial tests. It is evident that there is virtually no difference between the vertical and horizontal undrained shear strength, as concluded in section 3.2.1.2. Figure 44 shows the influence of the confining stress on the measured shear strength and is observed an increase of the shear strength with increasing confining stress until a maximum value in which the confining stress does not affect the shear strength anymore.

*Table 11. Soil properties in Møllenberg, Trondheim, Norway. Source:* (Hanson, 2012; Karlsrud et al., 2013).

| **Water content, w [%]** | **Sensitivity, $S_t$** | **Soil type** |
|---|---|---|
| **40** | 19 | Silty clay |

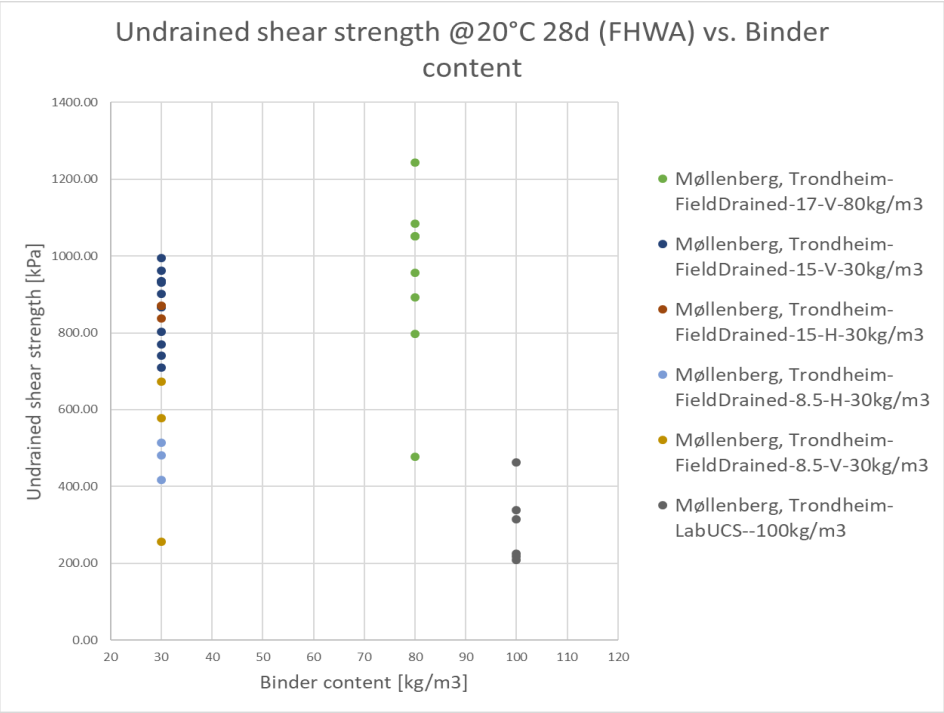


*Figure 43. Undrained shear strength for unconfined compression and drained triaxial tests at different binder content. Source: own elaboration from* (Hanson, 2012; Karlsrud et al., 2013).

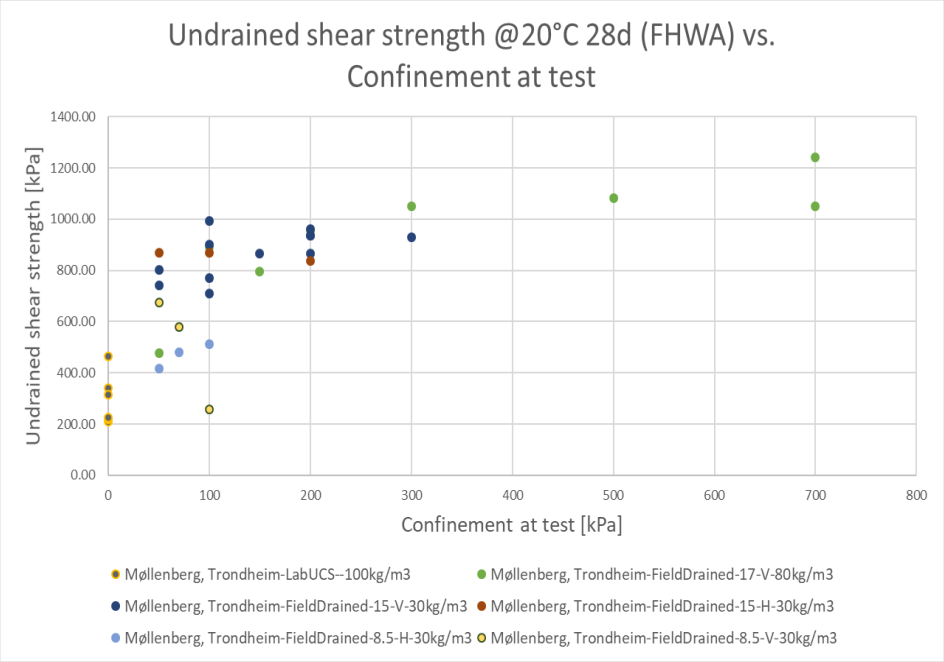


*Figure 44. Undrained shear strength at different confining stress. Source: own elaboration from* (Hanson, 2012; Karlsrud et al., 2013).

### *3.2.1.6. Schweigaardsgate, Oslo, Norway*

Similar to the previous case, only little information about the natural soil properties is available and it is reported in Table 12. In this site, laboratory and field tests were performed; unconfined compression tests were performed on laboratory mixed samples and FOPS was performed in field mixed samples. Figure 45 shows the results of the aforementioned tests at different confinement stress. It is observed big scatter in the unconfined compression tests as well as in the FOPS tests, with an increasing trend with increasing confining stress.

*Table 12. Soil properties in Schweigaardsgate, Oslo, Norway. Source:* (Karlsrud et al., 2013).

| Water content, w [%] | Plasticity index, $I_p$ | Sensitivity, $S_t$ |
|---|---|---|
| **40** | 25 | 4.5 |

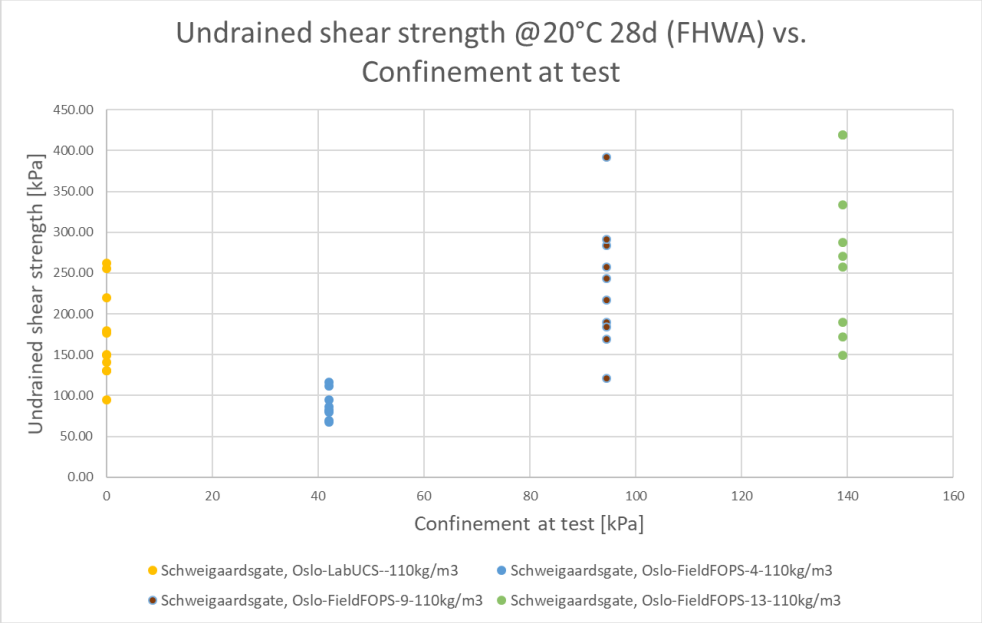


*Figure 45. Improved undrained shear strength at different confining stresses. Source: own elaboration from* (Karlsrud et al., 2013).

### *3.2.1.7. Trafikverket study*

The tests on this site were performed on laboratory mixed specimens and the results are reported in Figure 46, where a direct relation is observed between the improved undrained shear strength and the binder content. It is also observed a certain influence of the natural depth of the soil used for the mixture. The natural soil properties reported for this site can be observed in Table 13.

*Table 13. Soil properties in the Trafikverket study. Source:* (Trafikverket, 2011).

| Depth [m] | Density [t/m3] | Liquid Limit, LL [%] | Water Content, w [%] | Sensitivity, $S_t$ | Undrained shear strength [kPa] | Soil type |
|---|---|---|---|---|---|---|
| **1** | 1.45 | 100 | 90 | 10 | 6 | Silty clay |
| **2** | 1.45 | 100 | 100 | 13 | 6 | Silty clay |

| | | | | | | |
|---|---|---|---|---|---|---|
| **3** | 1.45 | 80 | 120 | 30 | 6 | Silty clay |
| **4** | 1.45 | 75 | 100 | 37 | 6 | Silty clay |
| **5** | 1.45 | 60 | 85 | 50 | 6 | Silty clay |
| **6** | 1.45 | 55 | 90 | 65 | 7.1 | Silty clay |
| **7** | 1.45 | 50 | 70 | 50 | 8.2 | Silty clay |
| **8** | 1.5 | 50 | 75 | 60 | 9.3 | Silty clay |
| **9** | 1.6 | 38 | 65 | 65 | 10.4 | Silty clay |
| **10** | 1.6 | 50 | 75 | 50 | 11.5 | Silty clay |
| **11** | 1.6 | 40 | 65 | 65 | 12.6 | Silty clay |
| **12** | 1.6 | 40 | 65 | 130 | 13.7 | Silty clay |
| **13** | 1.6 | 38 | 60 | 130 | 14.8 | Silty clay |

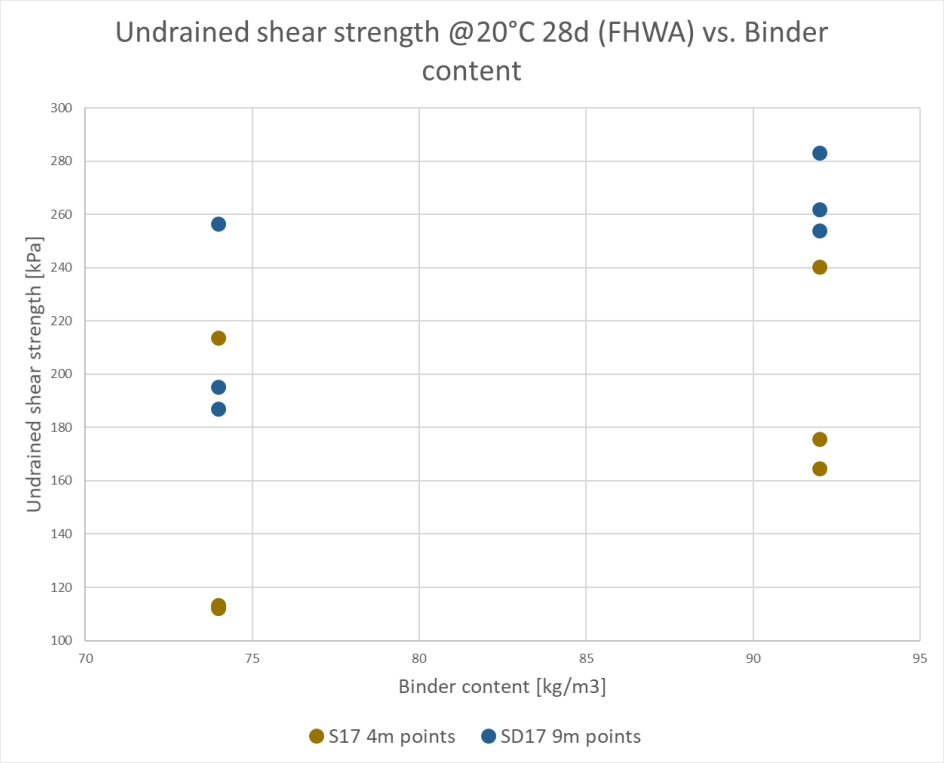


*Figure 46. Undrained shear strength at different binder content of soils from different depths. Source: own elaboration from* (Trafikverket, 2011).

#### *3.2.1.8. Skøyen, Oslo, Norway*

Figure 47 shows the result of unconfined compression tests on laboratory mixed samples at different binder contents. For the present site, it is observed a direct relation between the undrained shear strength and the binder content introduced to the natural soil. Very little information regarding the natural soil condition was reported and it can be observed in Table 14.

*Table 14. Soil properties in Skøyen, Oslo, Norway. Source:* (Karlsrud et al., 2013).

| Water content, w [%] | Plasticity index, $I_p$ |
|---|---|
| **35** | 16 |

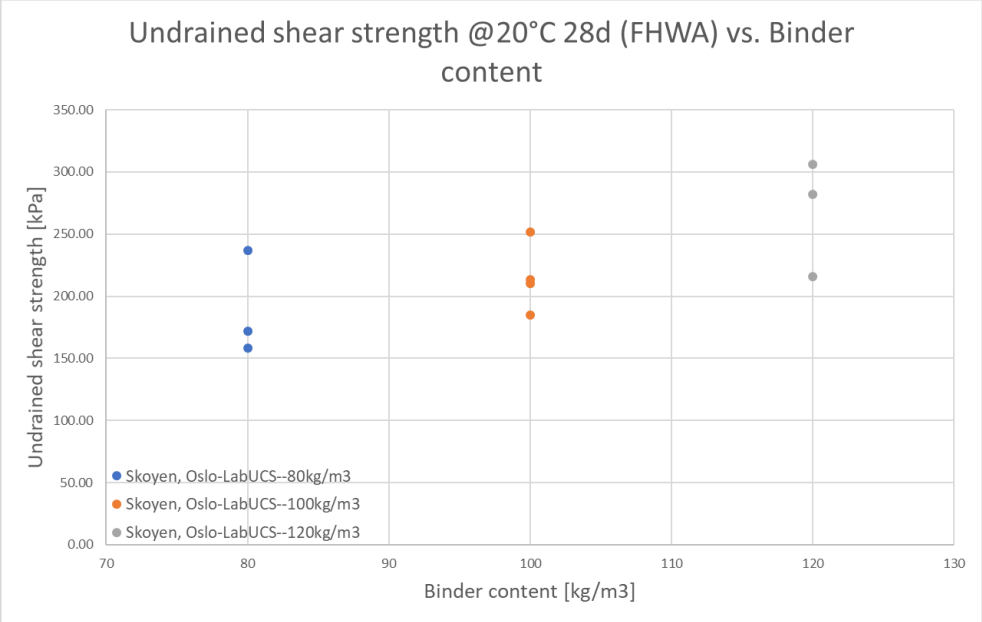


*Figure 47. Improved undrained shear strength at different binder content. Source: own elaboration from* (Karlsrud et al., 2013).

#### *3.2.1.9. Gothenburg, Sweden (Luleå University of Technology)*

For the considered site, the natural soil properties can be found in Table 15 and the data from the improved soil was obtained by means of unconfined compression tests performed on laboratory mixed samples. In Figure 48 the results of the performed unconfined compression tests at different binder contents can be observed. It is clear the direct relation between the undrained shear strength and the binder content introduced in the soil; it appears that at low binder contents, the improved undrained shear strength seems to develop differing from the expected linear trend observed in the previous data reported in the present section.

*Table 15. Soil properties in Gothenburg, Sweden. Source:* (Jonsson, 2017).

| Water content, w [%] | Density [ton/m3] | Dry unit weight [ton/m3] | Liquid limit, LL [%] | Plastic Limit, PL [%] | Undrained shear strength [kPa] |
|---|---|---|---|---|---|
| 31.2 | 1.55 | 1.18 | 37.17 | 19.62 | 13 |

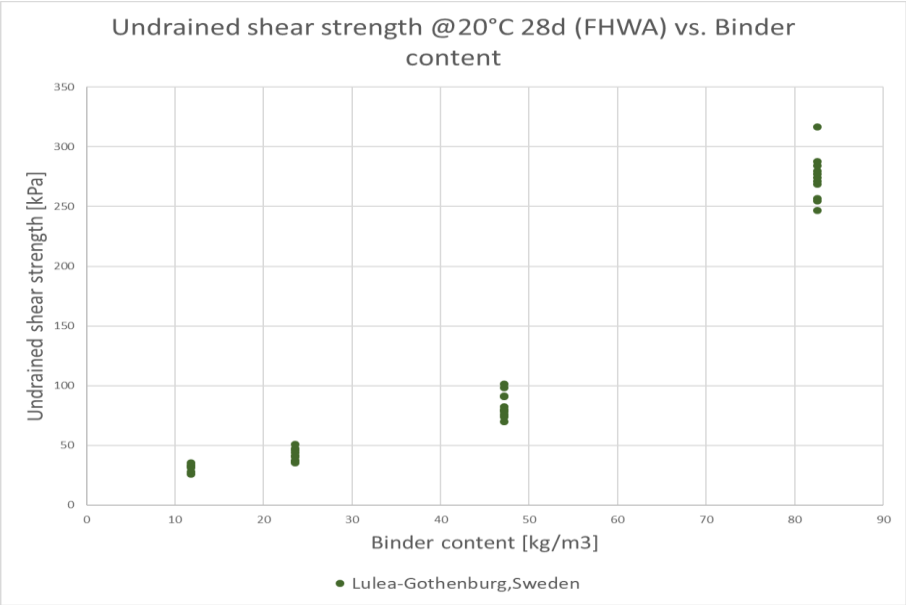


*Figure 48. Improved undrained shear strength at different binder content. Source: own elaboration from* (Jonsson, 2017).

## 3.2.2. Estimation of the improved undrained shear strength

### *3.2.2.1. Parameters used for the estimation*

To find an expression that can properly estimate the improved soil strength after adding binders, it is necessary to acknowledge that binder content, binder ratio, and natural soil properties are the three drivers of the final improved soil strength. Among the natural soil properties reported in the dataset, all were analyzed in order to confirm their influence in the improved shear strength of the stabilized soil. Considering liquid limit, water content, sensitivity, and undrained shear strength, graphical analysis is made in order to decide which property or properties are of direct influence to the improved shear strength; this is done by plotting the improved shear strength against the four mentioned soil properties and observing if a trend exists.

According to the data used, the natural undrained shear strength is the only soil property that strongly influences the improved shear strength, whereas the rest of the natural soil properties do not explicitly show any possible trend, for the ranges and data analyzed. The plot containing all the data comparing the improved and the natural shear strength can be observed in Figure 49. The rest of the plots made and some comments about the process can be found in Appendix B. The influence of the binder content and binder ratio is evident and is confirmed for each site in section 3.2.1, Figure 50 shows all the available data of improved shear strength against the total binder content in two data series for the 50/50 and 0/100 binder ratios. The direct relation between the improved strength and the binder content added is hereby confirmed and is also noted that depending on the binder ratio used, the resulting improved strength will vary. For the 0/100 a wide range of total binder content data is available, whereas for the 50/50 a smaller range is reported in the acquired data, therefore the estimation of the improved strength should be limited to the total binder content range here reported and a difference should be made between the two available binder ratios.

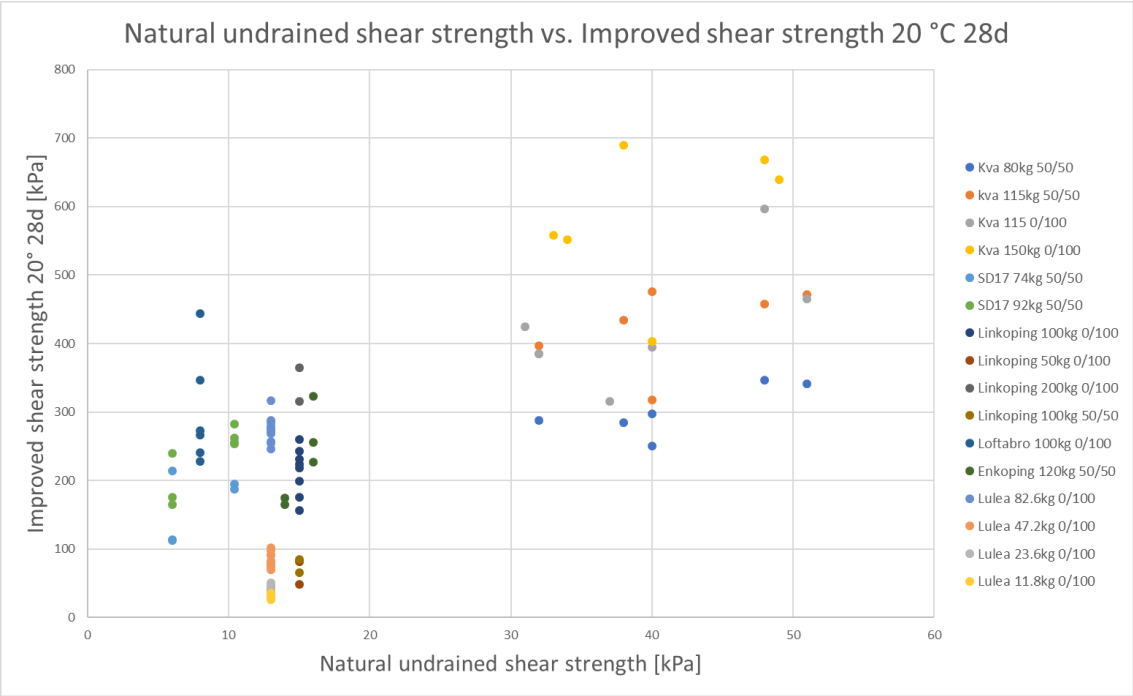


*Figure 49. Natural vs. improved undrained shear strength. Source: own elaboration.*

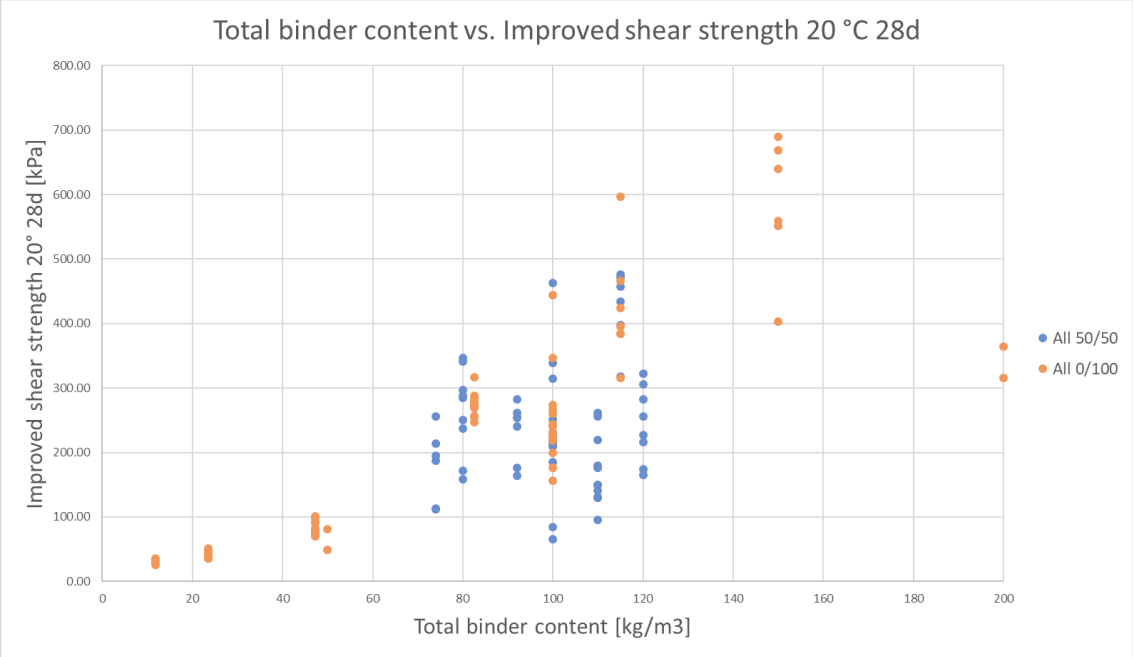


*Figure 50. Total binder content vs. Improved shear strength for 0/100 and 50/50 binder ratio for all sites. Source: own elaboration.*

### *3.2.2.2. Mathematical expressions used for the estimation*

Investigating the influence of the different soil properties into the improved undrained shear strength was done graphically and it was concluded that, with the available data, the only soil property that should be taken into account in the expression to estimate the improved undrained shear strength is the natural undrained shear strength of the soil, as reported in section 3.2.2.1. Also, separate analyses are made to assess both 0/100 and 50/50 binder ratios because, for each case, the composition of the total binder content differs, hence the influence of the binder content must also be different, therefore leading to different coefficients in the expression to estimate the improved shear strength.

Even though many mathematical expressions exist to model the available data, it is important to first analyze and establish the expected trend for the improved shear strength in both the binder content and the natural undrained shear strength taking as a base both Figure 49 and Figure 50 in order to generate the most suitable expression. In the binder content space, the improved soil shear strength is expected to follow an "S" shape starting from the natural undrained shear strength and reaching an upper limit which can be set by the available water to react with the binder or the hardened binder strength, a sketch of this behavior can be observed in Figure 51 (left). Considering the undrained shear strength space and, as stated before, it is expected that the improved shear strength follows the natural undrained shear strength at low binder contents, therefore initially generating a 1:1 relation as a baseline and shifting it toward higher values, maintaining the initial slope as the binder content increases; the expected behavior can be observed in Figure 51 (right).

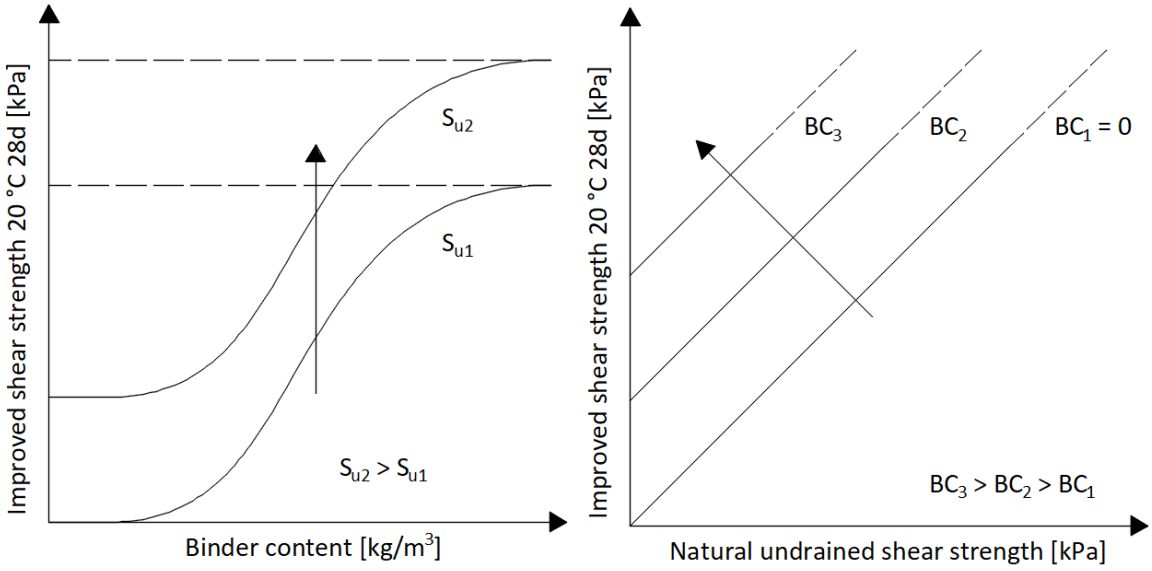


*Figure 51. Expected trend of the improved shear strength in the binder content space (left) and in the natural undrained shear strength space (right). Source: own elaboration.*

As mentioned at the beginning of section 3.2, high variability is expected in the measured improved shear strength per site and for a given binder content, this fact has been analyzed previously with reported coefficient of variation typically ranging from 0.30 to 0.60 but values as low as 0.15 and as high as 1.35 have also been found (Navin & Filz, 2005). The reported coefficient of variation in previous research will be compared to that of the present dataset in order to suggest a value for the

coefficient of variation to be considered when estimating the improved undrained shear strength using the proposed mathematical expression.

From Figure 51, several mathematical expressions are selected to be tested in order to represent the available data for both the binder content and the natural undrained shear strength space. The selected expressions are listed below:

- *Polynomial:* a simultaneous combination of binder content and natural undrained shear strength as independent variables were tested starting from a first-degree polynomial up to a fifth-degree polynomial. A division of polynomial up to fourth-degree was also tested.
    - Polynomial expression:

$$s_{u;impr;20°C;28d;est} = \beta_0 + \beta_1 * BC + \beta_2 * BC^2 + \cdots + \beta_5 * BC^5 + \beta_6 * s_{u;nat} + \cdots + \beta_{10} * {s_{u;nat}}^5 \quad (15)$$

    - Ratio of polynomial expressions:

$$s_{u;impr;20°C;28d;est} = \frac{\beta_0 + \beta_1 * BC + \cdots + \beta_4 * BC^4 + \beta_5 * s_{u;nat} + \cdots + \beta_8 * {s_{u;nat}}^4}{1 + \beta_9 * BC + \cdots + \beta_{12} * BC^4 + \beta_{13} * s_{u;nat} + \cdots + \beta_{16} * {s_{u;nat}}^4} \quad (16)$$

- *Sigmoid function:* with this function, the expected "S" shape can be reproduced and thus is used to represent the behavior in the binder content space in combination with a first-degree polynomial of the natural undrained shear strength.

$$s_{u;impr;20°C;28d;est} = \beta_0 \frac{1}{1 + e^{-(\beta_1 BC)}} + \beta_2 \frac{1}{1 + e^{-(\beta_3 s_{u;nat})}} + \beta_4 BC + \beta_5 s_{u;nat} \quad (17)$$

- *Exponential:* used to represent the behavior in the binder content space in combination with a first-degree polynomial of the natural undrained shear strength. Polynomials were also tested in the exponential function up to the second degree.
    - Exponential of a polynomial:

$$s_{u;impr;20°C;28d;est} = e^{\left(\beta_0 + \frac{\beta_1}{BC + \beta_2} - \left(\frac{\beta_3}{BC + \beta_4}\right)^2\right)} + \beta_5 s_{u;nat} + \beta_6 {s_{u;nat}}^2 + \beta_7 {s_{u;nat}}^3 \quad (18)$$

    - Exponential recovery:

$$s_{u;impr;20°C;28d;est} = \beta_0\left(1 - e^{-\beta_1 BC}\right) + \beta_2 s_{u;nat} \quad (19)$$

    - Ratio of exponential decay and exponential recovery:

$$s_{u;impr;20°C;28d;est} = \beta_0 \left(\frac{1 - e^{\frac{-BC}{\beta_1}}}{1 + e^{\frac{-BC}{\beta_2}}}\right) + \beta_3 * s_{u;nat} \quad (20)$$

Where $\beta_i$ are the fitting coefficients; $s_{u;impr;20°C;28d}$ is the undrained shear strength of the improved soil cured at 20 °C and for 28 days [kPa]; $s_{u;nat}$ is the natural undrained shear strength [kPa]; and $BC$ is the binder content [kg/m$^3$]

#### *3.2.2.3. Suitability of the selected expressions and determination of fitting coefficients*

In the present section, the suitability of each of the mathematical expressions presented in section 3.2.2.2 are tested and the fitting coefficients for each binder ratio calculated using the *curve_fit* function from Python. Only the results considered relevant for the present discussion are included, and the selected expressions and fitting coefficients are presented in the next section with additional remarks.

The equations presented in the previous section have two independent variables, therefore the correct representation of the expressions would be a surface, nevertheless, it is considered more convenient to present the shape of the expressions in two separate plots, one for each independent variable, for ease of comparison and to check whether the expressions are consistent to what is expected in geotechnical problems.

As mentioned in section 3.2.2.2, the estimated values of the most suitable mathematical expressions will be compared to the corresponding measured values and a calculated coefficient of variation will be presented and compared to the ones reported in previous research in order to propose a suggested coefficient of variation to take into account for design purposes.

##### 3.2.2.3.1. Polynomial

Polynomial expressions including both the binder content and the natural undrained shear strength as independent variables and starting from a first-degree up to a fifth-degree polynomial are implemented and tested in order to assess their suitability to represent the available data. Also, a ratio of polynomials up to fourth-degree is implemented.

- *Polynomial expression:* the suitability of a polynomial expression to represent the available data is first tested starting from a first-degree polynomial and increasing simultaneously the degree for both independent variables up to a fifth-degree polynomial. Also, the natural undrained shear strength is left as a first-degree expression and the degree of the binder content expression is increased separately. From this analysis, it is concluded that polynomial expressions from third up to fifth-degree are not correctly representing the available data, since with these high order expressions very high values or sudden drops in the estimation are obtained, behavior that is not desired to represent the actual physical mechanism, even though the $R^2$ values are in the order of 0.91.
  Linear or quadratic polynomials show more consistent estimations that are indeed more attached to the expected physical phenomenon than the higher-order polynomials, even though the $R^2$ values are in the order of 0.85, which would mean a less accurate model in purely statistical terms. From the results obtained, the simplified expression for the polynomial approach shown in Equation (15) can be written as:

$$s_{u;impr;20°C;28d;est} = \beta_0 + \beta_1 * BC + \beta_2 * s_{u;nat} + \beta_3 * {s_{u;nat}}^2 \quad (21)$$

*Fitting coefficients for both 0/100 and 50/50 binder ratio are determined and the most relevant presented in Table 16 and*

Table 17. The plots in both the binder content and natural undrained shear strength are presented in Figure 52, Figure 53 and Figure 54. It was decided to leave out the plots for the 50/50 binder ratio because essentially the graphs will look the same and will not add any value to the discussion. The $R^2$ value for the "BC-lin/Su-lin/Su-qua 1" and "BC-lin/Su-lin/Su-qua

2" coefficients is slightly higher than that of the "All-lin" coefficients, meaning that the fit is better numerically, but the concave shape that is evident in the natural undrained shear strength space is not a behavior expected in geotechnical problems, therefore the preferred set of fitting coefficients for the present case is the "All-lin".

*Table 16. Fitting coefficients and $R^2$ for the 0/100 samples. Source: own elaboration.*

| Multiplier | Coefficients | BC-lin/Su-lin/Su-qua 1 | BC-lin/Su-lin/Su-qua 2 | All-lin |
|---|---|---|---|---|
| **1** | $\beta_0$ | 40.4464 | 0.0000 | -81.5427 |
| $\boldsymbol{BC}$ | $\beta_1$ | 2.5566 | 2.5743 | 2.5230 |
| $\boldsymbol{s_{u;nat}}$ | $\beta_2$ | -6.4110 | -2.6995 | 6.0498 |
| $\boldsymbol{s_{u;nat}}^2$ | $\beta_3$ | 0.2235 | 0.1589 | 0.0000 |
| | $R^2$ | 0.8614 | 0.8761 | 0.8459 |

*Table 17. Fitting coefficients and R2 for the 50/50 samples. Source: own elaboration.*

| Multiplier | Coefficients | BC-lin/Su-lin/Su-qua 1 | BC-lin/Su-lin/Su-qua 2 | All-lin |
|---|---|---|---|---|
| **1** | $\beta_0$ | 74.5155 | 0.0000 | 50.0358 |
| $\boldsymbol{BC}$ | $\beta_1$ | 1.4020 | 2.1089 | 1.4986 |
| $\boldsymbol{s_{u;nat}}$ | $\beta_2$ | -1.3388 | -0.8173 | 3.6219 |
| $\boldsymbol{s_{u;nat}}^2$ | $\beta_3$ | 0.1122 | 0.1031 | 0.0000 |
| | $R^2$ | 0.4566 | 0.4435 | 0.4036 |

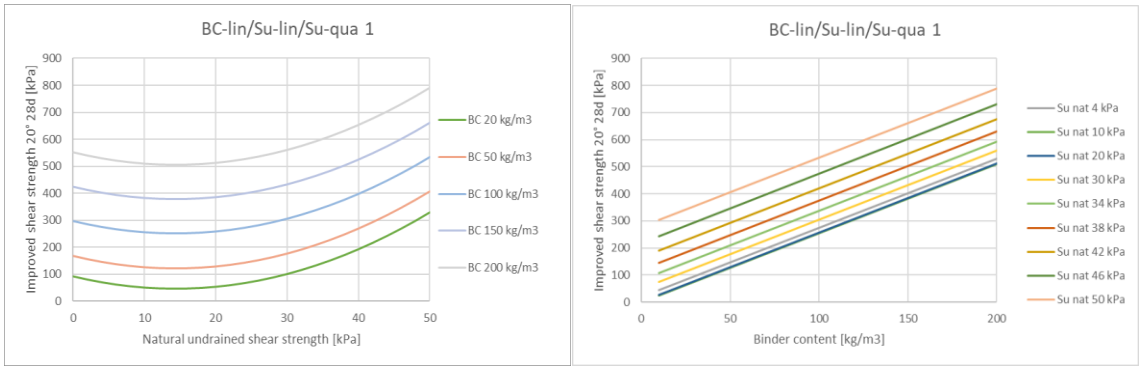


*Figure 52. Plots of Equation (21) using the "BC-lin/Su-lin/Su-qua 1" coefficients for the 0/100 binder ratio case in the natural undrained shear strength (left) and binder content (right) space. Source: own elaboration.*

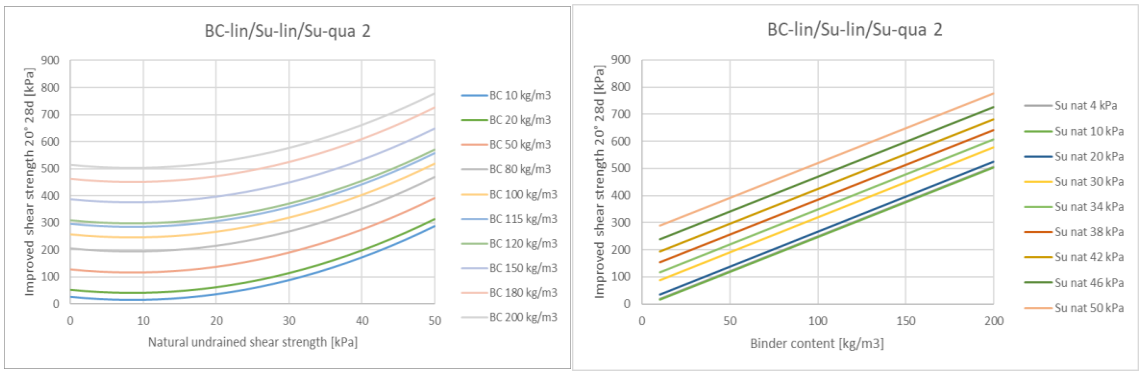


*Figure 53. Plots of Equation (21) using the "BC-lin/Su-lin/Su-qua 2" coefficients for the 0/100 binder ratio case in the natural undrained shear strength (left) and binder content (right) space. Source: own elaboration.*

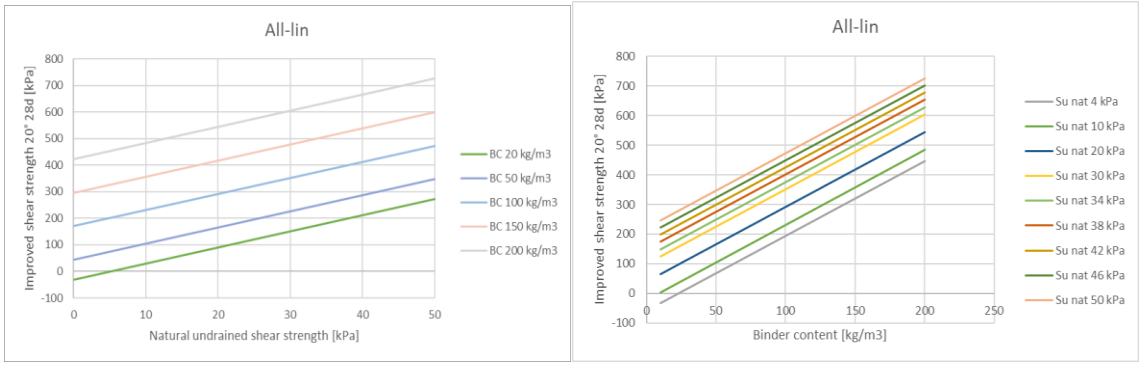


*Figure 54. Plots of Equation (21) using the "All-lin" coefficients for the 0/100 binder ratio case in the natural undrained shear strength (left) and binder content (right) space. Source: own elaboration.*

It is important to check whether the selected set of fitting coefficients are indeed correctly estimating the improved shear strength, for this purpose the estimated value of the improved shear strength for each data point is calculated and plotted alongside the measured value of the shear strength, this can be observed in Figure 55 and Figure 56 for the 0/100 and 50/50 binder ratio respectively. It is also important to check the variability of the measured results over the estimated values, for this purpose, for each pair of estimated-measured value a normalized deviation on the estimation is calculated as follows:

$$\Delta estimation_{norm} = \frac{S_{u;impr;20°C;28d;est} - S_{u;impr;20°C;28d;meas}}{S_{u;impr;20°C;28d;meas}} \quad (22)$$

Using Equation (22), the average normalized deviation found between the measured values and the estimated values using the "All-in" coefficients is 0.31 with a standard deviation of 0.39, meaning that the recommended values in found in previous research and presented at the beginning of section 3.2 could be used for the present analysis.

Lines showing the recommended upper and lower limits for a variation of both 30 % and 60 % (Navin & Filz, 2005) are included because, as stated in section 3.2, the coefficient of

variation of measured improved shear strength typically ranges from 0.30 to 0.60 (Navin & Filz, 2005), fact that should be taken into account when estimating improved shear strength values.

For the 0/100 binder ratio case, if a coefficient of variation of 30 % is assumed, more than 80 % of the data points are inside the area of estimation, whereas 97 % of the data points are inside the prediction area when a coefficient of variation of 60 % is considered. For the 50/50 binder ratio case, 75 % of the data points are inside the prediction area when assuming a coefficient of variation value of 30 %; when assuming a value of 60 %, 93 % of the data points are inside the estimation area. The $R^2$ values were not included in these plots because they will coincide with the ones presented in Table 16 and

Table 17 for the "All-lin" set of fitting coefficients. It is considered that the estimation of the improved shear strength can be done by using Equation (21) alongside with the "All-lin" coefficients set and considering a coefficient of variation of 30 % to obtain a clear scope of the possible results that the actual mixed soil could yield.

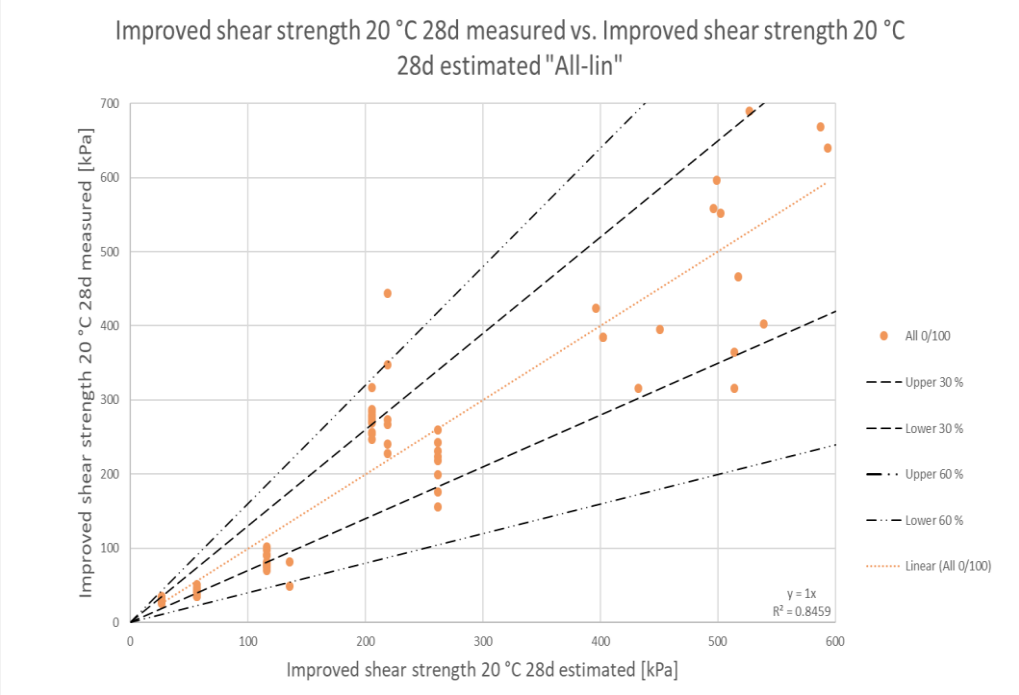


*Figure 55. Measured vs. estimated improved shear strength using the "All-lin" coefficients for the 0/100 binder ratio case. Source: own elaboration.*

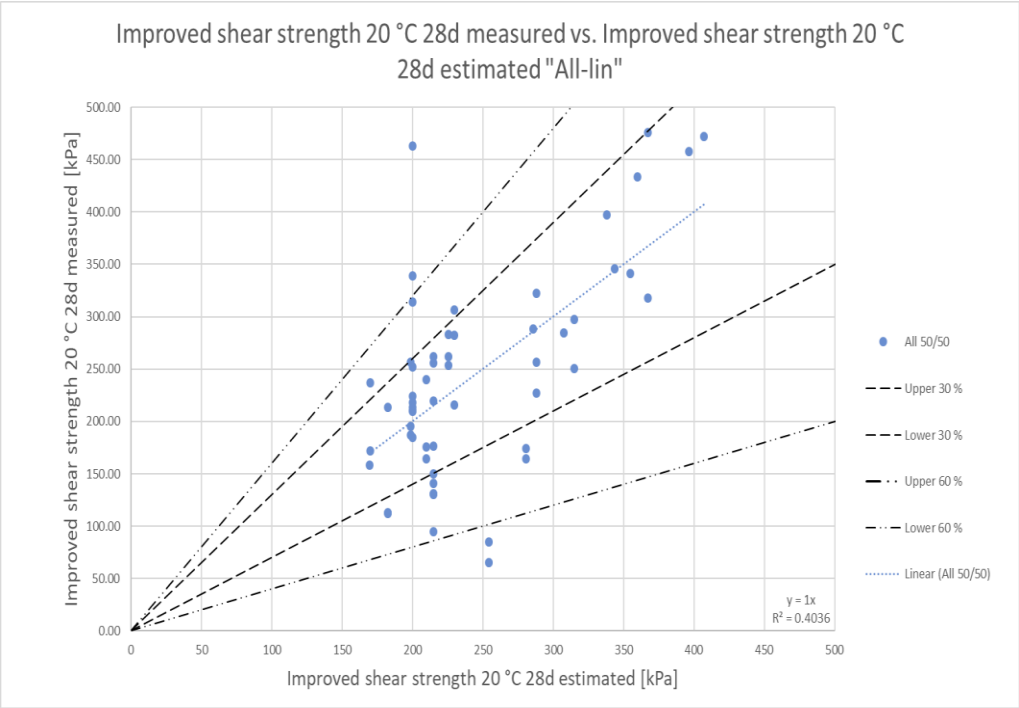


*Figure 56. Measured vs. estimated improved shear strength using the "All-lin" coefficients for the 50/50 binder ratio case. Source: own elaboration.*

- *Ratio of polynomial expressions:* the ratio of polynomial expressions is also considered as a mathematical expression that could represent the available data. When testing this type of expression, both very high and very low estimated values are obtained for some range of independent variables, moreover, the obtained shapes when plotting the expressions do not follow the expected physical phenomenon, therefore this type of function is discarded. An example of the estimated expression for a second-degree polynomial ratio can be observed in Figure 57.

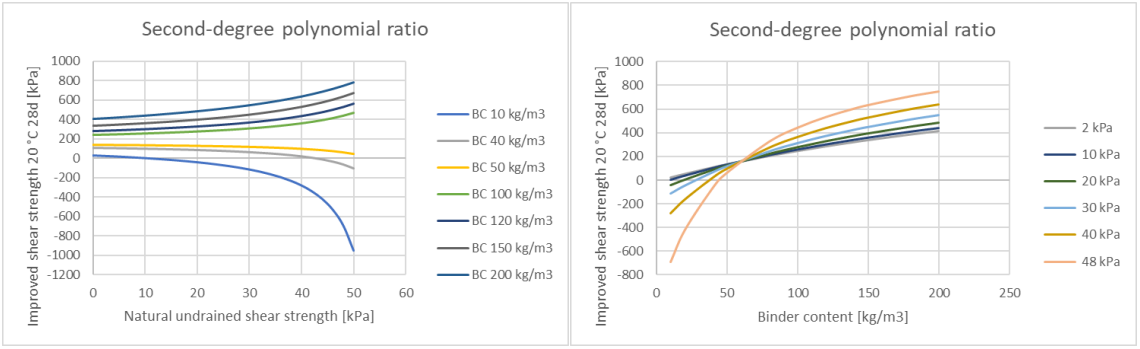


*Figure 57. Plots of a second-degree polynomial ratio for the 0/100 binder ratio case in the natural undrained shear strength (left) and binder content (right) space. Source: own elaboration.*

#### 3.2.2.3.2. Sigmoid function

Sigmoid functions in combination with linear function for both the binder content and the undrained shear strength were tested. When using the full Equation (17), the resulting plot shows linear trends for both independent variables, therefore this approach is discarded because it could simply be modelled by using linear functions. When using the sigmoid function for the binder content and a linear function for the natural undrained shear strength, the estimated coefficients lead to an expression which emulates to a certain extent the expected behavior but with values often going to a negative estimated improved strength. Lastly, only sigmoid functions are used for both the independent variables and this approach leads also to the expected behavior but with the same disadvantages of the previous case. None of the approaches using sigmoid functions are considered suitable for representing the available data. The coefficients for the different approaches are presented in Table 18, and the plots for the first set of fitting coefficients (columns 2 and 4 of Table 18) for the 0/100 samples is shown in Figure 58. The second set of fitting coefficients (columns 3 and 5 of Table 18) is discarded because even though the $R^2$ is better for the 0/100 samples, the $R^2$ is substantially lower for the 50/50 samples.

*Table 18. Fitting coefficients and $R^2$ for both the 0/100 and 50/50 samples. Source: own elaboration.*

| Coefficients | 0/100 | | 50/50 | |
|---|---|---|---|---|
| $\beta_0$ | -480.8933 | 1051.5427 | 251.9845 | 337.0774 |
| $\beta_1$ | -0.0460 | 0.0138 | 0.0138 | 0.0134 |
| $\beta_2$ | 0 | -1311.1314 | 0 | -93.7936 |
| $\beta_3$ | 0 | -0.0197 | 0 | -778.1462 |
| $\beta_4$ | 0 | 0 | 0 | 0 |
| $\beta_5$ | 13.5794 | 0 | 3.5457 | 0 |
| $R^2$ | 0.6876 | 0.8714 | 0.3493 | 0.0559 |

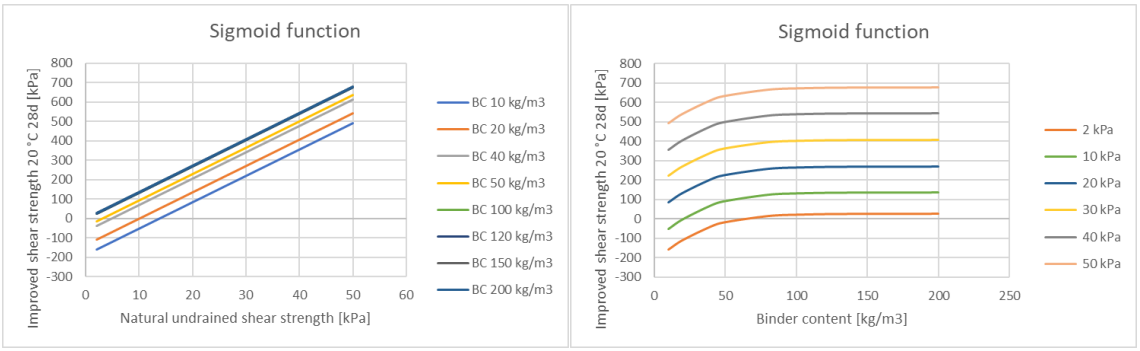


*Figure 58. Plots of the first set of fitting coefficients for the sigmoid function for the 0/100 binder ratio case in the natural undrained shear strength (left) and binder content (right) space. Source: own elaboration.*

#### 3.2.2.3.3. Exponential

Exponential expressions offer a certain degree of versatility to represent different graph shapes, these are considered to model the expected "S" shape in the binder content space accompanied with another exponential expression and/or a polynomial for the natural undrained shear strength representation.

- *Exponential of a polynomial:* the exponential of a polynomic function including the binder content is jointly implemented with a polynomic function including the natural undrained shear strength. From the analysis the second- and third-degree terms of the natural undrained shear strength are not of any use to properly represent the data. When only considering the first-degree term of the natural undrained shear strength and the exponential of a polynomial including the binder content, good agreement is obtained with the available data. Table 19 shows the obtained coefficients to represent the available data and Figure 59 shows the plots of Equation (18) in both the binder content and the natural undrained shear strength space.

*Table 19. Fitting coefficients and $R^2$ for both the 0/100 and 50/50 samples. Source: own elaboration*

| Coefficients | 0/100 | 0/50 |
|---|---|---|
| $\beta_0$ | 6.1272 | 1.2448 |
| $\beta_1$ | -42.5638 | -1589.8230 |
| $\beta_2$ | -20.5895 | -519.5808 |
| $\beta_3$ | -33.0872 | 5.7575 |
| $\beta_4$ | 4.9317 | 4.9071 |
| $\beta_5$ | 6.1272 | 1.2448 |
| $R^2$ | 0.8718 | 0.6221 |

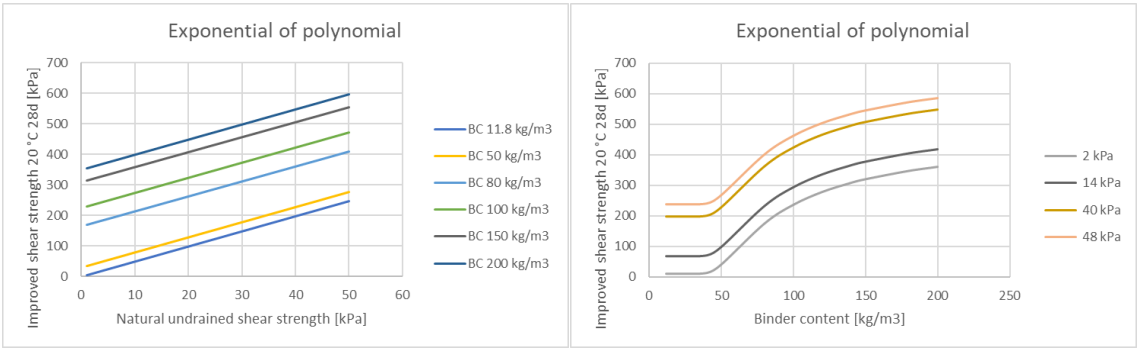


*Figure 59. Plots exponential of a polynomial for the 0/100 binder ratio case in the natural undrained shear strength (left) and binder content (right) space. Source: own elaboration.*

As the present function is considered to properly represent the available data, it is important to check whether the selected set of fitting coefficients are indeed correctly estimating the improved shear strength, for this purpose, a similar procedure to that of section 3.2.2.3.1 is followed. A normalized deviation is calculated obtaining an average value of 0.32 and a standard deviation of 0.38 thus confirming that the recommended values for coefficient of variation are also suitable for this case.

The estimated values are plotted alongside with the measured values of the improved shear strength, this can be observed in Figure 60 and Figure 61 for the 0/100 and 50/50 binder ratio respectively. Again, lines showing upper and lower limits for a variation of both 30 % and 60 % are included to express the possible variability.

For the 0/100 binder ratio case, if a coefficient of variation of 30 % is assumed, more than 85 % of the data points are inside the area of estimation, whereas 98 % of the data points are inside the prediction area when a coefficient of variation of 60 % is considered. For the 50/50 binder ratio case, 74 % of the data points are inside the prediction area when assuming a coefficient of variation value of 30 %; when assuming a value of 60 %, 94 % of the data points are inside the estimation area. With the obtained results, it is considered that with the set of coefficients available, a good estimation of the improved shear strength can be performed.

- *Exponential recovery:* the exponential recovery function for the binder content is implemented with a linear expression of the natural undrained shear strength. This function was expected to yield good results, but the obtained fit does not properly match neither the data nor the phenomenon, therefore these results are not included.

- *Ratio of exponential decay and exponential recovery:* this function emulated the behavior of the hyperbolic tangent, which, in principle should yield an "S" shaped plot. Contrary to what was expected, this expression resulted in a quasi-linear plot, therefore this approach is also disregarded as more simple expression could be used.

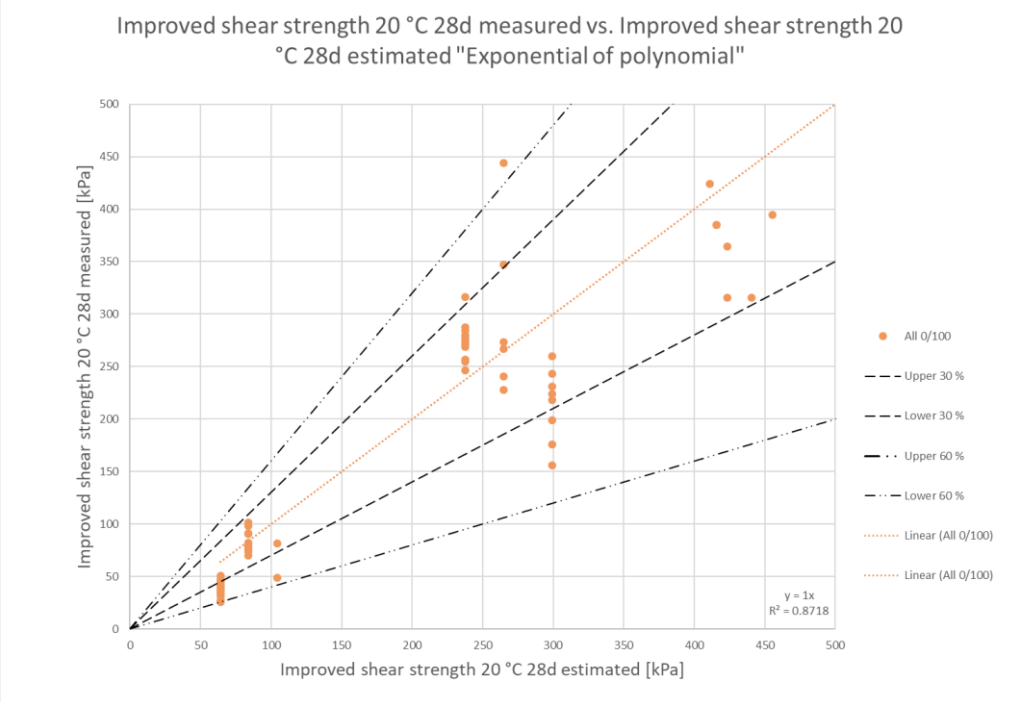


*Figure 60. Measured vs. estimated improved shear strength of the exponential of a polynomial function for the 0/100 binder ratio case. Source: own elaboration.*

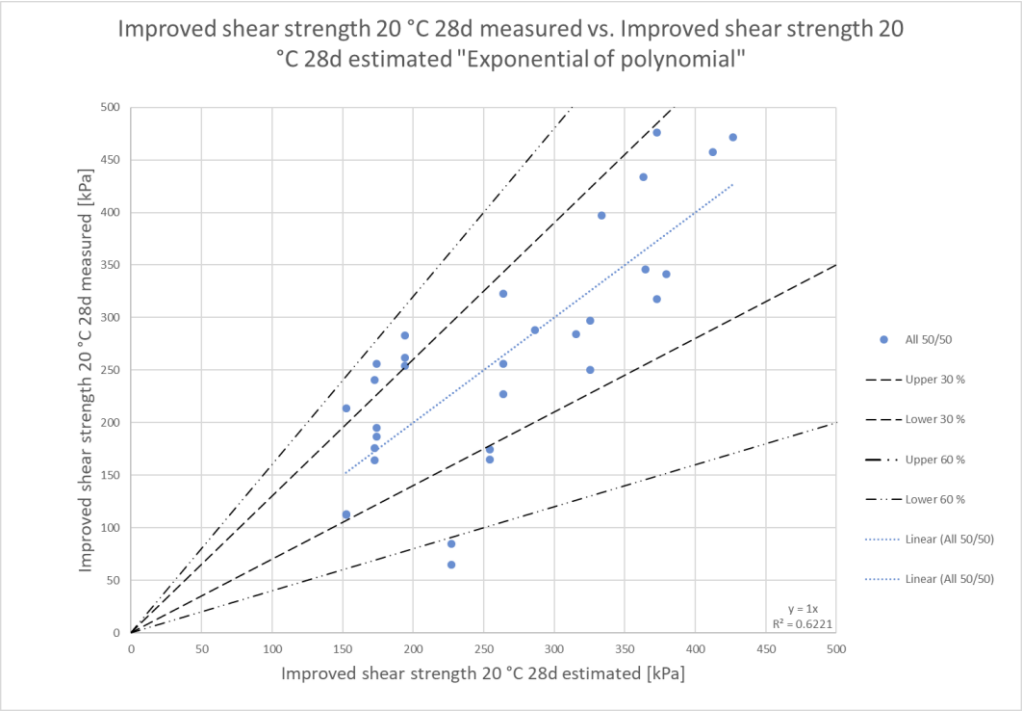


*Figure 61. Measured vs. estimated improved shear strength of the exponential of a polynomial function for the 50/50 binder ratio case. Source: own elaboration.*

#### *3.2.2.4. Comparison between obtained expressions*

After testing several mathematical expressions to fit the available data using the binder content and the natural undrained shear strength as independent variables to estimate the improved undrained shear strength coming from unconfined compression tests, only two proved to be of real use. As observed in section 3.2.2.3.1 and section 3.2.2.3.3, both a linear expression and an exponential of a polynomial along with a linear function can estimate the improved shear strength of the available data by only using the binder content and the natural shear strength as independent variables.

These mathematical expressions should be implemented with care because only a limited dataset is available for the determination of the expressions. Moreover, these expressions should only be used with Scandinavian soils which properties are within the range of the available dataset of the present study. The ranges within which these expressions should be used differ for 0/100 and 50/50 samples and are listed below:

- 0/100 binder ratio:
  - Binder content: from 11 kg/m$^3$ up to 200 kg/m$^3$.
  - Natural undrained shear strength: from 8 kPa to 51 kPa.
- 50/50 binder ratio:
  - Binder content: from 70 kg/m$^3$ up to 120 kg/m$^3$.
  - Natural undrained shear strength: from 8 kPa to 51 kPa.

Among the two mathematical expressions, the exponential of a polynomial including the binder content along with a first degree expression of the natural undrained shear strength is preferred because it is considered that it emulates better the expected physical phenomenon and yields slightly better results for the 50/50 binder ratio samples.

# 4. FULL-SCALE TEST MODELLING USING PLAXIS 2D

## 4.1. Methodology

Full-scale tests allow investigating almost any system in-place behavior of any possible engineered application. For the present study, it is relevant to increase the understanding between the connection of a laboratory or field-measured critical property, like the shear strength, and its influence on the final system behavior. For the case of stabilized soil placed in the passive zone of an excavation, the Swedish guideline states that the design value should be determined by means of a laboratory study while limiting the maximum value to use; in addition to this fact, the FHWA deep mixing manual also suggests the use of a laboratory study to determine the design values for stabilized soil properties but contrary to the Swedish case, it does not establish maximum values for strength. Moreover, the FHWA manual also suggest conducting full-scale tests to test the in-place performance of the material and its expected behavior when subjected to service conditions.

### 4.1.1. Modelled full-scale tests

The motivation to perform a 2D finite analysis of a full-scale test comes from the necessity to better understand the connection between results from laboratory and field tests, and the in-place behavior of the material assessed using a certain constitutive model, in order to be able to properly simulate the system behavior under the specified loading conditions. Two full-scale tests were performed in Sweden, in the proximities of the town of Enköping, about 70 km northwest of Stockholm (Ignat et al., 2016), geotechnical conditions at site are presented in Figure 62. Measurements from both stresses and displacements were taken, the results of these tests will be used for the calibration of the model using the Plaxis 2D software. The general top view of the tests can be observed in Figure 63 whereas the sensor placement is presented in Figure 64.

The sensors used for the calibration will be the strain gauges in the struts, which the author reports as a load; and the inclinometers, which are placed in the active and passive side of the excavation. Regarding the inclinometers, there are in total six per site, two in the active side of the excavation, 0.50 m behind the sheet pile wall; and four in the passive side of the excavation, of which two are placed inside the DSM columns at 1.50 m and 4.00 m away from the sheet pile wall, and the two remaining are placed in the unimproved soil at the same distances (Ignat et al., 2016). As only the inclinometers placed in the active side and the two placed at 1.50 m away from the sheet pile wall measure displacement due to the slip surface shape, the two remaining inclinometers placed at 4.00 m away from the sheet pile wall are disregarded.

It has to be noted that the principal difference between the two tests is the DSM rib center-to-center distance; in the first test is 3.00 m and in the second test is 1.50 m, from now on the former will be referred as Test 1 and the latter as Test 2. In both tests, the DSM ribs consist of overlapping soil-cement columns installed using a binder content of 120 kg/m$^3$ with 50 % quicklime and 50 % Portland cement. Each rib consists of a single row of 24 columns, each with a diameter of 0.60 m and a center-to-center distance of 0.50 m. The results of laboratory tests performed for this site on laboratory mixed samples are presented in section 3.2.1.1.

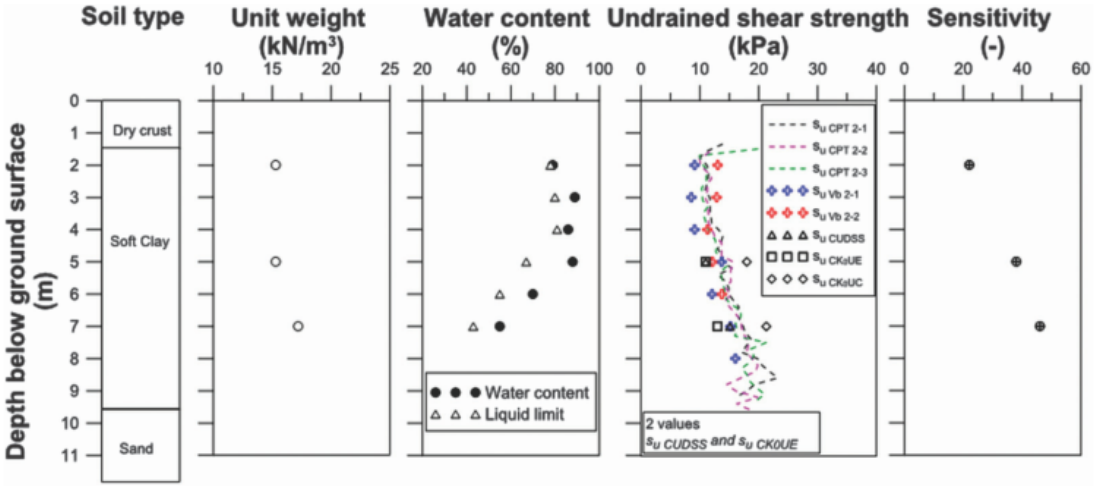


*Figure 62. Geotechnical conditions at test site. Source:* (Ignat et al., 2016).

As retaining walls, each test used two steel sheet pile walls, type VL604, parallel to each other with a crest length of 19.80 m, installed to a depth of 7.00 m on the loading side and to 7.50 m on the opposite side. The excavation area has a length of 14.00 m and a width of 12.00 m. The excavation was braced using HEB 300 steel beams at a level 1.00 m below surface and with a center-to-center distance of 3.00 to 3.50 m. The excavation between the sheet pile walls was planned to be 4.50 m depth with open slopes at each end of the excavation. Loading was performed using two containers placed over a square load distribution platform of 6.00 m by side.

For both tests, the loading was performed after the full completion of the excavation and the measure also includes the load of the load distribution platform. Test 1 failed at a load of 40.6 kPa with no modification of the excavation geometry. On the other hand, the excavation depth had to be changed for Test 2, because even when containers were fully loaded, failure did not appear. Failure was induced in Test 2 by increasing the excavation depth from 4.50 to 5.00 m and applying a load of 56.2 kPa. The failure mechanism in Test 1 was a rotational stability failure of the sheet pile wall, resulting in heave at the excavation bottom and settlements on the active side of the wall. A slip surface developed at failure starting at 6.00 m from the sheet pile wall to the active side, approximately at the far edge of the load distribution platform, and the toe of the slip surface located at about 3.00 m to 3.50 m from the wall on the passive side, a simulation of this slip surface can be observed in Figure 73. Test 2 presented a similar failure mechanism, but in contrast to Test 1, the failure in Test 2 was less brittle with stepwise increasing deformations (Ignat et al., 2016).

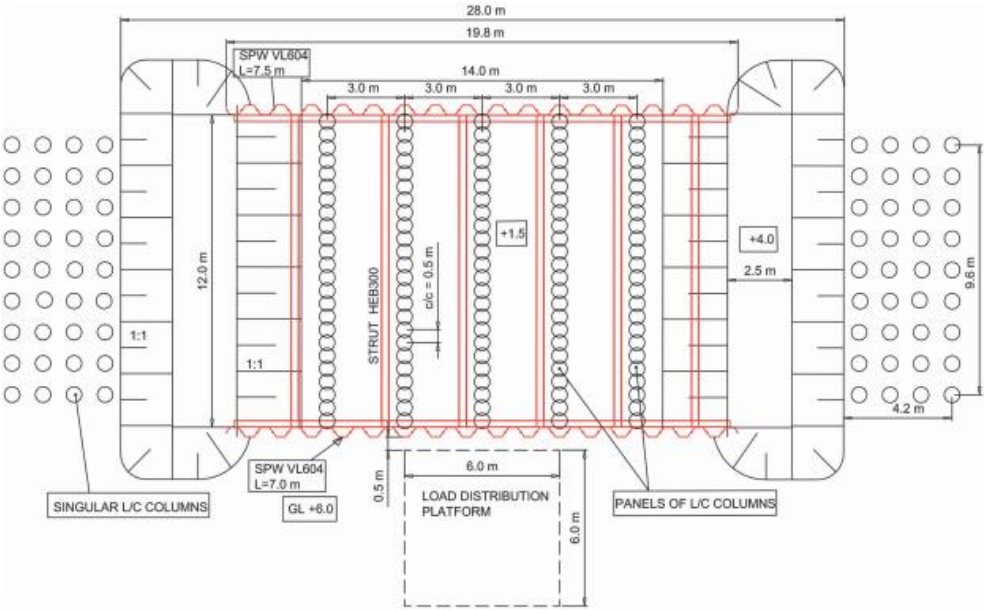


*Figure 63. Plan view of the full-scale tests. GL, ground level; L/C, lime-cement. Source:* (Ignat et al., 2016).

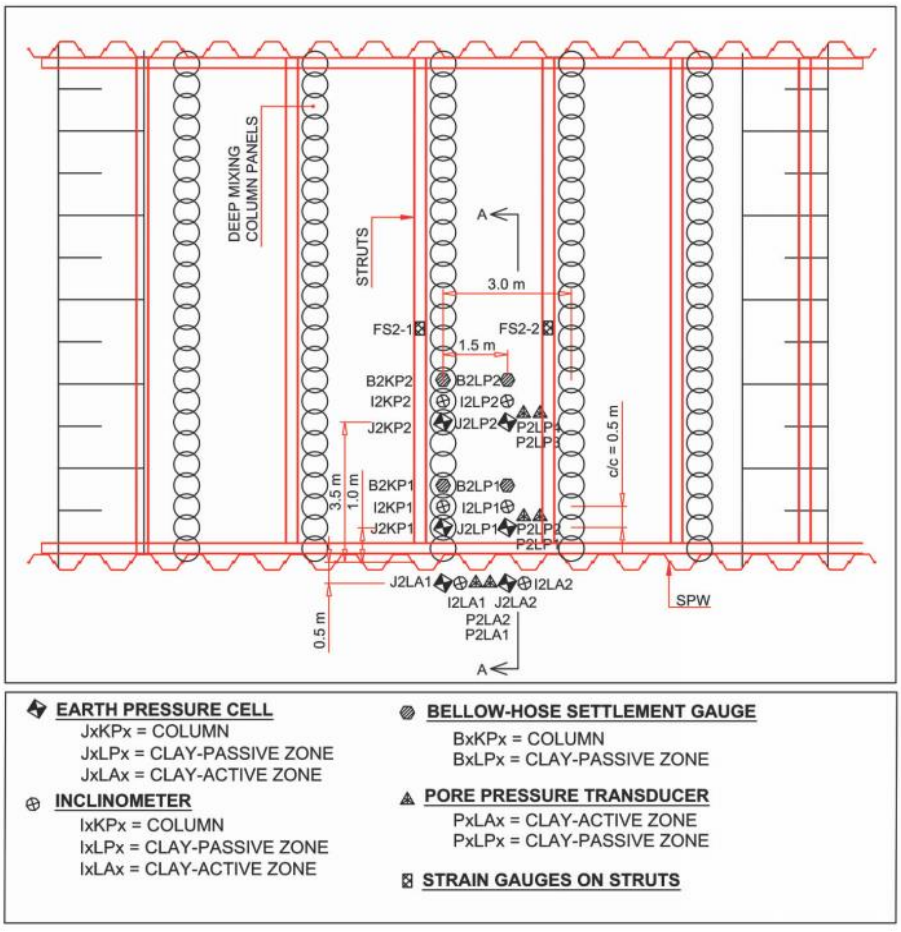


*Figure 64. Location of in situ instrumentation. Source:* (Ignat et al., 2016).

### 4.1.2. Model layout

The first step to model the full-scale test, is to define the ground layering of the site, this is done by interpreting the given geotechnical conditions at the test site (Ignat et al., 2016), presented in the previous section; it is observed that the ground level is at about +6.00 m and the excavation goes down to +1.50 m (or +1.00 m for Test 2), meaning 4.50 m depth (or 5.00 m for Test 2), the groundwater level was measured to be at about 0.50 m below the ground surface. The identified soil layers and the most relevant material properties to be used are shown in Table 20, the strength properties are obtained from Figure 62 and the stiffness properties are the result of the calibration process presented in section 4.2.2.1.2. The model dimensions set in Plaxis are 35 m width by 12 m depth. From the test layout presented in the previous section, it is observed that the excavation consisted of two sheet pile walls type VL604 parallel to each other such that the excavation width is 12 m; the sheet pile on the loading side was placed up to a depth of 7.00 m, whereas on the opposite side, the wall was placed up to 7.50 m depth, model implemented in Plaxis 2D can be observed in Figure 65. Steel HEB 300 beams were used for bracing, installed at 1.00 m below ground level and a center-to-center distance of 3.00 m and 3.50 are considered. The properties of the structural elements can be observed in Table 21.

### 4.1.3. Composite material approach

The installed soil-cement columns as bottom panels for passive support and the surrounding clay are modelled as a composite material with weighted strength and stiffness properties (Andromalos et al., 2001; Charbit, 2009; Trafikverket, 2011), therefore, a special material is needed in a 2D model to include the composite properties and to replace the soil cluster in the passive zone of the excavation, the weighted properties are calculated using Equation (12), presented in section 2.7.7. To calculate the area replacement ratio, the procedure followed by the reported full-scale test is used (Ignat et al., 2015), the result of this approach was confirmed by using a graphical method; both methods lead to similar results; Test 1 has a ratio of 18 % and Test 2 has a ratio of 36 %. The initial stiffness of the stabilized material was selected to be 250 time its peak strength as suggested in earlier studies (Navin & Filz, 2005; Trafikverket, 2011); this assumed value will be checked as it has also been reported that the horizontal stiffness of the improved soil is higher than the vertical (Hanson, 2012).

The composite material is modelled with both drained and undrained properties to assess the influence of each approach and the suggested values for computing drained properties from undrained test results (Helen Åhnberg, 2006, 2007; Ignat, 2018). The Mohr-Coulomb constitutive model was selected as the appropriate model to simulate the behavior of the composite material because the stabilized soil is a rather brittle material where failure occurs as a sudden decrease of strength at relatively low strain (H. Åhnberg & Johansson, 2005; Helen Åhnberg, 2006, 2007; S Baker et al., 2005; Ignat, 2015). A calculation example of the composite shear strength using Equation (12) will be presented below with some assumed values:

- In order to calculate the composite shear strength to be used in a 2D model, Equation (12) is used:

$$s_{u,comp} = s_{u,col} \cdot a + s_{u,soil} \cdot (1 - a)$$

- Considering an area replacement ratio of 18 % (for Test 1), an improved shear strength of 220 kPa and a natural undrained shear strength of 10 kPa, the resulting composite shear strength can be computed as:

$$s_{u,comp} = 220\ kPa \cdot \frac{18}{100} + 10 \cdot \left(1 - \frac{18}{100}\right) = 39.6\ kPa + 8.2\ kPa = 47.8\ kPa$$

- A similar procedure can be followed to calculate any composite stiffness or strength property.

### 4.1.4. Model construction stages

The amount of construction stages was selected based on the information provided by the reported full-scale test, a total of 12 phases among construction and loading stages of the system was implemented with an additional safety factor calculation. The phase names along with a brief description are presented below:

- Initial phase: model creation, material set up and generation of initial stresses.
- Installation DSM: the composite DSM material is activated in its correspondent soil cluster.
- Installation SPW: sheet pile walls and interfaces activated.
- Excavation +4.00m: soil cluster from +6.00 m to +4.00 m deactivated, lowering local water level inside the excavation.
- Strut installation: activation of the strut.
- Excavation +2.00m: soil cluster from +4.00 m to +2.00 m deactivated, lowering local water level inside the excavation.
- Excavation +1.50m (or +1.00m): soil cluster from +2.00 m to +1.50 m (or +1.00 m) deactivated, lowering local water level inside the excavation.
- Active surcharge loading 25 %: specified load activated.
- Active surcharge loading 50 %: specified load activated.
- Active surcharge loading 80 %: specified load activated.
- Active surcharge loading 100 %: specified load activated. This phase can be observed in Figure 65.
- Safety: safety factor calculation performed.

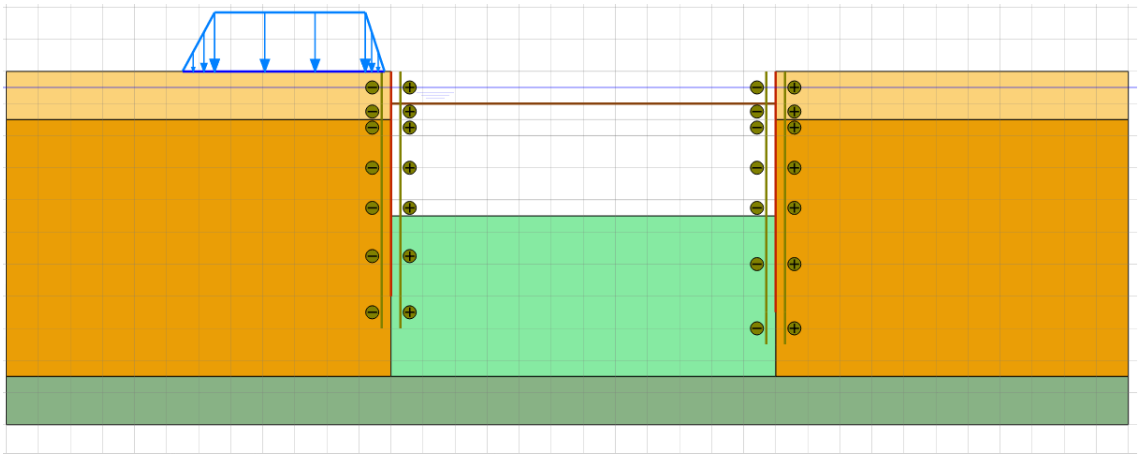

*Figure 65. Model layout in the loading stage. Source: own elaboration using Plaxis 2D.*

*Table 20. Used parameters for soil layers for the finite element model. Source: own elaboration from reported geotechnical conditions in (Ignat et al., 2016).*

| | | | | | | |
|---|---|---|---|---|---|---|
| General | Layers | | # | 1 | 2 | 3 |
| | | | **Material** | **Clay, hard crust** | **Clay, soft, sensitive** | **Sand/silt** |
| | | | Top of the layer [m] | 6.00 | 4.50 | -3.50 |
| | Material set | | Material model | Mohr-Coulomb | Mohr-Coulomb | Hardening soil |
| | | | Drainage type | Undrained (B) | Undrained (B) | Drained |
| | General properties | | γ_unsat [kN/m3] | 18 | 16.5 | 18 |
| | | | γ_sat [kN/m3] | 18 | 16.5 | 20 |
| Parameters | Stiffness | | E_50,ref [kN/m2] | | | 75000 |
| | | | E_eod,ref [kN/m2] | | | 75000 |
| | | | E_ur,ref [kN/m2] | | | 225000 |
| | | | Power m | | | 0.5 |
| | | | E' [kN/m2] | 3500 | 2500 | |
| | | | v' | 0.35 | 0.40 | |
| | Alternatives | | G [kN/m2] | 1296 | 892.9 | |
| | | | E_oed [kN/m2] | 5617 | 5357 | |
| | Strength | | s_u,ref [kPa] | 40 | 10 | |
| | | | phi_u [°] | 0 | 0 | |
| | | | c' [kPa] | | | 0 |
| | | | phi' [°] | | | 38 |
| | | | psi [°] | 0 | 0 | 0 |
| | Advanced | Stiffness | v'_ur | | | 0.2 |
| | | | p_ref [kN/m2] | | | 100 |
| | | | K_0,nc | | | 0.3843 |
| | | | E'_inc [kN/m2/m] | 0 | 300 | |
| | | | y_ref [m] | 6 | 5 | |
| | | Strength | c'_inc [kN/m2] | | | 0 |
| | | | s_u,inc [kPa/m] | 0 | 1.3 | |
| | | | y_ref [m] | 6 | 5 | 0 |
| | | | R_f | | | 0.9 |
| | | | Tension cut-off | | | x |
| | | | Tensile strength [kPa] | | | 0 |
| Interfaces | Strength | | Strength | Manual | Manual | Rigid |
| | | | R_inter | 0.5 | 0.6 | 1 |

*Table 21. Structural elements data. Source: own elaboration from reported structural elements (Ignat et al., 2016).*

| **Element** | **Type** | **Unit weight [kg/m3]** | **Young's modulus [kPa]** | **Wy [cm3 /m]** | **Iy [cm4/m ]** | **Weight [kg/ml]** | **Weight [kg/m2]** | **Area [m2 /m]** | **EA [kN/m]** | **EI [kN*m2 /m]** |
|---|---|---|---|---|---|---|---|---|---|---|
| **Sheet pile** | VL604 | 7800 | 2.10E+08 | 1618 | 31548 | 73.1 | 121.8 | 0.01 5615 | 3.28E+06 | 66250.8 |
| **Strut** | HEB300 | 7800 | 2.10E+08 | | | 117 | | 0.01 491 | 3.13E+06 | |

### 4.1.5. Simulations and back-calculation procedure

It is of importance to define the relation of the measured laboratory and field strength and stiffness properties, and the design value to be used in a finite element model to properly simulate the system behavior at failure, therefore, a set of simulations aimed to investigate the model response to a variation of the strength properties of the composite material, specially the undrained shear strength and the cohesion intercept, due to the fact that the internal friction angle is considered to be constant regardless of the strength level (Helen Åhnberg, 2006; Ignat, 2018). As mentioned in section 4.1.1, results from strain gauges in the struts and inclinometers placed in both active and passive side of the excavation will be used to back-calculate the composite material properties.

The first step of the back-calculation of the properties using Plaxis 2D will be aimed to determine the required composite shear strength for the system not to fail. To determine this condition, the model is tested using different composite shear strengths and the behavior is analyzed. If the model has already failed, the calculation will stop and the message “soil body seems to collapse” will be received. Even though Plaxis offers this capability, it is decided to determine the failure condition using a different method, by analyzing the relative shear plot given by Plaxis, especially near the loaded sheet pile wall, and the safety factor obtained in the safety factor calculation stage.

In the present research, it is considered that the composite material has failed when a considerable area of the relative shear plot has reached the unity in the final loading stage, such as in Figure 66; and the safety factor obtained in the safety factor calculation stage is close to the unity. The former because, as stated in section 4.1.3, stabilized soil is a rather brittle material where failure occurs as a sudden decrease of strength at relatively low strain (H. Åhnberg & Johansson, 2005; Helen Åhnberg, 2006, 2007; S Baker et al., 2005; Ignat, 2015), meaning that when a considerable volume of improved soil has mobilized its maximum strength it will fail and with it, the whole system. When the composite shear strength at which the system fails is determined, it is back-calculated using Equation (12) with the corresponding area replacement ratio per test and the natural undrained shear strength of the surrounding clay.

As a second step, the strut force reported is compared to the strut force obtained in the Plaxis calculation. The final step is to compare deformations of the sheet pile wall and the composite DSM body only in the loading stage because it is the critical stage, this is done graphically. The process of calibrating the stiffness of the system is iterative and has to be performed by seeking the best fit for the three available inclinometer measurements. This process is rather complex for several reasons:

- The inclinometers are only able to measure the deflection relative to its own position, meaning that if a mass movement exists, this translation of the inclinometer will not be recorded in the measurements unless an additional positioning is measured with an external tool.
- There are three available inclinometer measurements for the calibration and are located at different locations in the system. One located at 0.50 m behind the retaining wall, another located at 1.50 m from the wall in the passive side of the excavation in the natural soil and a last one also at 1.50 m from the retaining wall in the passive side of the excavation but in the improved soil. For the case of the composite soil, the aim is to obtain a deformation that matches an intermediate value of the reported deformations of both the unimproved and improved soil because the passive zone is modelled as a composite material while also

maintaining a match with the soil behind the wall; therefore an average fit for the three available inclinometers is aimed. The abovementioned process is done by varying the reference Young's modulus and Young's modulus gradient of the first layer (dry crust), the second layer (soft clay) and the composite soil until a similar shape and values are obtained.

## 4.2. Results

### 4.2.1. Determining failure condition

When a failure condition has been reached in Plaxis 2D, the message "soil body seems to collapse" is received during the model calculation. Nevertheless, the stabilized material is considered to be a much stiffer material than the natural soil, therefore a different failure criterion has to be implemented to be able to accurately describe the system behavior. When modelling the composite material for Test 1 with a stabilized material shear strength of 140 kPa, meaning a composite strength of 37 kPa, the result of the relative mobilized shear is presented in Figure 66. It is observed that a failure mechanism is triggering from the sheet pile towards the surface, but it has not reached the top of the stabilized material. In simulations where the strength values are lower, the mobilized relative shear is observed to reach its maximum value in almost all the stabilized soil cluster. This same procedure is also used to determine the failure composite strength for Test 2.

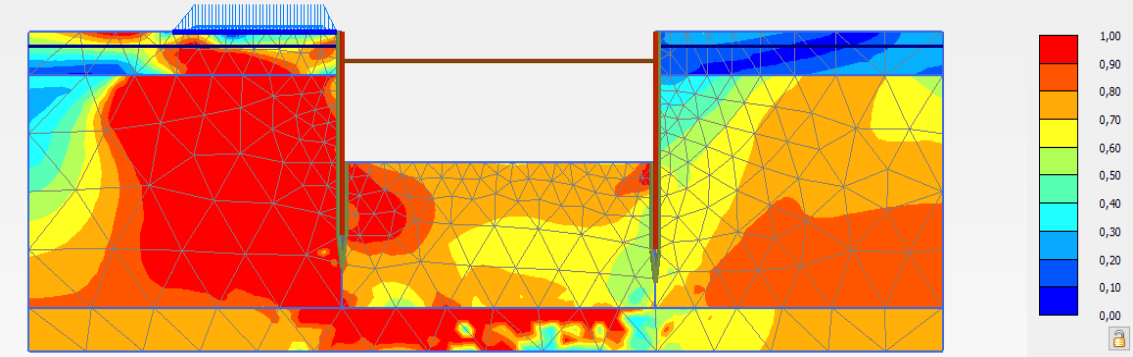


*Figure 66. Relative mobilized shear for a composite strength of 37 kPa in Test 1. Source: own elaboration using Plaxis 2D.*

### 4.2.2. Model calibration

In the present section, the procedure presented in section 4.1.5 is used to calibrate the strength and stiffness properties of the composite soil, meaning that the composite shear strength required for the model not to fail is determined prior to the model stiffness calibration; after the stiffness is calibrated, the influence of the strength parameter is checked. In the back-calculation process it is recognized the influence of the 3D effects as a 2D model is a plain strain situation and punctual effects as the positioning of the struts or the DSM column panels cannot be taken into account, as well as loading conditions; nevertheless, it has been proven that 2D models can, to a certain extent, be used to analyze 3D systems (Ignat et al., 2015). For each calibration, the corresponding discussion and conclusions will be exposed. The back-calculated properties of the composite material in undrained condition of Test 1 are presented in Table 22, the properties for the composite material of Test 2 will, in general, be the same, except for the shear strength and stiffness properties.

*Table 22. Back-calculated undrained properties of the composite material for Test 1. Source: own elaboration.*

| | | | |
|---|---|---|---|
| **General** | Material set | Material model | Mohr-Coulomb |
| | | Drainage type | Non-porous |
| | General properties | γ_unsat [kN/m3] | 16.5 |
| | | γ_sat [kN/m3] | 16.5 |
| **Parameters** | Stiffness | E [kN/m2] | 35000 |
| | | v [-] | 0.33 |
| | | E_inc [kN/m2/m] | 7000 |
| | | γ_ref [m] | 1.50 |
| | Alternatives | G [kN/m2] | 2989 |
| | | E_oed [kN/m2] | 11780 |
| | Strength | c' [kPa] | 36.7 |
| | | phi' [°] | 0 |
| | | psi [°] | 0 |
| **Interfaces** | Strength | Strength | Manual |
| | | R_inter | 0.8 |

#### *4.2.2.1. Composite material with undrained properties*

##### 4.2.2.1.1. Strength calibration

In this first step, several composite shear strengths are tested until a concentrated relative shear area equal to the unity is observed near the sheet pile wall and the safety factor has decreased to a value close to the unity, the general procedure is explained in section 4.2.1. It is of interest to obtain the composite undrained shear strength for the model not to fail, because at this point the mobilized shear strength at failure is equal to the input parameter in the 2D model, therefore this value can be compared to the obtained laboratory and field tests, as well as with the estimated strength calculated using the procedure proposed in the present research. The composite shear strengths for the model not to fail, along with the natural shear strength of the clay, the area improvement ratio and the back-calculated shear strength of the improved soil for each test are presented in Table 23.

*Table 23. Back-calculated values of improved shear strength. Source: own elaboration.*

| | $s_{u,comp}\ [kPa]$ | $s_{u,soil}\ [kPa]$ | $a\ [\%]$ | $s_{u,col}\ [kPa]$ |
|---|---|---|---|---|
| **TEST 1** | 37 | 14 | 18 | **140** |
| **TEST 2** | 76 | 14 | 36 | **185** |

In order to analyze the back-calculated strengths for Test 1 and Test 2, it is necessary to compare them to the measured laboratory and field values, and the estimated values obtained with the suggested mathematical expression of section 3.2.2. As two values for the natural undrained shear strength are available from the site data, the estimated strength values using the exponential of a polynomial expression range from 254 kPa to 264 kPa, if the suggested coefficient of variation presented in section 3.2, which was also checked with the available data, is assumed as a value of 0.30, yielding to expected lower values which range from 178 kPa and 185 kPa, whereas the expected higher values range from 330 kPa and 343 kPa. From laboratory unconfined compression test results on mixed samples from the site presented in section 3.2.1.1, the mean undrained shear

strength of the laboratory tests referred to 28 days curing time and 20 °C curing temperature is 229 kPa with a standard deviation of 64.54 kPa, yielding a coefficient of variation of 0.28.

For the full-scale test, several KPS (push-in resistance test), described in section 2.6.2.1, were performed on different installed columns 10 to 12 days after installation of the DSM column panels, the test results with the highlighted area of interest can be observed in Figure 67. From these tests, the minimum value is around 130 kPa, the mean value is approximately 270 kPa, and the maximum measured value is around 440 kPa. It has to be noted that these values are at 10-12 curing days, therefore, they have to be converted to 28 curing days values using Equation (1), resulting in a minimum value of 158 kPa, a mean of 328 kPa and a maximum of 534 kPa. All the aforementioned quantities are summarized in Table 24. It is important to note that in the reported full-scale test, it is not clearly stated what is the time span between installation and loading of the improved soil, therefore 28 curing days is assumed.

*Table 24. Undrained shear strength obtained by unconfined compression tests, KPS and average of the estimation referred to 28 days curing time (from exponential of a polynomial); values in kPa. Source: own elaboration from* (Ignat et al., 2016)

| **Unconfined compression test** | |
|---|---|
| Mean | 229.02 |
| Mean + σ | 293.56 |
| Mean - σ | 164.48 |
| **KPS** | |
| Mean | 327.90 |
| Max | 534.36 |
| Min | 157.88 |
| **Estimation (from the exponential of a polynomial)** | |
| Mean | 259 |
| Mean + σ | 337 |
| Mean - σ | 181 |

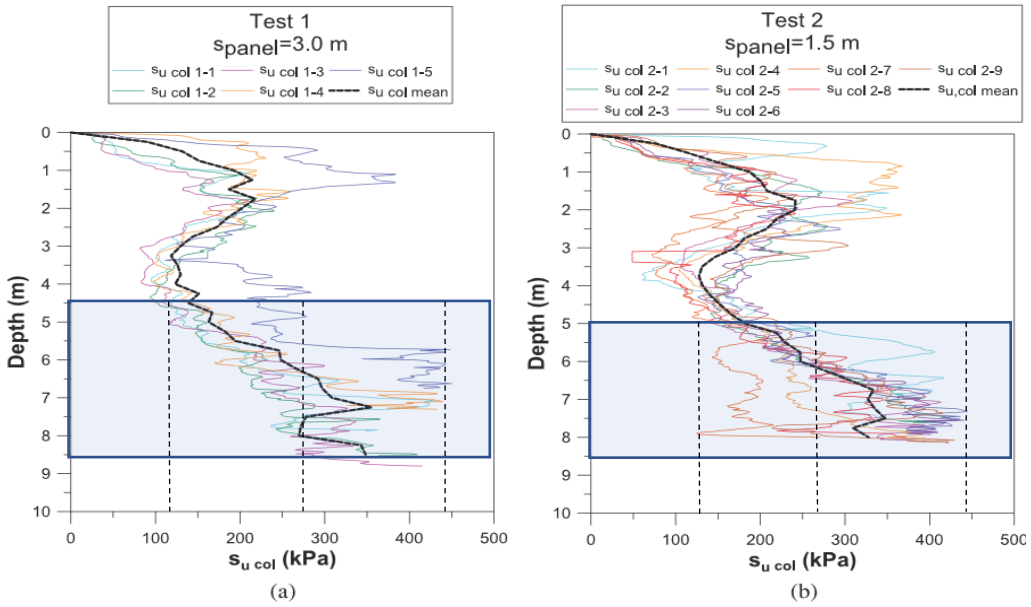


*Figure 67. Results of column penetration tests for (a) Test 1 and (b) Test 2. Source:* (Ignat et al., 2016).

It is important to point out that the back-calculated shear strength from Test 1 is lower than the one from Test 2, fact that was unexpected because, as Figure 67 clearly shows, both sites have similar quality of mixed material, but can be explained by the higher horizontal deformation of the improved soil present in Test 2 to that of Test 1, leading the former to mobilized more strength than the latter. Moreover, both values were back-calculated using Equation (12), meaning that in principle both should yield the same result. This discrepancy between results must be caused by reasons others than mixing quality, the ones considered to have the most impact on the obtained outcomes are:

- Strength model: the strength properties of the composite soil used in the Plaxis 2D model are calculated as a weighted average of the strength properties of the improved and unimproved soil using Equation (12), which assumes that all the strength of both the improved and unimproved soil can be mobilized simultaneously and completely, a situation that is most likely not occurring and that has been analyzed in previous research (Kitazume & Terashi, 2013; Sukpunya & Jotisankasa, 2016). To assess this possibility, Equation (13), which includes a term to reduce the allowable mobilized strength in the improved and unimproved soil, can be used. The magnitude of the term to reduce the strength that can be mobilized in the unimproved soil is the ratio of the undrained shear strength of soft soil mobilized at the peak shear strength of stabilized soil and the undrained shear strength of the soil. The magnitude of this term can be easily determined by comparing the stress-strain curves of the two materials, nevertheless, it is necessary to point out that for the case of an excavation, the strain that the materials experience might not be of the same magnitude, and are influenced by loading conditions and the retaining structure used. On the other hand, the term to reduce the improved soil strength has been proven to depend on the loading condition of the entire system and on the column installation geometry (Sukpunya & Jotisankasa, 2016); for the specific case of laterally loading column panels, this factor has not been quantified.
- Lower strength constraint: Comparing the back-calculated shear strength values obtained from the Plaxis 2D simulations, which can be observed in Table 23, the values obtained from laboratory and field tests, and estimated values, which are summarized in Table 24, it is clear that the back-calculated shear strength values are lower than the mean values obtained for each of the three methods. The back-calculated shear strength values tend to the mean shear strength value minus a standard deviation of the reported measured and estimated values, a fact that suggests that the allowable or available shear strength of the improved soil could be limited to the lowest measured or estimated shear strength value.
- System geometry: observing Table 23, it is evident that the back-calculated shear strength of Test 1 is lower than that of Test 2. As mentioned before, the only main difference of the two tests is the column panel center-to-center distance, in Test 1 is 3.00 m and in Test 2 is 1.50 m, meaning that the area replacement ratio for Test 2 is higher than for Test 1. This distance along with the selected retaining structure can be causing the low mobilized shear strength at failure. For both full-scale tests, the retaining structure is a braced sheet pile wall, which being a flexible structural element, can bend towards the less stiff unimproved soil and cause it to reach failure first and therefore cause the system to collapse with it. Considering Test 1, this could be the case, because as observed in Figure 68, the clay presents higher horizontal deformations than the DSM column. Observing Figure 69, which

refers to Test 2, it is observed that the improved material is experiencing a higher horizontal deformation than the unimproved soil and the back-calculated shear strength is higher in this situation, fact that suggests that the geometry and the selected structural element as retaining wall have an influence on the admissible shear strength.

It is clear that at least one of the abovementioned approaches is necessary to be considered for an excavation project, but most likely, a combination of the three situations is to control the allowable shear strength to be used for design. From the results, it seems that the allowable undrained shear strength will tend to the improved soil strength as the panels are closer together, but this effect should be further studied when a block improvement full-scale test, meaning 100 % of area improvement ratio, is tested.

#### 4.2.2.1.2. Stiffness calibration

As both the strut force and the horizontal deformations are affected by each of the stiffnesses present in the system, these two calibrations are done simultaneously as mentioned in section 4.1.5. The displacements to be calibrated are the ones measured during loading, in Figure 68 and Figure 69 the measured horizontal displacements at the end of the loading stage are highlighted and marked with a "(1)"; measurements during failure are disregarded because this progressive failure is not intended to be predicted by the model and also the measurements of the inclinometers might be corrupted due to the wall collapse. To compare the deformations calculated by Plaxis and the measured values in the loading stage only, the horizontal displacement plots presented in the full-scale report (Ignat et al., 2016) are overlapped with the values obtained from Plaxis at different percentages of load.

As stated in section 4.1.5, the horizontal displacement calibration is done by varying the reference Young's modulus and Young's modulus gradient of the first layer (dry crust), the second layer (soft clay) and the composite soil until a similar shape and values are obtained. The composite stiffness parameters used to calibrate the horizontal displacements are presented in Table 25, in this table, only the parameters for the composite soil are included because the soil parameters shown in Table 20 in section 4.1.1 include the result of the present procedure. The result of this calibration can be observed in Figure 68 for Test 1 and Figure 69 for Test 2. The measured and modelled strut forces for each test and each load condition are reported in Table 26.

*Table 25. Back-calculated composite stiffness properties. Source: own elaboration.*

| | $E_{50;ref;comp}\ [kPa]$ | $E_{50;inc;comp}\ [kPa/m]$ |
|---|---|---|
| **TEST 1** | 35000 | 7000 |
| **TEST 2** | 35000 | 8000 |

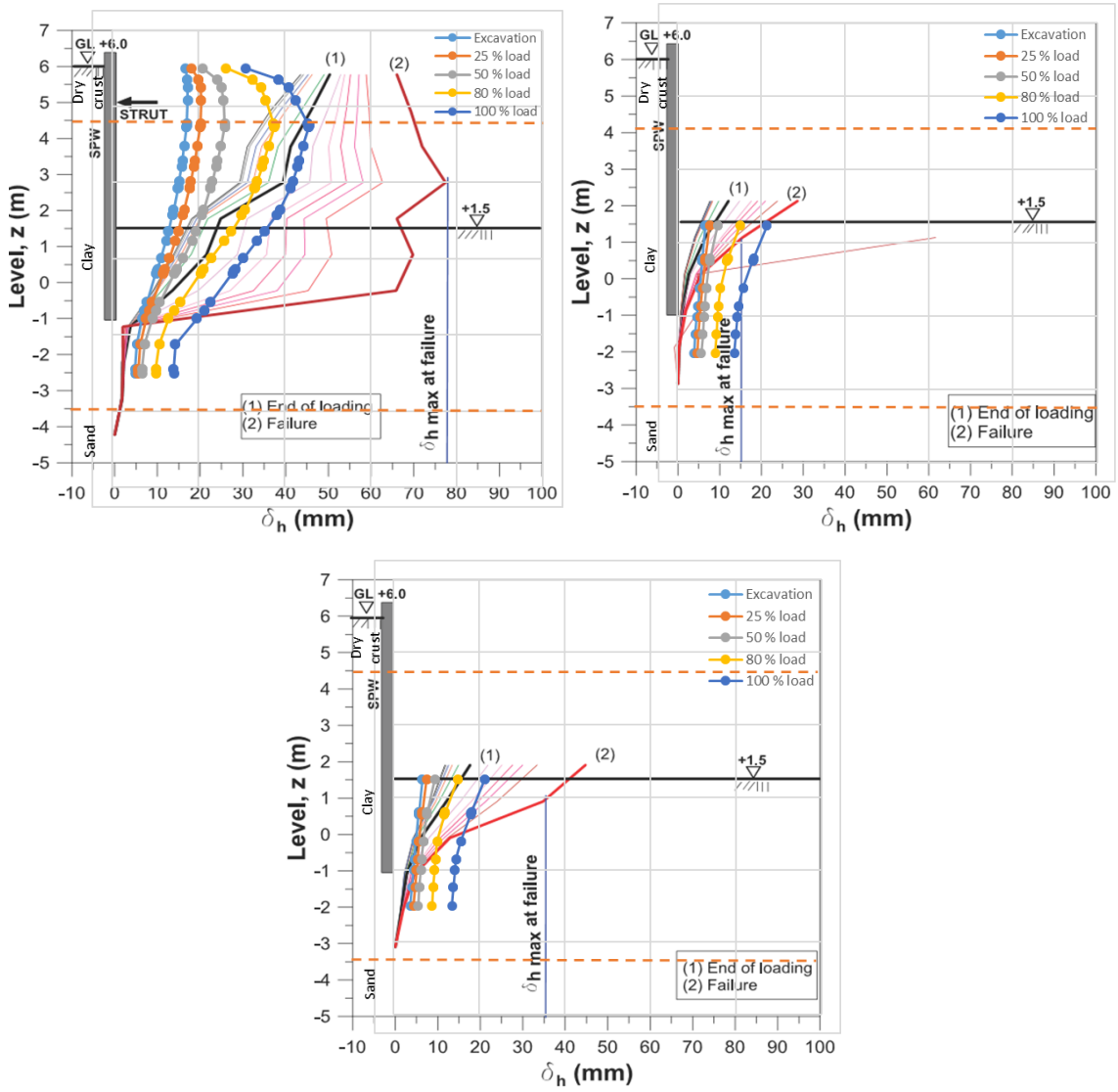


*Figure 68. Result of the stiffness calibration for Test 1 using strut spacing of 3.00 m in the active side 0.50 m behind the wall (left), DSM column (center) and the unimproved soil (right) 1.50 m away from the wall. Source: own elaboration over plots from* (Ignat et al., 2016).

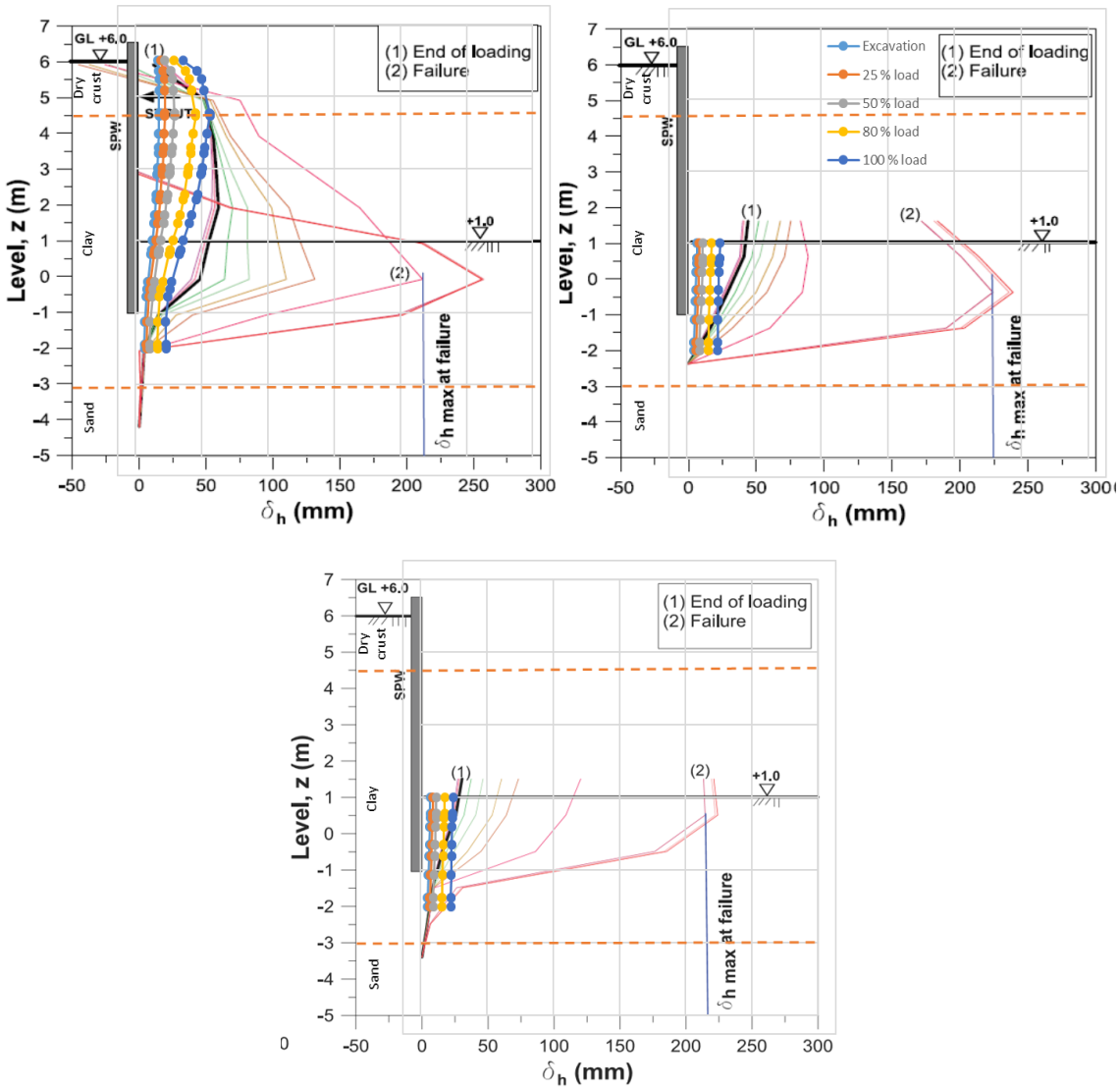


*Figure 69. Result of the stiffness calibration for Test 2 using strut spacing of 3.00 m in the active side 0.50 m behind the wall (left), DSM column (center) and the unimproved soil (right) 1.50 m away from the wall. Source: own elaboration over plots from* (Ignat et al., 2016).

*Table 26. Measured and modelled strut forces at different loading applied loads. Source: own elaboration (simulation) and* (Ignat et al., 2016) *(measured).*

| | | | | Strut spacing [m] | | |
|---|---|---|---|---|---|---|
| | | | | 3.00 | 3.50 | 4.00 |
| | % load | Load [kPa] | Measured [kN] | Simulated [kN] | | |
| Test 1 | 0 | 0 | 200 | 75 | 87 | 99 |
| | 25 | 10.2 | 210 | 100 | 116 | 132 |
| | 50 | 20.3 | 230 | 142 | 166 | 189 |
| | 80 | 32.5 | 290 | 219 | 255 | 291 |
| | 100 | 40.6 | 300 | 267 | 310 | 354 |

| | | | | | | |
|---|---|---|---|---|---|---|
| | 0 | 0 | 130 | 89 | 104 | 119 |
| | 25 | 14.05 | 150 | 118 | 137 | 156 |
| **Test 2** | 50 | 28.1 | 170 | 161 | 199 | 214 |
| | 80 | 44.96 | 350 | 250 | 307 | 333 |
| | 100 | 56.2 | 420 | 309 | 377 | 411 |

Figure 68 and Figure 69 show the horizontal displacements measured in the full-scale test overlapped with the simulation results of the same variable at different loading stages for Test 1 and Test 2 respectively. From the measured horizontal deformation of Test 1 in the active side, it is observed a cantilever-like deformation of the sheet pile wall, which is most likely happening because the inclinometer was not placed in line with one of the struts, and as the sheet pile is a flexible structural element, this bending can occur, especially considering the high center-to-center distance of the DSM column panels. The fact that a flexible structural element and a high center-to-center distance of the DSM column panels are present in this test, may be causing the higher horizontal deformation experienced by the unimproved soil in comparison with the improved soil.

Contrary to Test 1, in Test 2 the DSM column panel experiences more deformation than that of the unimproved soil, a fact that is caused by the lower center-to-center distance between panels, hence mobilizing more shear strength in the improved soil of Test 2 in comparison with the improved soil in Test 1. In Test 2, it seems that the inclinometer of the active side was placed almost in line with a strut, leading to measure the expected deformation behavior of a braced excavation.

Contrary to what was expected considering the result of the previous section, Table 25 shows that for both tests the composite stiffness properties at failure are virtually the same. This fact suggests that Equation (12) should also be revised regarding the calculation of stiffness properties, Table 27 shows the calculated composite stiffness using Equation (12), the Young's modulus of the improved soil is assumed to be 400 times its undrained shear strength obtained from unconfined compression tests; this high coefficient is used because, as proven in the present research, the horizontal stiffness of the improved material is higher than its vertical stiffness, therefore higher coefficients than presented in Table 2 should be used. It is observed that for the case of Test 2, the result is closer to the back-calculated value, meaning that in Test 2, the improved and unimproved soil are indeed working as a composite material. On the other hand, it is clear that for Test 1, there is an underestimation of the composite Young's modulus and that the improved soil is contributing to a greater extent to the system stiffness.

*Table 27. Calculated expected composite stiffness properties. $E_{50,col} = 400 s_{u,col}$; $s_{u,col}$ from unconfined compression test. Source: own elaboration*

| | $\boldsymbol{E_{50,col}\ [kPa]}$ | $\boldsymbol{E_{50,soil}\ [kPa]}$ | $\boldsymbol{a}$ [%] | $\boldsymbol{E_{50;comp}\ [kPa]}$ |
|---|---|---|---|---|
| **TEST 1** | 91000 | 2500 | 18 | **18600** |
| **TEST 2** | 91000 | 2500 | 36 | **34800** |

The stiffness gradient obtained from the back-calculation process can be explained by three mechanisms. First, the stiffness is related to the strength of the material, and as observed in Figure 67, the strength of the material increases with depth. Second, due to a stiffness degradation of the

material due to the excavation works and loading, meaning that the material will gradually lose stiffness while increasing deformations. Third, reduced confining vertical stress due to excavation and increased lateral stress.

Regarding the measured and modelled strut forces, it was decided to test the influence of the strut spacing in Plaxis because the author of the full-scale test stated that the struts were placed between 3.00 m to 3.50 m apart from each other. After testing the strut spacing, it is observed that when using a spacing of 3.50 m the results are closer to the measured values and, in the calibration process, it was observed that the deformations were not highly disturbed in the model by the variation of the strut spacing in the range used.

#### *4.2.2.2. Composite material with drained properties*

##### 4.2.2.2.1. Strength calibration

Previous research, shown in section 2.7.2, evidence that the drained friction angle of the improved material can be assumed to be around 33 ° regardless of the measured cohesion intercept magnitude. Nevertheless, as shown in section 2.4.1, the Swedish design guideline (Trafikverket, 2011) limits the drained friction angle design value to 32 °, therefore this value will be used as a fixed property in the present analysis. The Swedish design guideline also sets the magnitude of the allowable cohesion intercept value for improved soil installed in the passive side of an excavation to 0 kPa, but previous research suggests that it is related to the undrained shear strength of the improved material (Helen Åhnberg, 2007), as a result, higher values could be used for this property. Due to the abovementioned reasons, the strength calibration of the drained properties of the composite material will be limited only to the cohesion intercept leaving the drained friction angle value fixed to 32 °.

For the mentioned reasons, the only back-calculated strength property to be determined in this section is the cohesion intercept of the composite material. As the cohesion intercept has been shown to be related to the unconfined compression strength, see section 2.7.2, results from the undrained strength calibration from section 0 will be compared with the results obtained in the present section and with literature review.

To calculate the composite drained properties to be used in the Plaxis 2D model, it is also necessary to determine the drained properties of the clay surrounding the DSM column panels. Results of consolidated undrained compression triaxial tests performed on the clay at the test site at a depth of 7.00 m are shown in Figure 70. From these results, the drained properties of the natural clay can be estimated, resulting in a cohesion intercept of around 5 kPa and a drained friction angle of 15 °. To determine the composite drained properties, the weighted average method shown in section 2.7.7 is used, the composite drained friction angle for Test 1 and Test 2 is shown in Table 28.

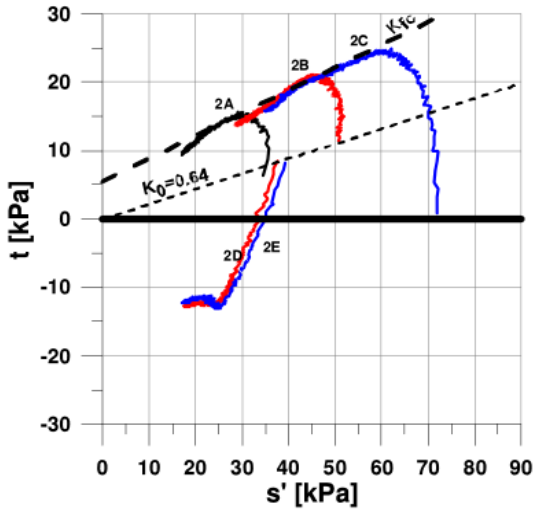


*Figure 70. Consolidated undrained compression triaxial test results on clay samples of 7.00 m depth. Source:* (Ignat, 2015).

*Table 28. Calculated composite drained friction angle. Source: own elaboration.*

| | $\phi'_{col}$ [°] | $\phi'_{soil}$ [°] | $a$ [%] | $\phi'_{comp}$ [°] |
|---|---|---|---|---|
| **TEST 1** | 32 | 15 | 18 | **18.4** |
| **TEST 2** | 32 | 15 | 36 | **21.7** |

Similar to section 4.2.2.1.1, several composite cohesion intercepts are tested until the failure criterion described in section 4.2.1 is reached. The composite cohesion intercepts for the model not to fail, along with the natural cohesion intercept of the clay, the area improvement ratio and the back-calculated cohesion intercepts of the improved soil for each test are presented in Table 29.

*Table 29. Back-calculated values of improved cohesion intercepts. Source: own elaboration*

| | $c'_{comp}$ [kPa] | $c'_{soil}$ [kPa] | $a$ [%] | $c'_{col}$ [kPa] |
|---|---|---|---|---|
| **TEST 1** | 20 | 5 | 18 | **87** |
| **TEST 2** | 35 | 5 | 36 | **88** |

In order to analyze the back-calculated strengths for Test 1 and Test 2, the same procedure used in section 4.2.2.1.1 is followed. In previous research, the undrained shear strength obtained from unconfined compression tests is compared to the cohesion intercept obtained from triaxial tests (Helen Åhnberg, 2007; Ignat, 2015), this approach is also followed in the present research to compare the back-calculated properties from a full-scale test. The measured field and laboratory values, alongside with the estimated values and the ratio between them and the back-calculated cohesion intercept are presented in Table 30.

*Table 30. Ratio between the back-calculated cohesion intercept and measured and estimated undrained shear strength of the improved soil. Source: own elaboration.*

| | | | **TEST 1** | | TEST 2 | |
|---|---|---|---|---|---|---|
| | | $s_{u;col}\ [kPa]$ | $c'_{col}\ [kPa]$ | $\frac{c'_{col}}{s_{u;col}}[kPa]$ | $\boldsymbol{c'_{col}\ [kPa]}$ | $\frac{c'_{col}}{s_{u;col}}[\boldsymbol{kPa}]$ |
| **UNCONFINED COMPRESSION TEST** | Mean | 229.02 | 87 | 0.38 | 88 | 0.38 |
| | Mean + σ | 293.56 | | 0.30 | | 0.30 |
| | Mean - σ | 164.48 | | 0.53 | | 0.54 |
| **KPS** | Mean | 327.90 | | 0.27 | | 0.27 |
| | Max | 534.36 | | 0.16 | | 0.16 |
| | Min | 157.88 | | 0.55 | | 0.56 |
| **ESTIMATION** | Mean | 259 | | 0.34 | | 0.34 |
| | Mean + σ | 337 | | 0.26 | | 0.26 |
| | Mean - σ | 181 | | 0.48 | | 0.49 |

Table 30 shows that the ratio of the back-calculated cohesion intercept and the measured and estimated undrained shear strength ranges from 0.16 to 0.56, this including the upper and lower limit values stated in Table 24. In previous research, it has been proven that the ratio between the magnitude of the cohesion intercept of the improved soil and its correspondent undrained shear strength is in the range of 0.13 to 0.33 (Helen Åhnberg, 2007; Ignat, 2015). When only taking into account the mean measured or estimated values, this range goes from 0.27 to 0.38; when taking upper values, the range is 0.16 to 0.30; and when taking lower values, it goes from 0.48 to 0.56. It is necessary to point out that both tests evidence the same back-calculated cohesion intercept, meaning that for drained analysis, this value appears to be constant regardless of the system geometry.

#### 4.2.2.2.2. Stiffness calibration

Similar to section 4.2.2.1.2, both the strut force and the horizontal deformations are calibrated simultaneously. The displacements to be calibrated are the ones measured during loading, in Figure 71 and Figure 72 the measured horizontal displacements at the end of the loading stage are highlighted and marked with a "(1)"; as previously decided in section 4.2.2.1.2, measurements during failure are disregarded for the calibration process. Following the established procedure of section 4.2.2.1.2, to compare the deformations calculated by Plaxis and the measured values in the loading stage only, the horizontal displacement plots presented in the full-scale report (Ignat et al., 2016) are overlapped with the values obtained from Plaxis at different percentages of load.

The back-calculated drained stiffness parameters used to calibrate the horizontal displacements are presented in Table 31 and the result of the calibration can be observed in Figure 71 for Test 1 and Figure 72 for Test 2. The measured and modelled strut forces for each test and each load condition are reported in Table 34.

*Table 31. Back-calculated composite drained stiffness properties. Source: own elaboration.*

| | $E'_{50;ref}$ $[kPa]$ | $E'_{50;inc}$ $[kPa/m]$ |
|---|---|---|
| **TEST 1** | 31000 | 6200 |
| **TEST 2** | 30000 | 7000 |

In the present section, only the drained stiffness properties of the composite material are calibrated as the stiffness properties of the natural soil were already determined in section 4.2.2.1.2 and are presented in Table 20 of section 4.1.1. It is important to point out that as back-calculated composite undrained stiffness values are already available from section 4.2.2.1.2, drained stiffnesses are determined from them and used as a first estimation that leads to a faster calibration process, this first estimation is presented in Table 32. The drained stiffnesses are determined using Equation (23) and assuming a Poisson's ratio equal to 0.35. Another comparison point are stiffness values calculated from improved and unimproved soil properties; these are shown in

Table 33.

$$E' = \frac{2}{3}(1+\upsilon)E_u \qquad (23)$$

*Table 32. First estimation of the drained stiffness parameters for the model calibration. Source: own elaboration.*

| | $E_{50;ref}$ $[kPa]$ | $E_{50;inc}$ $[kPa/m]$ | $E'_{50;ref}$ $[kPa]$ | $E'_{50;inc}$ $[kPa/m]$ |
|---|---|---|---|---|
| **TEST 1** | 35000 | 7000 | 31000 | 6200 |
| **TEST 2** | | 8000 | | 7100 |

*Table 33. Calculated expected drained composite stiffness properties. Source: own elaboration.*

| | $E_{50,col}$ $[kPa]$ | $E_{50,soil}$ $[kPa]$ | $E'_{50,col}$ $[kPa]$ | $E'_{50,soil}$ $[kPa]$ | $a$ [%] | $E_{50;comp}$ $[kPa]$ |
|---|---|---|---|---|---|---|
| **TEST 1** | 91000 | 2500 | 80600 | 2333 | 18 | **16500** |
| **TEST 2** | | | | | 36 | **30700** |

*Table 34. Measured and modelled strut forces at different loading applied loads. Source: own elaboration (simulation) and* (Ignat et al., 2016) *(measured).*

| | | | | **Strut spacing [m]** | | |
|---|---|---|---|---|---|---|
| | | | | 3.00 | 3.50 | 4.00 |
| | **% load** | **Load [kPa]** | **Measured [kN]** | **Simulated [kN]** | | |
| **Test 1** | 0 | 0 | 200 | 84 | 98 | 112 |
| | 25 | 10.2 | 210 | 106 | 124 | 141 |
| | 50 | 20.3 | 230 | 146 | 170 | 194 |
| | 80 | 32.5 | 290 | 219 | 255 | 291 |
| | 100 | 40.6 | 300 | 261 | 304 | 347 |
| **Test 2** | 0 | 0 | 130 | 101 | 118 | 134 |
| | 25 | 14.05 | 150 | 133 | 152 | 173 |
| | 50 | 28.1 | 170 | 194 | 208 | 238 |
| | 80 | 44.96 | 350 | 292 | 316 | 361 |
| | 100 | 56.2 | 420 | 355 | 386 | 437 |

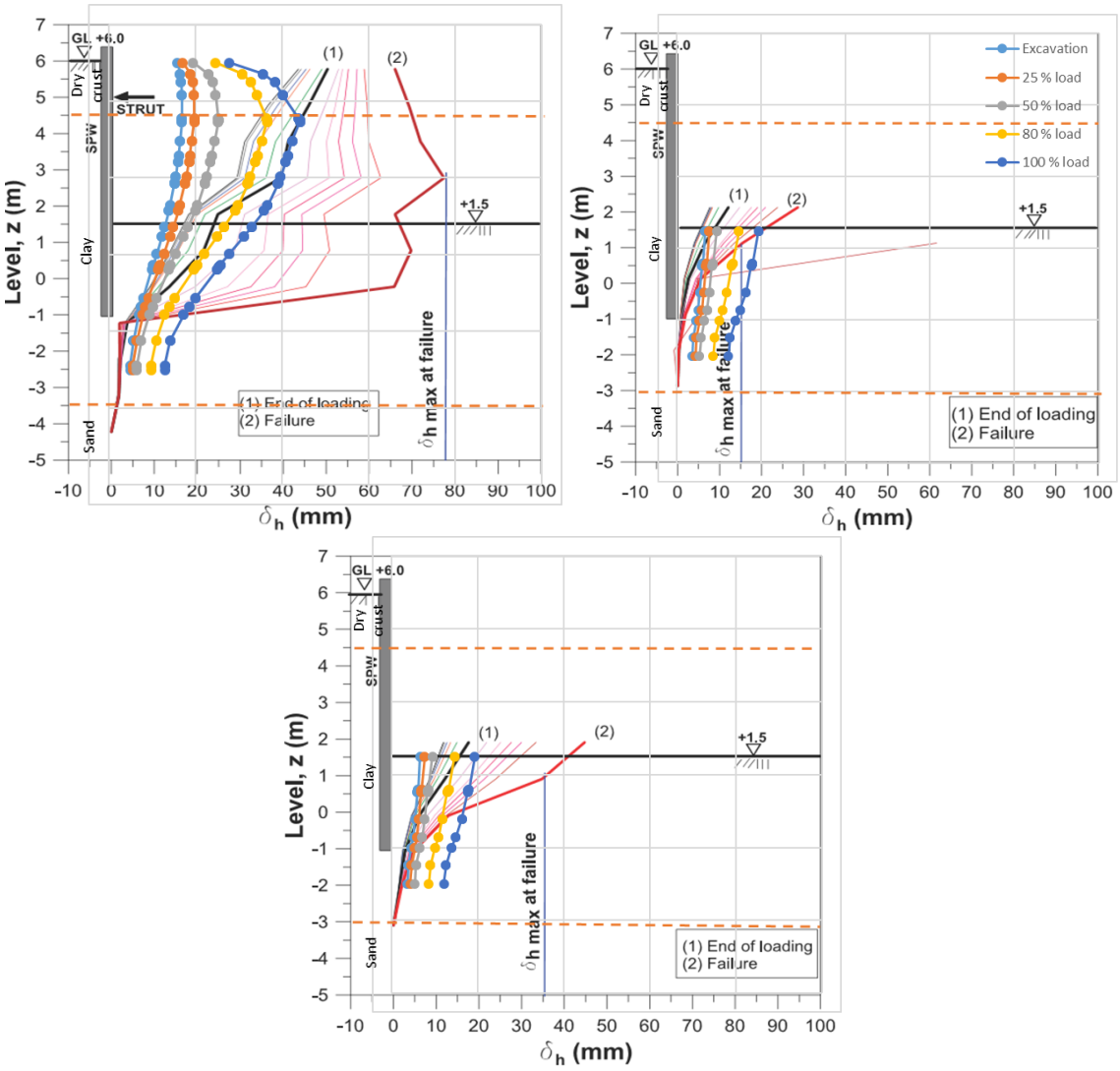


*Figure 71. Result of the stiffness calibration for Test 1 using strut spacing of 3.00 m in the active side 0.50 m behind the wall (top left), DSM column (top right) and the unimproved soil (bottom) 1.50 m away from the wall. Source: own elaboration over plots from* (Ignat et al., 2016).

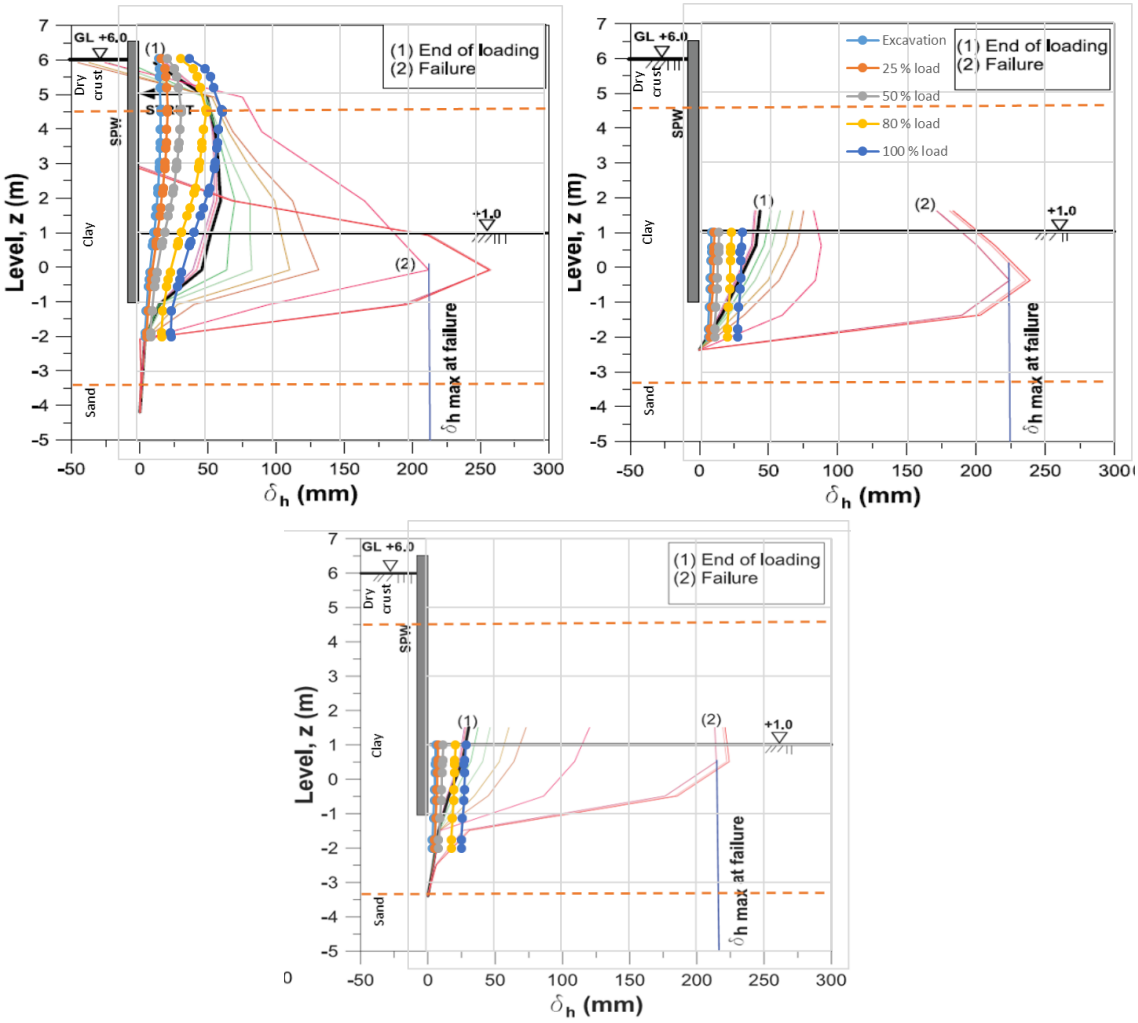


*Figure 72. Result of the stiffness calibration for Test 2 using strut spacing of 3.00 m in the active side 0.50 m behind the wall (top left), DSM column (top right) and the unimproved soil (bottom) 1.50 m away from the wall. Source: own elaboration over plots from* (Ignat et al., 2016).

Figure 71 and Figure 72 show the horizontal displacements measured in the full-scale test overlapped with the simulation results of the same variable at different loading stages for Test 1 and Test 2 respectively. As previously stated in section 4.2.2.1.2, deformations in the active side of Test 1 have a cantilever-like bend, which can be explained by the inclinometer being placed in between struts. Also, a higher horizontal deformation is measured in the unimproved soil cause by the high center-to-center distance of the DSM column panels and the flexible characteristics of the retaining structure.

Similar to the findings in the undrained case, the DSM column panels installed in Test 2 experience more horizontal deformations than those in Test 1, therefore more shear strength is being mobilized by the improved soil in Test 2 than in Test 1. The deformations measured in Test 2 match better the Plaxis 2D simulations than those in Test 1 most likely because of the positioning of the inclinometers in each test, as expressed in section 4.2.2.1.2.

Regarding the back-calculated stiffness of Test 1, it again overestimates the calculated value from the improved and unimproved soil properties, but it is in perfect accordance with the results of the undrained stiffness back-calculation process, which was the expected result. On the other hand, the back-calculated drained stiffness from Test 2 is in accordance with the results of both the undrained back-calculated value and with the value obtained from improved and unimproved soil properties. The stiffness gradients obtained from the drained back-calculation process are in perfect accordance with the ones obtained in the undrained back-calculation process.

Regarding the measured and modelled strut forces, it was decided to follow the same procedure applied in section 4.2.2.1.2 to test the influence of the strut spacing in Plaxis 2D, because it was reported that the struts were placed between 3.00 m to 3.50 m apart from each other. After testing the strut spacing, it is observed that when using a spacing of 3.50 m the results are closer to the measured values and, in the calibration process, it was observed that the deformations were not highly disturbed in the model by the variation of the strut spacing in the range used.

#### *4.2.2.3. Comparison between back-calculated drained and undrained properties*

To assess the relationship between the drained and undrained properties, it is necessary to compare the results of the back-calculated strength and stiffness properties. The strength properties that are to be compared are the back-calculated undrained shear strength and the back-calculated cohesion intercept, as the drained friction angle was set to a fixed value. In previous research, it has been proven that the ratio between the magnitude of the cohesion intercept of the improved soil and its correspondent undrained shear strength is in the range of 0.13 to 0.33 (Helen Åhnberg, 2007; Ignat, 2015), the ratios of the back-calculated undrained shear strength and the back-calculated cohesion intercept are shown in Table 35, additional relations were calculated for the present dataset and these are reported in Table 8.

*Table 35. Back-calculated undrained shear strength, cohesion intercept and the cohesion-undrained shear strength ratio for the improved soil of Test 1 and Test 2. Source: own elaboration.*

| | $s_{u;col;bc}\ [kPa]$ | $c'_{col}\ [kPa]$ | $\frac{c'_{col}}{s_{u;col}}\ [kPa]$ |
|---|---|---|---|
| **TEST 1** | 140 | 87 | 0.62 |
| **TEST 2** | 185 | 88 | 0.47 |

As stated in section 4.2.2.1.1, the improved soil in Test 1 mobilizes a lower undrained shear strength than the improved soil in Test 2 and this difference in mobilized strength can be explained by a wrong strength model, a constraint due to the lowest strength and by the influence of the system geometry.

Table 35 shows that the back-calculated cohesion intercept for both tests is virtually the same, meaning that perhaps a drained analysis is a better approach when modelling DSM column panels as bottom struts with surrounding clay as a composite material. When compared the back-calculated cohesion intercepts and undrained shear strength values for each test, it is observed that both yield into a high value of the $c'_{col}/s_{u;col}$ ratio comparing to the literature, a result that supports the findings for the undrained case, in which there are three possible areas in which the analysis could be improved.

Comparing the estimated values obtained with the proposed mathematical expression of section 3.2.2, it is observed that there is not a good agreement between the estimated improved undrained shear strength value and the back-calculated value from the undrained analysis. On the other hand, when considering the drained analysis, it is observed in Table 30 that the back-calculated cohesion intercept can be estimated using the suggested range of values of 0.15 to 0.25 (Helen Åhnberg, 2006, 2007) for the ratio of the cohesion intercept and the improved undrained shear strength. And as the estimated improved undrained shear strength is in good accordance with the measured values, this proposed values for the mentioned ratio can be implemented when using the mathematical expression proposed in section 3.2.2 to estimate the cohesion intercept as well.

Regarding the stiffness properties, it is observed that the back-calculated drained and undrained Young's modulus have a good agreement between analyses. Nevertheless, the composite stiffness calculated as the weighted average of properties is not a good estimation when considering cases of low area improvement ratio. On the contrary, when considering cases of high area improvement ratio, the weighted average approach leads to a good prediction of the stiffness properties in both undrained and drained cases. It is also observed that the undrained stiffness of the improved soil can be estimated as around 400 times its undrained shear strength, and therefore is proven the higher lateral stiffness compared to the vertical.

When calibrating the system deformations, it was not possible to completely obtain the exact shapes measured by the inclinometers. When observing Figure 68, Figure 69, Figure 71 and Figure 72, it is evident that the deformation slope could no be completely followed especially in the passive side of the excavation. This discrepancies between the model and the measured values could be originated by different sources:

- 3D effects, as the model is assuming a composite material with weighted properties.
- A soil model that is not capable to properly emulate what is happening on field.
- Strong stress dependence of the stiffness and strength degradation especially at the excavation bottom.

From the obtained results, it is considered that the undrained shear strength obtained from unconfined compression tests or from the proposed estimation expression cannot directly be used to determine the design strength and stiffness properties of the improved soil and the weighted average procedure should be revised for the undrained case. Drained analysis showed consistent results; therefore, its use is advised using a fixed friction angle of 32 ° and estimating the cohesion intercept from the improved undrained shear strength assuming a ratio between these two magnitudes of 0.15 to 0.25, which would yield to safe estimates. For both drained and undrained stiffness properties, the horizontal Young's modulus is proven to be higher than the vertical by both the back-calculated and experimental results. The value of the Young's modulus can be estimated from the strength properties.

### 4.2.3. Failure mechanism

The failure mechanism present in the model shows a clear shear band from the tip of the sheet pile to the top of the stabilized soil cluster at about 3.00 to 3.50 m away from the sheet pile, meaning that around 6 columns will be affected by the failure mechanism and extending all the way to the furthest edge of the load distribution platform, a similar failure mechanism was reported in the full scale test, see section 4.1.1; the failure mechanism can be observed in Figure 73.

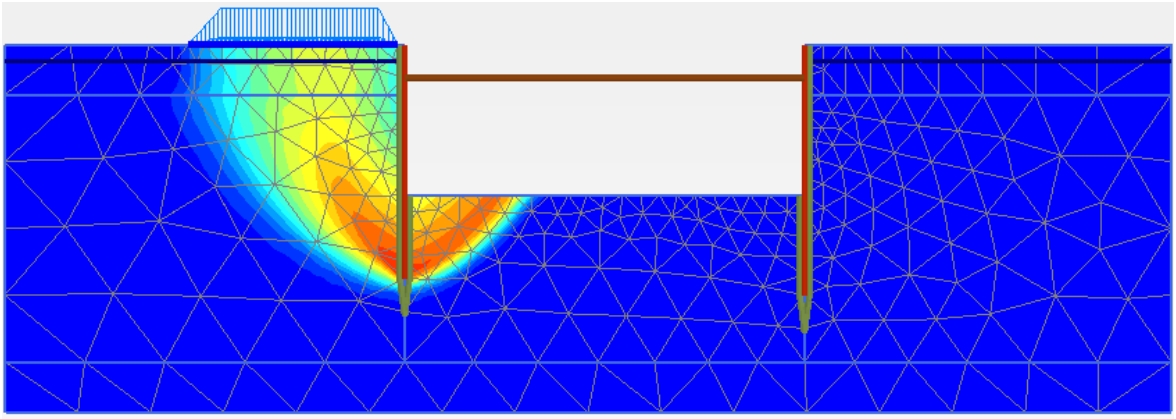

*Figure 73. Total deformations plot for a composite strength of 37 kPa. Source: own elaboration using Plaxis 2D.*

# 5. SUGGESTED DESIGN AND PLANNING CONSIDERATIONS

## 5.1. Laboratory and field study

In any civil project, it is mandatory to follow the local design code recommendations regarding soil investigation and design. Soil investigation generally includes boreholes, CPT, SPT, and laboratory analysis over soil samples to obtain index and strength properties, among others. But when assessing whether or not use soil mixing, design manuals and design codes (Bruce et al., 2013; Trafikverket, 2011) recommend to perform a laboratory mix study, with the implications that laboratory mix studies will use project budget and time. Depending on the project magnitude, a full-scale test is also highly recommended. An estimated improved undrained shear strength can be calculated with the mathematical expression suggested in section 3.2.2 using only the natural undrained shear strength and the binder content to be used to determine whether Deep Soil Mixing is a suitable technique for the project being developed; if this technique is considered as a plausible option, a laboratory mix study should follow to confirm the estimation.

The laboratory mix study is meant to investigate the actual improved strength of a specific type of soil mixed with a specific type of binder. It should, in principle, include a thorough investigation regarding the influence of the available binders at different binder contents and binder ratios reacting with the soil present at the project. The usual available binder types are Portland cement and lime, but there has been recent research over the possible use of other types (H. Åhnberg & Johansson, 2005) obtaining also good results but with less documentation about their use. The usual binder contents used in the investigations range between 30 kg/m$^3$ and 150 kg/m$^3$ and the binder ratios range from 0/100 (100 % cement), 50/50 (50 % cement and 50 % another binder) and 30/70 (30 % cement and 70% another binder). This complete laboratory study could be avoided if an estimation of the expected improved shear strength is available, and then only focus on endorsing the obtained estimation with fewer tests.

Once the binder ratio and binder content to be used is selected, mixed specimens should be prepared and cured at 20 °C and tested at a curing time of interest for the project, typically 28 to 90 days is preferred, but, as was discussed in the present research, any curing time could be used as long as the estimation in time is performed using Equation (1). It is recommended that more than one sample for the selected curing times is prepared in order to minimize the influence of inhomogeneities in the results.

When mixing the soil, it is of importance to obtain the index properties and the undrained shear strength of the soil sample used for the mix at hand, because, in the present research, it has been proven that the natural undrained shear strength is of great influence in the final improved shear strength. The tests performed on the improved soil specimens should be selected based on the stress conditions to be subjected in the project, the unconfined compression test being the most mentioned in literature. In fact, the unconfined compression test has proven to be a good reference to estimate the drained properties of the improved soil, therefore only this test should be enough to characterize the improve soil. The achieved strength on field should be confirmed by means of any penetration test available, see section 2.6.2, or by extracting cores of improved material and testing them.

## 5.2. Design considerations

At the moment of selecting strength design values, the stress conditions at which the improved material will be submitted, and the geometric arrangement used on site are to be considered carefully when selecting the strength and stiffness design value. From the present research, it has been shown that a drained analysis yields to more consistent result than an undrained analysis, therefore the former is recommended to assess the improved soil.

If DSM column panels are to be used, and as the present research has shown, it is highly recommended to select a center-to-center distance of the column panels less or equal than 1.50 m or perform a block improvement since the strength and stiffness model proposed by the weighted average loses accuracy when the DSM columns panels a further apart. Regarding the strength properties, the present findings suggest that the lower possible strength obtained from tests should be taken as an upper limit value for design considerations in undrained conditions.

It has also been shown than, for a drained analysis, a fixed value of 32 ° in the friction angle and a cohesion intercept of 0.15 to 0.25 of the improved undrained shear strength is a safe estimate that could be used for design and yields more consistent results than the undrained analysis. According to the results of the present research, the cohesion intercept can be safely estimated from both the improved undrained shear strength obtained from laboratory tests and from the proposed mathematical expression to estimate the improved undrained shear strength.

## 5.3. Installation procedure

From experiences in the West Link project in Gothenburg and the Møllenberg project in Trondheim, the column placement should be planned carefully before installation. It has been proven that the installation order contributes to poor verticality (Hanson, 2012), if a column is installed directly next to another, the drill rod will tend to deviate to the recently mixed column due to the decrease of strength in that soil body area. Results reveal that new columns should not be installed overlapped to others when more than two days after installation have been passed. The recommendation is thus to install a fraction of the columns at the beginning of the day and the rest of the overlapping columns at the end of the day. It is also recommended to install extra columns near connection points with the retaining structure to ensure structural continuity, as shown in Figure 5.

# 6. CONCLUSIONS, RECOMMENDATIONS AND FUTURE RESEARCH

## 6.1. Conclusions

From the data available, it has been found that the improved soil strength can be estimated in Scandinavian countries by means of the natural undrained shear strength of the soil and the binder content to be used during the mixing. It is considered that the linear expression performs reasonable estimations, but the exponential of a polynomial is preferred. This linear trend in the natural undrained shear strength is expected because the baseline of the improvement should be the natural undrained shear strength, and as the binder content increases, the improved shear strength should increase proportionally. For extremely soft soils, even if a high binder content is added, the magnitude of the improved strength is limited by the quality of the soil; whereas for the case of extremely hard soils, the strength improvement should be limited to that of the hardened cement.

In the binder content space, at low binder contents the improved strength should tend to the natural undrained shear strength and at high binder contents, the improved strength value should be limited by both the soil quality and the water available to react with the binder. It is evident that the undrained shear strength is not the only soil property affecting the improved strength, but from the data available, it was the only one showing a clear correlation.

In geotechnical engineering design problems, it is recognized that the measured properties of a soil specimen in the laboratory might not represent the in-place bulk behavior of the material in an engineered system due to the assumptions made to calculate or measure determined properties. In order to evaluate the general system behavior of an engineering project and the accuracy of the measured or estimated material property, full-scale tests can be performed. Two full-scale tests in which a braced steel sheet pile wall interacting with panels of overlapping DSM columns and loaded until failure were available to be analyzed in the present research. The Swedish design code and other authors recommend the use of weighted average properties to calculate the design properties of a soil mass in which improved and unimproved soil are present (Kitazume & Terashi, 2013; Trafikverket, 2011); this weighted average strength and stiffness model assumes full interaction between improved and unimproved soil.

The weighted average procedure should be carefully implemented, especially in cases in which a low area replacement ratio is used. For the case of high area replacement ratios, the results suggest that the assumption of a composite soil is valid, nevertheless, the threshold of this application is still not determined. It appears that the upper value for design shear strength should be limited to the lowest measured value in either field or laboratory when considering undrained analysis; when considering drained analysis, the cohesion intercept can be estimated from test results or from the proposed mathematical expression, and the friction angle can be assumed to be a fixed value. The weighted average methodology was originally devised and applied to embankment problems (Bruce et al., 2013), in which the improved and unimproved soil are submitted to specific loading conditions that might not be present in the passive zone of a braced excavation, thus is should be implemented with care for different loading conditions.

The use of the Deep Soil Mixing technique has been proven to improve natural strength and stiffness properties and with it, improve the behavior of an engineering system. When using Deep Soil Mixing as excavation support for braced excavations, its practice is recommended especially if a high area

replacement ratio is to be used, because when high area replacement ratios are used, the proposed methodology for estimating design properties is accurate and thus leads to design parameters that represent the in-place behavior of the soil mass in the passive zone of the excavation. It is necessary to validate the applicability of the weighted average procedure to determine the strength and stiffness properties of composite materials used in the passive zone of an excavation, because according to the results of the present research, the procedure loses accuracy when dealing with low area replacement ratios for materials placed in the passive zone of an excavation.

## 6.2. Recommendations and future research

It is observed in the gathered data from different countries and researchers, a lack of measuring the index and strength properties of the soils to be used for the investigation. From the experience in the present research, it is highly recommended to measure the index and strength properties of the soil specimen to be used in a mix study, because with this specific information per specimen, a better analysis could be made, and perhaps a better understanding of the soil properties influencing the improved strength can be obtained. It is also recommended to include a mineralogy analysis of the soil to be used for research, in order to build a database that includes every soil property that can be obtained and be able to relate it to the improved soil strength, because when using binder different that cement, mineralogy could play a bigger role in the final improved soil strength. Therefore, a thorough investigation of different index properties and soil mineralogy should be performed to obtain a deeper understanding of the processes involved in the developing of the improved strength.

In Deep Soil Mixing applications, the influence of the available water in the improved shear strength is still unknown. It is observed that for Scandinavian soils the water content is usually in the same order of magnitude than the liquid limit, meaning that in these soils a relatively high amount of water is available to react with the binders. To measure this influence, it is proposed to compare the improved shear strength results from specimens in which the hardening process is performed by curing isolated or sealed samples, to samples that are allowed the intake of water from an external source. These further investigations are recommended to be performed as the actual expected behavior in the binder content space is an “S” shaped graph and a linear shape in the natural undrained shear strength space. Alongside this study, it is also proposed to investigate the influence of the binder content on a soil starting from extremely low binder contents, until extremely high binder contents; from this study it is expected to obtain a minimum binder content with which the soil will start to improve its strength and a maximum binder content at which there will be no further improvement. These two different experiments are related in respect to the varying ratio of available water to binder content, therefore they could be performed simultaneously.

Regarding the relevance of the weighted average approach for excavations problems, a setup similar to the one performed by (Sukpunya & Jotisankasa, 2016) is recommended. Small-scale models that emulate the loading condition of a braced excavation should be performed in order to determine a factor that modifies the maximum available strength of the improved soil for this specific condition. This investigation should include different penetration depth of the retaining structure, different retaining structure, different center-to-center distance of the DSM column panels and different composition of the DSM columns panels, using one or more rows.

It is also recommended to perform material model investigation because, in the present research, there is evidence that the improved material could be subjected to strength and stiffness degradation when excavated and interacting with a retaining structure. This has not been done yet for full-scale tests and could yield to a better understanding of the discrepancies between the low and high area replacement ratios back-calculated properties.

# REFERENCES


Åhnberg, H., & Johansson, S. E. (2005). Increase in strength with time in soils stabilised with different types of binder in relation to the type and amount of reaction products. *Deep Mixing*, 195–202.

Åhnberg, Helen. (2006). *Strength of stabilised soils – A laboratory study on clays and organic soils stabilised with different types of binder*. *Construction*.

Åhnberg, Helen. (2007). On yield stresses and the influence of curing stresses on stress paths and strength measured in triaxial testing of stabilized soils, 54–66. https://doi.org/10.1139/T06-096

Åhnberg, Helen, Johansson, S. E., Retelius, A., Ljungkrantz, C., Holmgvist, L., & Holm, G. (1995). *Cement and lime for deep stabilization of soil [Cement och kalk för djupstabilisering av jord]*. Linköping.

Andersson, C. (2010). Installation effects of lime-cement columns.

Andromalos, K., Hegazy, Y., & Jasperse, B. (2001). Stabilization Of Soft Soils By Soil Mixing. *Geotechnical Special Publication*, *112*, 1–12.

Baker, S, Sällfors, G., & Alén, C. (2005). Deformation properties of lime/cement columns. Evaluation from in-situ full scale tests of stabilised clay. In *International Conference on Deep Mixing Best Practice and Recent Advances*. Stockholm.

Baker, Sadek. (2000). *Deformation behavior of Lime/Cement stabilized clay*. Chalmers University of Technology.

Bruce, C., Collin, J., Berg, R., Filz, G., Terashi, M., & Yang, D. (2013). Federal Highway Administration Design Manual: Deep Mixing for Embankment and Foundation Support. *U.S. Department of Transportion, Federal Highway Administration*, (october), 244. Retrieved from http://www.fhwa.dot.gov/publications/research/infrastructure/structures/bridge/13046/index.cfm

Charbit, B. (2009). *Numerical analysis of laterally loaded lime / cement columns*. Royal Institute of Technology (KTH).

CUR. (2008). *Van Onzekerheid naar Betrouwbaarheid - Handrekening voor geotechnisch ontwerpers* (Rapport 20). Gouda.

Hanson, S. (2012). *Lime/cement stabilization at E6 Trondheim-Størdal, Trondheim dayzone west*. Norwegian University of Science and Technology, Trondheim.

Ignat, R. (2015). Field and laboratory tests of laterally loaded rows of lime-cement columns.

Ignat, R. (2018). *Ground Improvement by Dry Deep Mixing Lime-Cement Column Panels as Excavation Support*. KTH, Royal Institute of Technology.

Ignat, R., Baker, S., Larsson, S., & Liedberg, S. (2015). Two- and three-dimensional analyses of excavation support with rows of dry deep mixing columns. *Computers and Geotechnics*, *66*, 16–30. https://doi.org/10.1016/j.compgeo.2015.01.011

Ignat, R., Baker, S., Liedberg, S., & Larsson, S. (2016). Behavior of braced excavation supported by

panels of deep mixing columns. *Canadian Geotechnical Journal*, *53*(10), 1671–1687. https://doi.org/10.1139/cgj-2016-0137

Jonsson, C. (2017). *Deep stabilization with cement columns - A laboratory study*. Luleå University of Technology.

Karlsrud, K., Eggen, A., Nerland, Ø., & Haugen, T. (2013). Some Norwegian experiences related to use of dry-mixing methods to improve stability of excavations and natural slopes in soft clays.

Kitazume, M., & Terashi, M. (2013). *The Deep Mixing Method*. Taylor & Francis Group.

Larsson, R. (1977). *Basic behaviour of Scandinavian soft clays*. Linköping.

Liyapathirana, D. S., & Kelly, R. B. (2010). Interpretation of the lime column penetration test (pp. 0–10). https://doi.org/10.1088/1757-899X/10/1/012088

Löfroth, H. (2005). Properties of 10-year-old lime-cement columns. In *International Conference on Deep Mixing Best Practice and Recent Advances* (p. 255). Stockholm: Swedish Deep Stabilization Research Centre (SD).

Massarsch, K. R., & Topolnicki, M. (2005). Regional Report: European Practice of Soil Mixing Technology. In *International Conference on Deep Mixing Best Practice and Recent Advances*. Stockholm: Swedish Deep Stabilization Research Centre (SD).

Monnet, J. (2015). Pressuremeter Tests (PMT, SBP) and Variants. In *In Situ tests in geotechnical engineering*. London: ISTE Ltd.

Navin, M. P., & Filz, G. M. (2005). Statistical Analysis of Strength Data from Ground Improved with DMM Columns. In *International Conference on Deep Mixing Best Practice and Recent Advances* (p. 282). Stockholm: Swedish Deep Stabilization Research Centre (SD).

Sukpunya, A., & Jotisankasa, A. (2016). Large simple shear testing of soft Bangkok clay stabilized with soil–cement-columns and its application. *Soils and Foundations*, *56*(4), 640–651. https://doi.org/10.1016/j.sandf.2016.07.005

Terashi, M. (2005). Keynote Lecture: Design of deep mixing in infrastructure applications. In *International Conference on Deep Mixing Best Practice and Recent Advances* (p. 118). Stockholm: Swedish Deep Stabilization Research Centre (SD).

Timoney, M. J., & McCabe, B. A. (2017). Strength verification of stabilized soil – cement columns : a laboratory investigation of the push-in resistance test ( PIRT ), *805*(January), 789–805.

Trafikverket. (2011). Trafikverkets tekniska krav för geokonstruktioner - TK Geo 13. https://doi.org/ISBN: 978-91-7467-114-8

# APPENDIX

## A. Stabilized soil measured properties per site

### Enköping, Sweden

*Table 36. Data points from Enköping, Sweden. Source:* (Ignat, 2015).

| Mix | Test | Depth natural [m] | Binder content [kg/m$^3$] | Lime [%] | Cement [%] | Measured shear strength [kPa] | Curing time [days] | Curing time @20°C [days] | Curing temp [°C] | Shear Strength [kPa] 20 °C 28d |
|---|---|---|---|---|---|---|---|---|---|---|
| **Lab** | UCS | 5 | 120 | 50 | 50 | 126.5 | 28 | 7 | 7 | 164.6437 |
| **Lab** | UCS | 5 | 120 | 50 | 50 | 161.5 | 84 | 18 | 7 | 174.3179 |
| **Lab** | UCS | 7 | 120 | 50 | 50 | 174.5 | 28 | 7 | 7 | 227.1172 |
| **Lab** | UCS | 7 | 120 | 50 | 50 | 222.5 | 56 | 12 | 7 | 256.3061 |
| **Lab** | UCS | 7 | 120 | 50 | 50 | 299 | 84 | 18 | 7 | 322.731 |
| **Lab** | CIUC | 5 | 120 | 50 | 50 | 89.5 | 28 | 7 | 7 | 116.487 |
| **Lab** | CIUC | 5 | 120 | 50 | 50 | 87.5 | 28 | 7 | 7 | 113.884 |
| **Lab** | CIUC | 5 | 120 | 50 | 50 | 112 | 28 | 7 | 7 | 145.7715 |
| **Lab** | CIUC | 5 | 120 | 50 | 50 | 137.5 | 28 | 7 | 7 | 178.9605 |
| **Lab** | CIUC | 5 | 120 | 50 | 50 | 132 | 28 | 7 | 7 | 171.8021 |
| **Lab** | CIUE | 5 | 120 | 50 | 50 | 99.5 | 28 | 7 | 7 | 129.5023 |
| **Lab** | CIUE | 5 | 120 | 50 | 50 | 102 | 28 | 7 | 7 | 132.7562 |
| **Lab** | CIUE | 5 | 120 | 50 | 50 | 108.5 | 28 | 7 | 7 | 141.2161 |
| **Lab** | CIUC | 7 | 120 | 50 | 50 | 106.5 | 28 | 7 | 7 | 138.6131 |
| **Lab** | CIUC | 7 | 120 | 50 | 50 | 123.5 | 28 | 7 | 7 | 160.7391 |
| **Lab** | CIUC | 7 | 120 | 50 | 50 | 115 | 28 | 7 | 7 | 149.6761 |
| **Lab** | CIUC | 7 | 120 | 50 | 50 | 177 | 28 | 7 | 7 | 230.371 |
| **Lab** | CIUC | 7 | 120 | 50 | 50 | 234.5 | 28 | 7 | 7 | 305.209 |
| **Lab** | CIUE | 7 | 120 | 50 | 50 | 109 | 28 | 7 | 7 | 141.8669 |
| **Lab** | CIUE | 7 | 120 | 50 | 50 | 99.5 | 28 | 7 | 7 | 129.5023 |
| **Lab** | CIUE | 7 | 120 | 50 | 50 | 100 | 28 | 7 | 7 | 130.1531 |

## Gothenburg, Sweden (West Link project)

*Table 37. Data points from Gothenburg, Sweden of the West Link project. Source: West Link project data.*

| Mix | Test | Depth natural [m] | Binder content [kg/m3] | Lime [%] | Cement [%] | Measured shear strength [kPa] | Curing time [days] | Curing time @20°C [days] | Curing temp [°C] | Shear Strength [kPa] 20 °C 28d |
|---|---|---|---|---|---|---|---|---|---|---|
| **Lab** | UCS | 12 | 80 | 50 | 50 | 246.3 | 13 | 13 | 20 | 288.1897 |
| **Lab** | UCS | 12 | 115 | 50 | 50 | 339.6 | 13 | 13 | 20 | 397.3577 |
| **Lab** | UCS | 13 | 80 | 30 | 70 | 237 | 13 | 13 | 20 | 277.308 |
| **Lab** | UCS | 13 | 115 | 30 | 70 | 329.3 | 13 | 13 | 20 | 385.3059 |
| **Lab** | UCS | 14 | 115 | | 100 | 328.8 | 13 | 13 | 20 | 384.7209 |
| **Lab** | UCS | 14 | 115 | | 100 | 328.8 | 13 | 13 | 20 | 384.7209 |
| **Lab** | UCS | 14 | 150 | 30 | 70 | 516 | 13 | 13 | 20 | 603.7591 |
| **Lab** | UCS | 15 | 150 | | 100 | 471.4 | 13 | 13 | 20 | 551.5737 |
| **Lab** | UCS | 17 | 80 | 50 | 50 | 254.1 | 13 | 13 | 20 | 297.3162 |
| **Lab** | UCS | 17 | 115 | 50 | 50 | 271.6 | 13 | 13 | 20 | 317.7926 |
| **Lab** | UCS | 18 | 80 | 30 | 70 | 269.9 | 13 | 13 | 20 | 315.8034 |
| **Lab** | UCS | 18 | 115 | 30 | 70 | 376.2 | 13 | 13 | 20 | 440.1825 |
| **Lab** | UCS | 19 | 115 | | 100 | 337.5 | 13 | 13 | 20 | 394.9006 |
| **Lab** | UCS | 19 | 150 | 30 | 70 | 403.4 | 13 | 13 | 20 | 472.0086 |
| **Lab** | UCS | 20 | 150 | | 100 | 571 | 13 | 13 | 20 | 668.1132 |
| **Lab** | UCS | 22 | 80 | 50 | 50 | 295.8 | 13 | 13 | 20 | 346.1084 |
| **Lab** | UCS | 22 | 115 | 50 | 50 | 390.9 | 13 | 13 | 20 | 457.3826 |
| **Lab** | UCS | 23 | 80 | 30 | 70 | 328.3 | 13 | 13 | 20 | 384.1359 |
| **Lab** | UCS | 23 | 115 | 30 | 70 | 304.1 | 13 | 13 | 20 | 355.82 |
| **Lab** | UCS | 24 | 115 | | 100 | 509.9 | 13 | 13 | 20 | 596.6216 |
| **Lab** | UCS | 24 | 150 | 30 | 70 | 504.4 | 13 | 13 | 20 | 590.1862 |
| **Lab** | UCS | 25 | 150 | | 100 | 546.7 | 13 | 13 | 20 | 639.6804 |
| **Lab** | UCS | 13 | 150 | | 100 | 492.3 | 15 | 15 | 20 | 558.5398 |
| **Lab** | UCS | 14 | 150 | 30 | 70 | 403.2 | 15 | 15 | 20 | 457.4513 |
| **Lab** | UCS | 14 | 115 | | 100 | 374 | 15 | 15 | 20 | 424.3223 |
| **Lab** | UCS | 15 | 80 | 30 | 70 | 257.9 | 15 | 15 | 20 | 292.6009 |
| **Lab** | UCS | 15 | 115 | 30 | 70 | 411.5 | 15 | 15 | 20 | 466.868 |
| **Lab** | UCS | 16 | 80 | 50 | 50 | 250.6 | 15 | 15 | 20 | 284.3187 |
| **Lab** | UCS | 16 | 115 | 50 | 50 | 382.3 | 15 | 15 | 20 | 433.7391 |
| **Lab** | UCS | 18 | 150 | | 100 | 607.9 | 15 | 15 | 20 | 689.694 |
| **Lab** | UCS | 19 | 150 | 30 | 70 | 450.6 | 15 | 15 | 20 | 511.229 |
| **Lab** | UCS | 19 | 115 | | 100 | 278.5 | 15 | 15 | 20 | 315.9727 |
| **Lab** | UCS | 20 | 80 | 30 | 70 | 301.5 | 15 | 15 | 20 | 342.0673 |
| **Lab** | UCS | 20 | 115 | 30 | 70 | 383.7 | 15 | 15 | 20 | 435.3275 |
| **Lab** | UCS | 21 | 80 | 50 | 50 | 220.8 | 15 | 15 | 20 | 250.509 |

| | | | | | | | | | | |
|---|---|---|---|---|---|---|---|---|---|---|
| **Lab** | UCS | 21 | 115 | 50 | 50 | 419.4 | 15 | 15 | 20 | 475.831 |
| **Lab** | UCS | 23 | 150 | | 100 | 355.3 | 15 | 15 | 20 | 403.1062 |
| **Lab** | UCS | 24 | 150 | 30 | 70 | 463.4 | 15 | 15 | 20 | 525.7513 |
| **Lab** | UCS | 24 | 115 | | 100 | 410.4 | 15 | 15 | 20 | 465.62 |
| **Lab** | UCS | 25 | 80 | 30 | 70 | 374.7 | 15 | 15 | 20 | 425.1165 |
| **Lab** | UCS | 25 | 115 | 30 | 70 | 396.7 | 15 | 15 | 20 | 450.0767 |
| **Lab** | UCS | 26 | 80 | 50 | 50 | 300.7 | 15 | 15 | 20 | 341.1597 |
| **Lab** | UCS | 26 | 115 | 50 | 50 | 415.9 | 15 | 15 | 20 | 471.8601 |
| **Lab** | TX | 14 | 115 | 30 | 70 | 730 | 14 | 14 | 20 | 840.526 |
| **Lab** | TX | 25 | 115 | 30 | 70 | 892.1 | 14 | 14 | 20 | 1027.169 |
| **Lab** | TX | 19 | 115 | 30 | 70 | 937.8 | 28 | 28 | 20 | 939.5643 |
| **Lab** | TX | 20 | 115 | 30 | 70 | 1023 | 28 | 28 | 20 | 1024.925 |
| **Lab** | TX | 14 | 80 | 30 | 70 | 605.8 | 14 | 14 | 20 | 697.5215 |
| **Lab** | TX | 25 | 80 | 30 | 70 | 589.1 | 14 | 14 | 20 | 678.293 |
| **Lab** | TX | 19 | 80 | 30 | 70 | 763.8 | 28 | 28 | 20 | 765.2369 |
| **Lab** | TX | 20 | 80 | 30 | 70 | 892.1 | 28 | 28 | 20 | 893.7783 |

## Linköping, Sweden

*Table 38. Data points from Linköping, Sweden. Source:* (H. Åhnberg & Johansson, 2005; Helen Åhnberg, 2006, 2007).

| **Mix** | **Test** | **Depth natural [m]** | **Binder content [kg/m3]** | **Lime [%]** | **Cement [%]** | **Measured shear strength [kPa]** | **Curing time [days]** | **Curing time @20°C [days]** | **Curing temp [°C]** | **Shear Strength [kPa] 20 °C 28d** |
|---|---|---|---|---|---|---|---|---|---|---|
| **Lab** | TXU | 5 | 100 | 0 | 100 | 155 | 1 | 0.1 | 7 | 536.96 |
| **Lab** | TXU | 5 | 100 | 0 | 100 | 170 | 1 | 0.1 | 7 | 588.92 |
| **Lab** | TXU | 5 | 100 | 0 | 100 | 172.5 | 1 | 0.1 | 7 | 597.58 |
| **Lab** | TXU | 5 | 100 | 0 | 100 | 235 | 1 | 0.1 | 7 | 814.09 |
| **Lab** | TXU | 5 | 100 | 0 | 100 | 200 | 28 | 7 | 7 | 260.31 |
| **Lab** | TXU | 5 | 100 | 0 | 100 | 245 | 28 | 7 | 7 | 318.88 |
| **Lab** | TXU | 5 | 100 | 0 | 100 | 245 | 28 | 7 | 7 | 318.88 |
| **Lab** | TXU | 5 | 100 | 0 | 100 | 275 | 28 | 7 | 7 | 357.92 |
| **Lab** | TXU | 5 | 100 | 0 | 100 | 310 | 400 | 84 | 7 | 269.30 |
| **Lab** | TXU | 5 | 100 | 0 | 100 | 400 | 400 | 84 | 7 | 347.49 |
| **Lab** | TXU | 5 | 100 | 0 | 100 | 400 | 400 | 84 | 7 | 347.49 |
| **Lab** | TXU | 5 | 100 | 0 | 100 | 450 | 400 | 84 | 7 | 390.92 |
| **Lab** | TXD | 5 | 100 | 0 | 100 | 140 | 1 | 0.1 | 7 | 484.99 |
| **Lab** | TXD | 5 | 100 | 0 | 100 | 235 | 1 | 0.1 | 7 | 814.09 |
| **Lab** | TXD | 5 | 100 | 0 | 100 | 240 | 28 | 7 | 7 | 312.37 |
| **Lab** | TXD | 5 | 100 | 0 | 100 | 275 | 28 | 7 | 7 | 357.92 |

| | | | | | | | | | | |
|---|---|---|---|---|---|---|---|---|---|---|
| **Lab** | TXD | 5 | 100 | 0 | 100 | 310 | 400 | 84 | 7 | 269.30 |
| **Lab** | TXD | 5 | 100 | 0 | 100 | 315 | 400 | 84 | 7 | 273.65 |
| **Lab** | UCS | 5 | 100 | 0 | 100 | 57.5 | 1 | 0.1 | 7 | 199.19 |
| **Lab** | UCS | 5 | 100 | 0 | 100 | 75 | 1 | 0.1 | 7 | 259.82 |
| **Lab** | UCS | 5 | 100 | 0 | 100 | 120 | 28 | 7 | 7 | 156.18 |
| **Lab** | UCS | 5 | 100 | 0 | 100 | 135 | 28 | 7 | 7 | 175.71 |
| **Lab** | UCS | 5 | 100 | 0 | 100 | 167.5 | 28 | 7 | 7 | 218.01 |
| **Lab** | UCS | 5 | 100 | 0 | 100 | 177.5 | 28 | 7 | 7 | 231.02 |
| **Lab** | UCS | 5 | 100 | 0 | 100 | 257.5 | 400 | 84 | 7 | 223.70 |
| **Lab** | UCS | 5 | 100 | 0 | 100 | 280 | 400 | 84 | 7 | 243.24 |
| **Lab** | TXU | 5 | 50 | 0 | 100 | 100 | 28 | 7 | 7 | 130.15 |
| **Lab** | TXU | 5 | 50 | 0 | 100 | 125 | 28 | 7 | 7 | 162.69 |
| **Lab** | TXU | 5 | 50 | 0 | 100 | 125 | 28 | 7 | 7 | 162.69 |
| **Lab** | TXU | 5 | 50 | 0 | 100 | 135 | 28 | 7 | 7 | 175.71 |
| **Lab** | TXD | 5 | 50 | 0 | 100 | 100 | 28 | 7 | 7 | 130.15 |
| **Lab** | TXD | 5 | 50 | 0 | 100 | 155 | 28 | 7 | 7 | 201.74 |
| **Lab** | TXD | 5 | 50 | 0 | 100 | 210 | 28 | 7 | 7 | 273.32 |
| **Lab** | UCS | 5 | 50 | 0 | 100 | 37.5 | 28 | 7 | 7 | 48.81 |
| **Lab** | UCS | 5 | 50 | 0 | 100 | 62.5 | 28 | 7 | 7 | 81.35 |
| **Lab** | TXU | 5 | 200 | 0 | 100 | 325 | 28 | 7 | 7 | 423.00 |
| **Lab** | TXU | 5 | 200 | 0 | 100 | 385 | 28 | 7 | 7 | 501.09 |
| **Lab** | TXU | 5 | 200 | 0 | 100 | 415 | 28 | 7 | 7 | 540.14 |
| **Lab** | TXD | 5 | 200 | 0 | 100 | 500 | 28 | 7 | 7 | 650.77 |
| **Lab** | TXD | 5 | 200 | 0 | 100 | 575 | 28 | 7 | 7 | 748.38 |
| **Lab** | TXD | 5 | 200 | 0 | 100 | 725 | 28 | 7 | 7 | 943.61 |
| **Lab** | UCS | 5 | 200 | 0 | 100 | 242.5 | 28 | 7 | 7 | 315.62 |
| **Lab** | UCS | 5 | 200 | 0 | 100 | 280 | 28 | 7 | 7 | 364.43 |
| **Lab** | TXU | 5 | 100 | 50 | 50 | 120 | 28 | 7 | 7 | 156.18 |
| **Lab** | TXU | 5 | 100 | 50 | 50 | 120 | 28 | 7 | 7 | 156.18 |
| **Lab** | TXU | 5 | 100 | 50 | 50 | 150 | 28 | 7 | 7 | 195.23 |
| **Lab** | TXU | 5 | 100 | 50 | 50 | 185 | 28 | 7 | 7 | 240.78 |
| **Lab** | TXD | 5 | 100 | 50 | 50 | 100 | 28 | 7 | 7 | 130.15 |
| **Lab** | TXD | 5 | 100 | 50 | 50 | 185 | 28 | 7 | 7 | 240.78 |
| **Lab** | TXD | 5 | 100 | 50 | 50 | 280 | 28 | 7 | 7 | 364.43 |
| **Lab** | TXD | 5 | 100 | 50 | 50 | 385 | 28 | 7 | 7 | 501.09 |
| **Lab** | UCS | 5 | 100 | 50 | 50 | 50 | 28 | 7 | 7 | 65.08 |
| **Lab** | UCS | 5 | 100 | 50 | 50 | 65 | 28 | 7 | 7 | 84.60 |

## Löftabro, Sweden

*Table 39. Data points from Löftabro, Sweden. Source:* (H. Åhnberg & Johansson, 2005; Helen Åhnberg, 2006, 2007).

| Mix | Test | Depth natural [m] | Binder content [kg/m3] | Lime [%] | Cement [%] | Measured shear strength [kPa] | Curing time [days] | Curing time @20°C [days] | Curing temp [°C] | Shear Strength [kPa] 20 °C 28d |
|---|---|---|---|---|---|---|---|---|---|---|
| **Lab** | TXU | 3 | 100 | 0 | 100 | 85 | 1 | 0.1 | 7 | 294.46 |
| **Lab** | TXU | 3 | 100 | 0 | 100 | 110 | 1 | 0.1 | 7 | 381.07 |
| **Lab** | TXU | 3 | 100 | 0 | 100 | 155 | 1 | 0.1 | 7 | 536.96 |
| **Lab** | TXU | 3 | 100 | 0 | 100 | 170 | 28 | 7 | 7 | 221.26 |
| **Lab** | TXU | 3 | 100 | 0 | 100 | 205 | 28 | 7 | 7 | 266.81 |
| **Lab** | TXU | 3 | 100 | 0 | 100 | 210 | 28 | 7 | 7 | 273.32 |
| **Lab** | TXU | 3 | 100 | 0 | 100 | 220 | 28 | 7 | 7 | 286.34 |
| **Lab** | TXU | 3 | 100 | 0 | 100 | 300 | 365 | 75 | 7 | 263.63 |
| **Lab** | TXU | 3 | 100 | 0 | 100 | 350 | 365 | 75 | 7 | 307.57 |
| **Lab** | TXU | 3 | 100 | 0 | 100 | 260 | 365 | 75 | 7 | 228.48 |
| **Lab** | TXD | 3 | 100 | 0 | 100 | 170 | 28 | 7 | 7 | 221.26 |
| **Lab** | TXD | 3 | 100 | 0 | 100 | 260 | 28 | 7 | 7 | 338.40 |
| **Lab** | TXD | 3 | 100 | 0 | 100 | 325 | 28 | 7 | 7 | 423.00 |
| **Lab** | UCS | 3 | 100 | 0 | 100 | 175 | 28 | 7 | 7 | 227.77 |
| **Lab** | UCS | 3 | 100 | 0 | 100 | 185 | 28 | 7 | 7 | 240.78 |
| **Lab** | UCS | 3 | 100 | 0 | 100 | 205 | 28 | 7 | 7 | 266.81 |
| **Lab** | UCS | 3 | 100 | 0 | 100 | 210 | 28 | 7 | 7 | 273.32 |
| **Lab** | UCS | 3 | 100 | 0 | 100 | 395 | 365 | 75 | 7 | 347.12 |
| **Lab** | UCS | 3 | 100 | 0 | 100 | 505 | 365 | 75 | 7 | 443.79 |

## Møllenberg, Trondheim, Norway

*Table 40. Data points from the Møllenberg project in Trondheim, Norway. Source:* (Hanson, 2012; Karlsrud et al., 2013).

| Mix | Test | Depth natural [m] | Binder content [kg/m3] | Lime [%] | Cement [%] | Measured shear strength [kPa] | Curing time [days] | Curing time @20°C [days] | Curing temp [°C] | Shear Strength [kPa] 20 °C 28d |
|---|---|---|---|---|---|---|---|---|---|---|
| **Field** | Drained | 17 | 80 | 50 | 50 | 750 | 592 | 592 | 20 | 478.10 |
| **Field** | Drained | 17 | 80 | 50 | 50 | 1400 | 592 | 592 | 20 | 892.45 |
| **Field** | Drained | 17 | 80 | 50 | 50 | 1250 | 592 | 592 | 20 | 796.83 |
| **Field** | Drained | 17 | 80 | 50 | 50 | 1500 | 592 | 592 | 20 | 956.20 |
| **Field** | Drained | 17 | 80 | 50 | 50 | 1650 | 592 | 592 | 20 | 1051.82 |
| **Field** | Drained | 17 | 80 | 50 | 50 | 1700 | 592 | 592 | 20 | 1083.69 |

| | | | | | | | | | | |
|---|---|---|---|---|---|---|---|---|---|---|
| **Field** | Drained | 17 | 80 | 50 | 50 | 1650 | 592 | 592 | 20 | 1051.82 |
| **Field** | Undrained | 17 | 80 | 50 | 50 | 1950 | 592 | 592 | 20 | 1243.06 |
| **Field** | Drained | 15 | 30 | 50 | 50 | 1250 | 561 | 561 | 20 | 801.97 |
| **Field** | Drained | 15 | 30 | 50 | 50 | 1200 | 561 | 561 | 20 | 769.89 |
| **Field** | Drained | 15 | 30 | 50 | 50 | 1550 | 561 | 561 | 20 | 994.45 |
| **Field** | Drained | 15 | 30 | 50 | 50 | 1350 | 561 | 561 | 20 | 866.13 |
| **Field** | Drained | 15 | 30 | 50 | 50 | 1350 | 561 | 561 | 20 | 866.13 |
| **Field** | Drained | 15 | 30 | 50 | 50 | 1500 | 561 | 561 | 20 | 962.37 |
| **Field** | Drained | 15 | 30 | 50 | 50 | 1450 | 561 | 561 | 20 | 930.29 |
| **Field** | Drained | 15 | 30 | 50 | 50 | 1100 | 540 | 540 | 20 | 708.98 |
| **Field** | Drained | 15 | 30 | 50 | 50 | 1400 | 540 | 540 | 20 | 902.34 |
| **Field** | Drained | 15 | 30 | 50 | 50 | 1450 | 540 | 540 | 20 | 934.57 |
| **Field** | Undrained | 15 | 30 | 50 | 50 | 1150 | 540 | 540 | 20 | 741.21 |
| **Field** | Undrained | 15 | 30 | 50 | 50 | 1450 | 540 | 540 | 20 | 934.57 |
| **Field** | Drained | 15 | 30 | 50 | 50 | 1350 | 540 | 540 | 20 | 870.11 |
| **Field** | Drained | 15 | 30 | 50 | 50 | 1350 | 540 | 540 | 20 | 870.11 |
| **Field** | Drained | 15 | 30 | 50 | 50 | 1300 | 540 | 540 | 20 | 837.89 |
| **Field** | Drained | 8.5 | 30 | 50 | 50 | 1050 | 560 | 560 | 20 | 673.80 |
| **Field** | Drained | 8.5 | 30 | 50 | 50 | 900 | 560 | 560 | 20 | 577.54 |
| **Field** | Drained | 8.5 | 30 | 50 | 50 | 400 | 560 | 560 | 20 | 256.69 |
| **Field** | Drained | 8.5 | 30 | 50 | 50 | 650 | 560 | 560 | 20 | 417.11 |
| **Field** | Drained | 8.5 | 30 | 50 | 50 | 750 | 560 | 560 | 20 | 481.29 |
| **Field** | Drained | 8.5 | 30 | 50 | 50 | 800 | 560 | 560 | 20 | 513.37 |
| **Lab** | UCS | 0 | 100 | 50 | 50 | 140 | 14 | 3 | 7 | 209.41 |
| **Lab** | UCS | 0 | 100 | 50 | 50 | 180 | 42 | 8 | 7 | 217.74 |
| **Lab** | UCS | 0 | 100 | 50 | 50 | 150 | 14 | 3 | 7 | 224.37 |
| **Lab** | UCS | 0 | 100 | 50 | 50 | 280 | 42 | 8 | 7 | 338.70 |
| **Lab** | UCS | 0 | 100 | 50 | 50 | 210 | 14 | 3 | 7 | 314.11 |
| **Lab** | UCS | 0 | 100 | 50 | 50 | 383 | 42 | 8 | 7 | 463.29 |

## Schweigaardsgate, Oslo, Norway

*Table 41. Data points from the Schweigaardsgate project in Oslo, Norway. Source:* (Karlsrud et al., 2013).

| **Mix** | **Test** | **Depth natural [m]** | **Binder content [kg/m3]** | **CKD** | **Lime [%]** | **Cement [%]** | **Measured shear strength [kPa]** | **Curing time [days]** | **Curing time @20°C [days]** | **Curing temp [°C]** | **Shear Strength [kPa] 20 °C 28d** |
|---|---|---|---|---|---|---|---|---|---|---|---|
| **Lab** | UCS | 6.4 | 110 | | 50 | 50 | 54 | 7 | 2 | 7 | 94.94 |
| **Lab** | UCS | 6.4 | 110 | | 50 | 50 | 87 | 14 | 3 | 7 | 130.13 |

| | | | | | | | | | | | |
|---|---|---|---|---|---|---|---|---|---|---|---|
| **Lab** | UCS | 6.4 | 110 | | 50 | 50 | 109 | 21 | 5 | 7 | 149.95 |
| **Lab** | UCS | 10 | 110 | | 50 | 50 | 80 | 7 | 2 | 7 | 140.65 |
| **Lab** | UCS | 10 | 110 | | 50 | 50 | 118 | 14 | 3 | 7 | 176.50 |
| **Lab** | UCS | 10 | 110 | | 50 | 50 | 95 | 21 | 5 | 7 | 130.69 |
| **Lab** | UCS | 16.4 | 110 | | 50 | 50 | 125 | 7 | 2 | 7 | 219.77 |
| **Lab** | UCS | 16.4 | 110 | | 50 | 50 | 175 | 14 | 3 | 7 | 261.76 |
| **Lab** | UCS | 16.4 | 110 | | 50 | 50 | 186 | 21 | 5 | 7 | 255.88 |
| **Lab** | UCS | 12.4 | 110 | 50 | | 50 | 85 | 7 | 2 | 7 | 149.44 |
| **Lab** | UCS | 12.4 | 110 | 50 | | 50 | 120 | 14 | 3 | 7 | 179.49 |
| **Field** | FOPS | 4 | 110 | | 50 | 50 | 50 | 3 | 3 | 20 | 86.14 |
| **Field** | FOPS | 4 | 110 | | 50 | 50 | 65 | 3 | 3 | 20 | 111.98 |
| **Field** | FOPS | 4 | 110 | | 50 | 50 | 50 | 7 | 7 | 20 | 67.67 |
| **Field** | FOPS | 4 | 110 | | 50 | 50 | 60 | 7 | 7 | 20 | 81.20 |
| **Field** | FOPS | 4 | 110 | | 50 | 50 | 60 | 7 | 7 | 20 | 81.20 |
| **Field** | FOPS | 4 | 110 | | 50 | 50 | 70 | 7 | 7 | 20 | 94.74 |
| **Field** | FOPS | 4 | 110 | | 50 | 50 | 60 | 14 | 14 | 20 | 69.08 |
| **Field** | FOPS | 4 | 110 | | 50 | 50 | 75 | 21 | 21 | 20 | 79.42 |
| **Field** | FOPS | 4 | 110 | | 50 | 50 | 110 | 21 | 21 | 20 | 116.49 |
| **Field** | FOPS | 9 | 110 | | 50 | 50 | 70 | 3 | 3 | 20 | 120.60 |
| **Field** | FOPS | 9 | 110 | | 50 | 50 | 110 | 3 | 3 | 20 | 189.51 |
| **Field** | FOPS | 9 | 110 | | 50 | 50 | 125 | 7 | 7 | 20 | 169.17 |
| **Field** | FOPS | 9 | 110 | | 50 | 50 | 160 | 7 | 7 | 20 | 216.54 |
| **Field** | FOPS | 9 | 110 | | 50 | 50 | 190 | 7 | 7 | 20 | 257.14 |
| **Field** | FOPS | 9 | 110 | | 50 | 50 | 210 | 7 | 7 | 20 | 284.21 |
| **Field** | FOPS | 9 | 110 | | 50 | 50 | 215 | 7 | 7 | 20 | 290.98 |
| **Field** | FOPS | 9 | 110 | | 50 | 50 | 160 | 14 | 14 | 20 | 184.22 |
| **Field** | FOPS | 9 | 110 | | 50 | 50 | 230 | 21 | 21 | 20 | 243.56 |
| **Field** | FOPS | 9 | 110 | | 50 | 50 | 370 | 21 | 21 | 20 | 391.81 |
| **Field** | FOPS | 13 | 110 | | 50 | 50 | 100 | 3 | 3 | 20 | 172.28 |
| **Field** | FOPS | 13 | 110 | | 50 | 50 | 110 | 3 | 3 | 20 | 189.51 |
| **Field** | FOPS | 13 | 110 | | 50 | 50 | 110 | 7 | 7 | 20 | 148.87 |
| **Field** | FOPS | 13 | 110 | | 50 | 50 | 190 | 7 | 7 | 20 | 257.14 |
| **Field** | FOPS | 13 | 110 | | 50 | 50 | 200 | 7 | 7 | 20 | 270.68 |
| **Field** | FOPS | 13 | 110 | | 50 | 50 | 310 | 7 | 7 | 20 | 419.55 |
| **Field** | FOPS | 13 | 110 | | 50 | 50 | 310 | 7 | 7 | 20 | 419.55 |
| **Field** | FOPS | 13 | 110 | | 50 | 50 | 250 | 14 | 14 | 20 | 287.85 |
| **Field** | FOPS | 13 | 110 | | 50 | 50 | 290 | 14 | 14 | 20 | 333.91 |

## Trafikverket study

*Table 42. Data points from the Trafikverket study. Source:* (Trafikverket, 2011).

| Mix | Test | Depth natural [m] | Binder content [kg/m3] | Lime [%] | Cement [%] | Measured shear strength [kPa] | Curing time [days] | Curing time @20°C [days] | Curing temp [°C] | Shear Strength [kPa] 20 °C 28d |
|---|---|---|---|---|---|---|---|---|---|---|
| **Lab** | UCS | 4 | 74 | 50 | 50 | 75 | 14 | 3 | 7 | 112.18 |
| **Lab** | UCS | 4 | 74 | 50 | 50 | 87 | 28 | 7 | 7 | 113.23 |
| **Lab** | UCS | 4 | 74 | 50 | 50 | 200 | 90 | 19 | 7 | 213.58 |
| **Lab** | UCS | 9 | 74 | 50 | 50 | 125 | 14 | 3 | 7 | 186.97 |
| **Lab** | UCS | 9 | 74 | 50 | 50 | 150 | 28 | 7 | 7 | 195.23 |
| **Lab** | UCS | 9 | 74 | 50 | 50 | 240 | 90 | 19 | 7 | 256.30 |
| **Lab** | UCS | 4 | 92 | 50 | 50 | 110 | 14 | 3 | 7 | 164.54 |
| **Lab** | UCS | 4 | 92 | 50 | 50 | 135 | 28 | 7 | 7 | 175.71 |
| **Lab** | UCS | 4 | 92 | 50 | 50 | 225 | 90 | 19 | 7 | 240.28 |
| **Lab** | UCS | 9 | 92 | 50 | 50 | 175 | 14 | 3 | 7 | 261.76 |
| **Lab** | UCS | 9 | 92 | 50 | 50 | 195 | 28 | 7 | 7 | 253.80 |
| **Lab** | UCS | 9 | 92 | 50 | 50 | 265 | 90 | 19 | 7 | 283.00 |

## Skøyen, Oslo, Norway

*Table 43. Data points from the Skøyen project in Oslo, Norway. Source:* (Karlsrud et al., 2013).

| Mix | Test | Depth natural [m] | Binder content [kg/m3] | Lime [%] | Cement [%] | Measured shear strength [kPa] | Curing time [days] | Curing time @20°C [days] | Curing temp [°C] | Shear Strength [kPa] 20 °C 28d |
|---|---|---|---|---|---|---|---|---|---|---|
| **Lab** | UCS | 0 | 80 | 50 | 50 | 115 | 21 | 5 | 7 | 158.20 |
| **Lab** | UCS | 0 | 80 | 50 | 50 | 125 | 21 | 5 | 7 | 171.96 |
| **Lab** | UCS | 0 | 80 | 50 | 50 | 205 | 55 | 11 | 7 | 236.85 |
| **Lab** | UCS | 0 | 100 | 50 | 50 | 105 | 7 | 2 | 7 | 184.61 |
| **Lab** | UCS | 0 | 100 | 50 | 50 | 153 | 21 | 5 | 7 | 210.48 |
| **Lab** | UCS | 0 | 100 | 50 | 50 | 155 | 21 | 5 | 7 | 213.23 |
| **Lab** | UCS | 0 | 100 | 50 | 50 | 218 | 55 | 11 | 7 | 251.87 |
| **Lab** | UCS | 0 | 120 | 50 | 50 | 157 | 21 | 5 | 7 | 215.98 |
| **Lab** | UCS | 0 | 120 | 50 | 50 | 205 | 21 | 5 | 7 | 282.01 |
| **Lab** | UCS | 0 | 120 | 50 | 50 | 265 | 55 | 11 | 7 | 306.18 |

## Gothenburg, Sweden (Luleå University of Technology)

*Table 44. Data points from Gothenburg, Sweden. Source:* (Jonsson, 2017).

| Mix | Test | Binder content [kg/m3] | Lime [%] | Cement [%] | Measured shear strength [kPa] | Curing time @ 20 °C [days] | Shear Strength [kPa] @ 20 °C 28d |
|---|---|---|---|---|---|---|---|
| **Lab** | UCS | 82.6 | 0 | 100 | 312.385 | 90 | 256.80 |
| **Lab** | UCS | 82.6 | 0 | 100 | 385 | 90 | 316.49 |
| **Lab** | UCS | 82.6 | 0 | 100 | 340 | 90 | 279.50 |
| **Lab** | UCS | 82.6 | 0 | 100 | 330 | 90 | 271.28 |
| **Lab** | UCS | 82.6 | 0 | 100 | 310 | 90 | 254.84 |
| **Lab** | UCS | 82.6 | 0 | 100 | 300 | 90 | 246.62 |
| **Lab** | UCS | 82.6 | 0 | 100 | 212.5 | 7 | 287.60 |
| **Lab** | UCS | 82.6 | 0 | 100 | 210 | 7 | 284.21 |
| **Lab** | UCS | 82.6 | 0 | 100 | 205 | 7 | 277.44 |
| **Lab** | UCS | 82.6 | 0 | 100 | 202.5 | 7 | 274.06 |
| **Lab** | UCS | 82.6 | 0 | 100 | 327.095 | 90 | 268.89 |
| **Lab** | UCS | 47.2 | 0 | 100 | 96.755 | 90 | 79.54 |
| **Lab** | UCS | 47.2 | 0 | 100 | 100 | 90 | 82.21 |
| **Lab** | UCS | 47.2 | 0 | 100 | 95 | 90 | 78.10 |
| **Lab** | UCS | 47.2 | 0 | 100 | 92.5 | 90 | 76.04 |
| **Lab** | UCS | 47.2 | 0 | 100 | 90 | 90 | 73.98 |
| **Lab** | UCS | 47.2 | 0 | 100 | 85 | 90 | 69.87 |
| **Lab** | UCS | 47.2 | 0 | 100 | 75 | 7 | 101.50 |
| **Lab** | UCS | 47.2 | 0 | 100 | 72.5 | 7 | 98.12 |
| **Lab** | UCS | 47.2 | 0 | 100 | 67.5 | 7 | 91.35 |
| **Lab** | UCS | 47.2 | 0 | 100 | 67 | 7 | 90.68 |
| **Lab** | UCS | 47.2 | 0 | 100 | 97.1 | 90 | 79.82 |
| **Lab** | UCS | 23.6 | 0 | 100 | 45.135 | 90 | 37.10 |
| **Lab** | UCS | 23.6 | 0 | 100 | 50 | 90 | 41.10 |
| **Lab** | UCS | 23.6 | 0 | 100 | 49 | 90 | 40.28 |
| **Lab** | UCS | 23.6 | 0 | 100 | 45 | 90 | 36.99 |
| **Lab** | UCS | 23.6 | 0 | 100 | 43.5 | 90 | 35.76 |
| **Lab** | UCS | 23.6 | 0 | 100 | 44.5 | 90 | 36.58 |
| **Lab** | UCS | 23.6 | 0 | 100 | 37.5 | 7 | 50.75 |
| **Lab** | UCS | 23.6 | 0 | 100 | 34 | 7 | 46.02 |
| **Lab** | UCS | 23.6 | 0 | 100 | 35 | 7 | 47.37 |
| **Lab** | UCS | 23.6 | 0 | 100 | 32.5 | 7 | 43.99 |
| **Lab** | UCS | 23.6 | 0 | 100 | 43.175 | 90 | 35.49 |
| **Lab** | UCS | 11.8 | 0 | 100 | 23.835 | 7 | 32.26 |
| **Lab** | UCS | 11.8 | 0 | 100 | 26 | 7 | 35.19 |
| **Lab** | UCS | 11.8 | 0 | 100 | 24.5 | 7 | 33.16 |

| | | | | | | | |
|---|---|---|---|---|---|---|---|
| **Lab** | UCS | 11.8 | 0 | 100 | 20.5 | 7 | 27.74 |
| **Lab** | UCS | 11.8 | 0 | 100 | 19 | 7 | 25.71 |
| **Lab** | UCS | 11.8 | 0 | 100 | 23.16 | 7 | 31.34 |

## B. Influence of soil natural properties in the improved shear strength of stabilized soil

In this section, the plots which prove that the water content, liquid limit and sensitivity do not greatly influence the improved shear strength of a stabilized soil are presented, these correspond to Figure 74, Figure 75 and Figure 76. For the data analyzed, no visible trend is observed and therefore these natural soil properties are discarded for the final expression to estimate the improved shear strength.

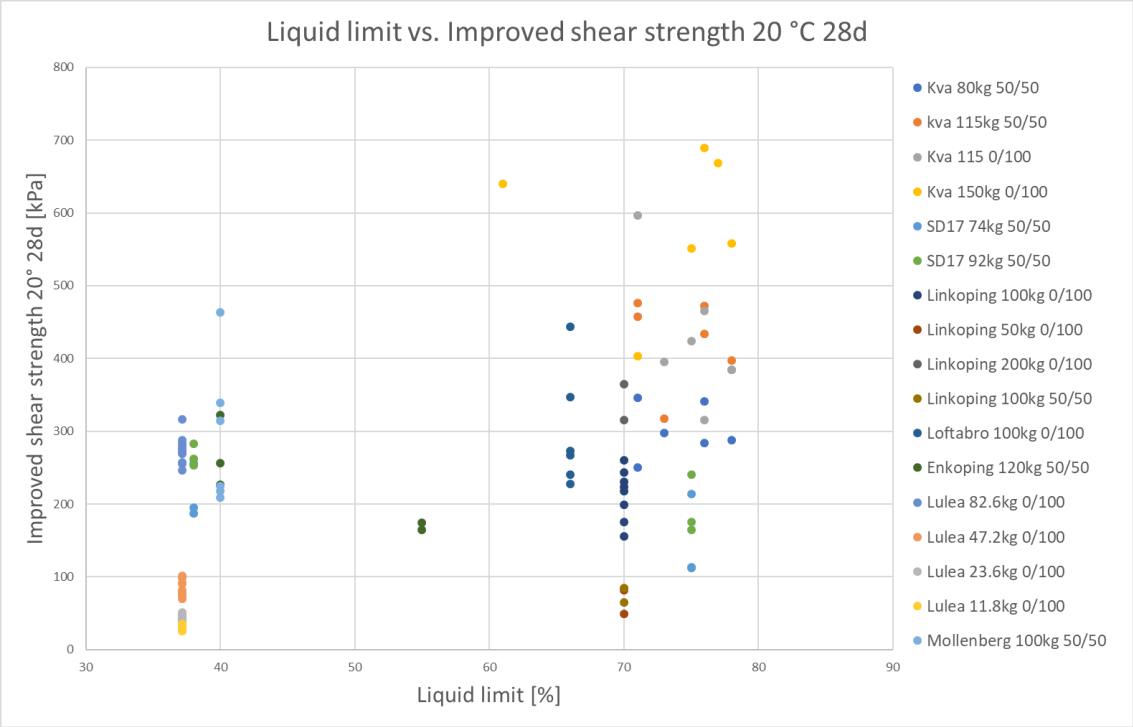


*Figure 74. Liquid limit vs. improved shear strength for all the available data. Source: own elaboration.*

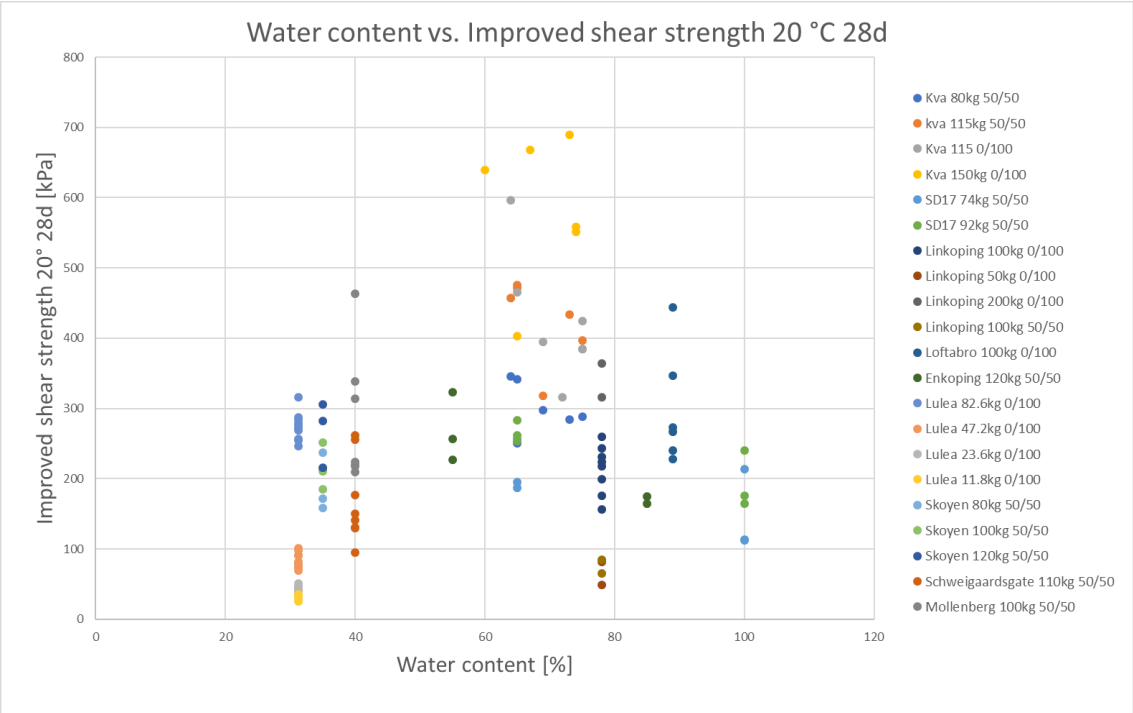


*Figure 75. Water content vs. improved shear strength for all the available data. Source: own elaboration.*

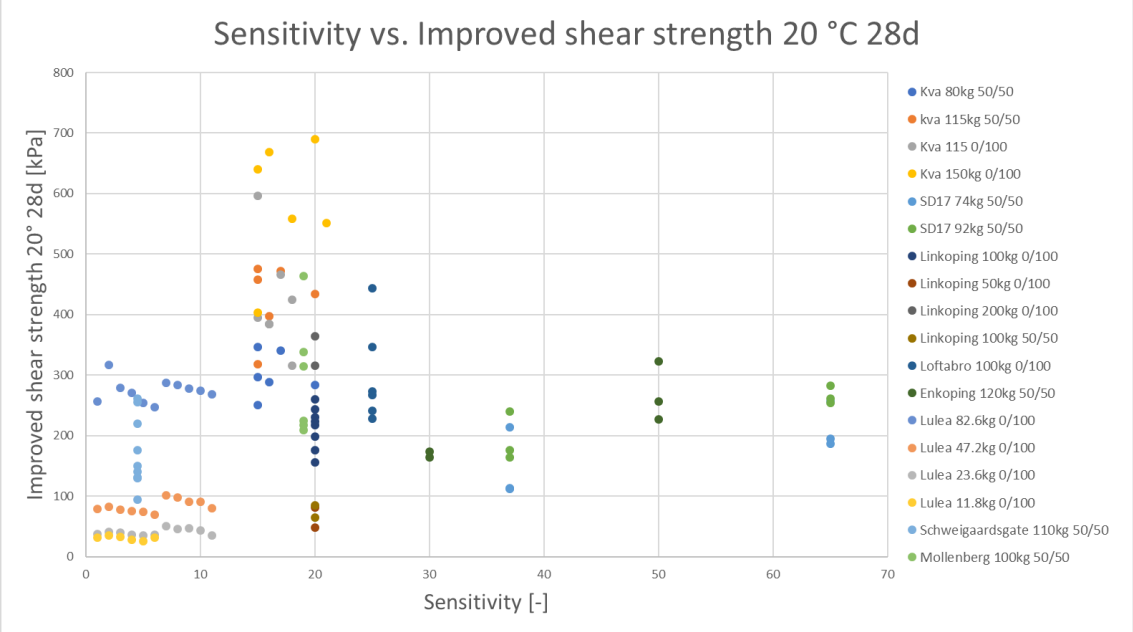


*Figure 76. Sensitivity vs. improved shear strength for all the available data. Source: own elaboration.*